MICROSTRUCTURE AND MECHANICAL PROPERTIES OF 2024-T3 AND 7075-T6

ALUMINUM ALLOYS AND AUSTENITIC STAINLESS STEEL 304

AFTER BEING EXPOSED TO HYDROGEN PEROXIDE

Except where reference is made to the work of others, the work described in this
dissertation is my own or was done in collaboration with my advisory
committee. This dissertation does not include proprietary,
restricted or classified information.

_____
Nofrijon Bin Imam Sofyan

Certificate of Approval:

_____   _____
Jeffrey W. Fergus   William F. Gale, Chair
Associate Professor   Alumni Professor
Mechanical Engineering   Mechanical Engineering

_____   _____
Barton C. Prorok   ZhongYang Cheng
Associate Professor   Associate Professor
Mechanical Engineering   Mechanical Engineering

_____   _____
German Mills   George T. Flowers
Associate Professor   Interim Dean
Chemistry and Biochemistry   Graduate School

MICROSTRUCTURE AND MECHANICAL PROPERTIES OF 2024-T3 AND 7075-T6

ALUMINUM ALLOYS AND AUSTENITIC STAINLESS STEEL 304

AFTER BEING EXPOSED TO HYDROGEN PEROXIDE

Nofrijon Bin Imam Sofyan

A Dissertation

Submitted to

the Graduate Faculty of

Auburn University

in Partial Fulfillment of the

Requirements for the

Degree of

Doctor of Philosophy

Auburn, Alabama

August 9, 2008

MICROSTRUCTURE AND MECHANICAL PROPERTIES OF 2024-T3 AND 7075-T6

ALUMINUM ALLOYS AND AUSTENITIC STAINLESS STEEL 304

AFTER BEING EXPOSED TO HYDROGEN PEROXIDE

Nofrijon Bin Imam Sofyan

_____
Signature of Author

_____
Date of Graduation

This dissertation is dedicated to my parents Rosnah and Imam Sofyan, my wife Linda, and my children Aga and Fiona. My parents have been an inspiration to me and instilled a sense of commitment to reach my goals. My wife has tolerated my absence for far too long and has maintained her support of my goals. I hope that my success in obtaining this degree will make my children proud of me and aware that no goal is too high to obtained.

VITA

Nofrijon Bin Imam Sofyan, son of Rosnah and Imam Sofyan of Taeh Bukik, was born on December 15, 1967 in Taeh Bukik, West Sumatera, Indonesia. He graduated from SMA Dangung-Dangung High School in 1987 and immediately entered Andalas University, Padang. He graduated with honors from Andalas University in April 1992 with a bachelor degree in chemistry. He then worked as a teacher at Indonesian College of the Arts and Sciences, Surakarta, Central Java, for 5 years. During the last two years of that period, he also served as the head of office of information and technology at the same school. He entered graduate school at the University of Indonesia, Jakarta, in 1997 and received a masters degree in materials science in 1999. He worked on the staff of the Research Center for Materials Science at the same school before entering the Doctoral program in 2000. In October 2001 he joined Materials Engineering at Auburn University as a research scholar in his effort to finish his doctoral degree, but then he decided to join Materials Engineering as a full time graduate student. He entered Materials Engineering Doctoral Program in Spring 2003. He married Lindawati, S., daughter of Janilas and Syamsuar of Ampang Godang, on January 11, 1995 and have two lovely children. Their son Aga Ridhova was born on May 3, 1996 and their daughter Fiona Angellinnov was born on December 1, 1997.

DISSERTATION ABSTRACT

MICROSTRUCTURE AND MECHANICAL PROPERTIES OF 2024-T3 AND 7075-T6

ALUMINUM ALLOYS AND AUSTENITIC STAINLESS STEEL 304

AFTER BEING EXPOSED TO HYDROGEN PEROXIDE

Nofrijon Bin Imam Sofyan

Doctor of Philosophy, August 9, 2008
(M.S., University of Indonesia, 1999)
(B.S., Andalas University, 1992)

191 Typed Pages

Directed by William F. Gale

The effect of hydrogen peroxide used as a decontaminant agent on selected aircraft metallic materials has been investigated. The work is divided into three sections; bacterial attachment behavior onto an austenitic stainless steel 304 surface; effect of decontamination process on the microstructure and mechanical properties of aircraft metallic structural materials of two aluminum alloys, i.e. 2024-T3 and 7075-T6, and an austenitic stainless steel 304 as used in galley and lavatory surfaces; and copper dissolution rate into hydrogen peroxide. With respect to bacterial attachment, the results show that surface roughness plays a role in the attachment of bacteria onto metallic surfaces at certain extent. However, when the contact angle of the liquid on a surface

increased to a certain degree, detachment of bacteria on that surface became more difficult. In its relation to the decontamination process, the results show that a corrosion site, especially on the austenitic stainless steel 304 weld and its surrounding HAZ area, needs more attention because it could become a source or a harborage of bio-contaminant agent after either incidental or intentional bio-contaminant delivery. On the effect of the decontamination process on the microstructure and mechanical properties of aircraft metallic structural materials, the results show that microstructural effects are both relatively small in magnitude and confined to a region immediately adjacent to the exposed surface. No systematic effect is found on the tensile properties of the three alloys under the conditions examined. The results of this investigation are promising with respect to the application of vapor phase hydrogen peroxide as a decontaminant agent to civilian aircraft, in that even under the most severe circumstances that could occur; only very limited damage was observed. The results from the dissolution of copper by concentrated liquid hydrogen peroxide showed that the rate of copper dissolution increased for the first 15 minutes of the reaction time with an activation energy of 19 kJ/mol, and then the fraction of copper dissolved became constant. This constant dissolution was expected to be due to the formation of copper hydroxide, which was observed to precipitate after the solution settled for some time. However, because the final consumption of hydrogen peroxide was not controlled, the exact reason for this constant dissolution cannot be determined at this time. The value of activation energy is within the range of activation energy found in the literature for other dissolution process. The low activation energy for dissolution of pure copper correlates with the observation of dissolution of copper from intermetallic particles in the aluminum alloys.

ACKNOWLEDGMENTS

All the praises and thanks be to Allah, the Almighty. Following, the author would like to express his deep sense of gratitude to Dr. William F. Gale for his constant support, guidance and encouragement during the period of work, and for his genuine concern for the well-being and success of his students. The author is indebted to Dr. Jeffrey W. Fergus for his invaluable help and advice throughout the course of work; without him the author would not be where he is now. Thanks are also due to the committee members Dr. ZhongYang Cheng, Dr. Barton C. Prorok, and Dr. German Mills for their versatility in tackling a different field of research and in their understanding through the projects; to Dr. Curtis G. Shannon, Dr. Michael L. McKee and Dr. David M. Stanbury for their help and valuable discussion; to Dr. Hyacinth S. Gale for her constant help and support; to his colleagues in Dr. Gale's group, not only for their assistance, but also for their friendship during his time in Materials Engineering Program: Daniel A. Butts, Venu Krishnardula, Rajeev Aluru, Chad Callender, Raghu Viswanathan, ShihFeng Chou, and Mobbassar Hassan SK; and to Mr. Roy Howard for being a source of constant help. The author would also like to express his sincere thanks to his parents for their love, prayers, and endless support and to his wife Linda and his two beloved children Aga and Fiona for their unconditional love, devotion, understanding, and patience for the past five years.

Style manual or journal used: <u>Metallurgical and Materials Transactions A</u>

Computer software used: <u>Microsoft Office 2007, SAS 9.0, and Image Pro 4.3</u>

TABLE OF CONTENTS

LIST OF FIGURES

LIST OF TABLES

LIST OF ACRONYMS

ACER: Airliner Cabin Environment Research

AEM: Analytical Electron Microscopy

ANOVA: Analysis of Variance

ASTM: American Society for Testing Materials

ATCC: American Type Culture Collection

BHI: Brain Heart Infusion

BIs: Biological Indicators

BWA: Biological Warfare Agents

CBED: Convergent Beam Electron Diffraction

CFU: Colony Forming Unit

CWA: Chemical Warfare Agent

EDM: Electrical Discharge Machine

EDS: Energy Dispersive Spectrometry

EDA: Ethylene Diamine

EDTA: Ethylene Diamine Tetraacetic Acid

EPA: Environmental Protection Agency

FAA: Federal Aviation Administration

FE-SEM: Field Emission Scanning Electron Microscope

FIFRA:	Federal Insecticide, Fungicide, and Rodenticide Act
GP:	Guinier-Preston
HALT:	High Accelerated Life Testing
HAZ:	Heat Affected Zone
HPAI:	Highly Pathogenic Avian Influenza
HPV:	Hydrogen Peroxide Vapor
kJ:	Kilojoules
QCT:	Quantitative Carrier Test
RH:	Relative Humidity
RPM:	Revolutions per Minute
SAD:	Selected Area Diffraction
SARS:	Severe Acute Respiratory Syndrome
SAS:	Statistical Analysis System
SCC:	Stress Corrosion Cracking
SCFM:	Standard Cubic Feet per Minute
SCMM:	Standard Cubic Meter per Minute
SEM:	Scanning Electron Microscope
SSSS:	Supersaturated Solid Solution
TEM:	Transmission Electron Microscope
TIG:	Tungsten Inert Gas
UTW:	Ultrathin Window
VHP:	Vaporized Hydrogen Peroxide
WHO:	World Health Organization

1. INTRODUCTION

There has been a long history of biological and chemical agents use for warfare and terrorism along with the growth and modernization of human life. The use of these agents has increased significantly during the World War I [1]. Fortunately, with the awareness of people who wanted to live peacefully, the use of biological and chemical as warfare agents has decreased after World War II, especially after the United Nations Convention on the "Prohibition of the Development, Production, and Stockpiling of Bacteriological and Toxin Weapons and Their Destruction" was ratified by member nations in 1972 [2].

The achievements in the field of biotechnology, biochemistry, and genetic engineering nowadays have brought human race to a new era and bright future. Nevertheless, like many other things, there will be a dark side of this technology. One aspect of this "dark side" is the application of science and technology for illegal manufacture and abuse in biological and chemical weapons by terrorists or by rogue nation leaders [1]. For that reason the use of chemical or biological warfare agents in either a domestic terrorist attack or military conflict for the purpose of causing people to die remains a threat [3].

Chemical warfare agents may be defined as poisonous chemicals that may generate irritating or debilitating effects, make materials deteriorate or areas unusable, or may cause lethal effects to human and other living organisms. According to the United States Military [4], chemical warfare agents that may cause lethal effects can be classified into four categories: nerve agents, blister agents, choking agents, and blood agents. This classification is basically based on the effects of the agents have on human or living animals as indicated by the agent names. For example, nerve agents will attack nerves and muscle system; blister agents will attack and destroy cell tissues resulting in severe blisters; choking agents cause irritation and inflammation of the bronchial tubes and lungs causing choking; and blood agents will react and disrupt the oxygen-carrying properties of the blood resulting in lethal effect. The damaging effect of these agents to human and/or to other animals depends on the type, concentration, and method of delivery.

Biological agents, on the other hand, are actually pathogens or toxins derived and/or produced by living microorganisms. These agents may cause disease or poisoning in people, animals or plants, and may also cause materials to deteriorate. Depending on the type of agents used, when used directly, these agents can be used to cause diseases such as anthrax, cholera, plague, or diphtheria, and when used indirectly can be used to infect crops or livestock and so to reduce the supply of food. Several other living microorganisms that can be used for biological warfare purpose include bacteria, rickettsiae, viruses, and fungi [4]. The diseases caused by these agents may spread in a variety of ways including ingestion of the infected plants or animals, bites from infected animals and/or insects, or inhaling the microorganisms that produce the toxin.

The threat of using chemical and biological warfare agents for the purpose of causing other people to die has been transformed into reality and made particularly evident by the *Bacillus antharacis* spores attack by terrorist to civilians in Washington D.C. and Sterling, Virginia, in 2001 [5, 6]. As a matter of fact, other than these two attacks, several other terrors that caused massive disruption and widespread fear into a society had also been released at several other places. For example, the Aum Shinrikyo Sarin attack on the Tokyo subway in 1995 and, most recently, employment of chlorine tankers by insurgent elements in Iraq [7-11].

Apart from intentional abuse of chemical and biological warfare agents for terrorist purposes, there are also natural occurrences of epidemics that need to be taken care of very carefully. Some examples are given as following. In 2003, severe acute respiratory syndrome (SARS) that initiated as endemic in Hong Kong has became epidemic and emerged as a new acute respiratory disease that spread rapidly across the world [12]. Only one year after the SARS outbreak, in 2004, highly pathogenic avian influenza (HPAI) viruses of the H5N1 subtype were spreading and circulating in eastern and South East Asia causing epidemic effects [13]. In the case of HPAI viruses, several Asian countries in that area including Cambodia, China, Indonesia, Japan, Laos, Malaysia, South Korea, Thailand, and Vietnam have reported outbreaks in their poultries [14]. It is suspected that this HPAI type of virus could have resulted from development of a pandemic strain because it was never detected before [15-16]. Even though the biggest impact was on poultry, however, animal-to-human and human-to-human transmission of the virus also has been described, most recently in families who live close to the poultry

3

in Thailand and Indonesia; many of them were fatal including 52 of which have been reported to the World Health Organization (WHO) [17-18].

The rapid spreading of these epidemics is believed by many investigators to be due to the weak control of the outbreak at the early stages of the epidemic [19-23]. SARS for example, at the early stage and even during the outbreak, was transmitted efficiently among workers, patients, and visitors at the healthcare facility. The weak control also has been acknowledged through documented hospital outbreaks of SARS that occurred in several countries following the outbreaks. The affected countries including Canada, China, Hong Kong, Singapore, Taiwan, and Vietnam also have highlighted the weak infection control of infrastructure present in their healthcare facilities [24-26]. Some data from researchers also have indicated that the SARS virus is largely spread by direct or indirect contact with the infected person, while other researchers have found that the airborne transmission of the virus could also responsible for the spread of SARS outbreaks [27-29].

If one were to take a look back to the time, long before these two epidemics, in 1918/1919, the world was swept by an influenza pandemic that killed more than 40 million of people in its wake [30]. This influenza pandemic almost circled the world that most of humanity felt and suffered from it. In the U.S. alone, an estimated 675,000 people died of influenza during this pandemic [31]. The interesting part is that, circulation of the virus followed the mass movements of the armies and aboard ships during the World War I. Because of that it is believed the mass movement of the armies probably caused the pandemic's rapid diffusion and attack [32-34].

4

As so many people travel nowadays using air transportation, airliners could again be one of the terrorist targets as was the case when they were used for attacking the World Trade Center in New York in 2001. At the same time, if pathogen control over the flight is weak, aircraft may become a vector for spreading an endemic, which then can be easily transformed into an epidemic, or even a pandemic. Thus, with the background of these recent events, the possibility of more biological and chemical emergencies, either incidental or deliberate, cannot be ignored [35].

Hence, there will be always growing concerns related to both naturally occurring pathogens and unintentional bio-chemical contamination or deliberate terrorist attacks that involve these chemical and biological warfare agents. These growing concerns have necessitated consideration and implementation of science and technology as a response to chemical and biological terrorism and/or epidemics/pandemics in which civil aviation represents a key potential vector. This response is needed especially to counter the attack and/or at least to reduce the possibility of lingering effects in case an incident or attack occurs unexpectedly, whilst at the same time trying to prevent such events in the future. One of the possibilities to counter these horrific bio-chemical events is by developing effective sensors and at the same time a decontamination defense.

As part of their role in the Air Transportation Center of Excellence for Airliner Cabin Environment Research (ACER), under funding received from the U.S. Office of Aerospace Medicine, Federal Aviation Administration (FAA), Auburn University, Boise State University, and Purdue University are surveying, selecting, and testing sensor and decontamination technologies for further evaluation or implementation on the civilian

aircraft. This dissertation focuses on the latter, so called on-the-ground airliner decontamination.

The main idea of this project is basically to be able to take the action of decontaminating an airliner on-the-ground following either deliberate or unintentional incidents of biological contamination and enable return to service. Due to the inherent properties of the chemical used as a decontaminant agent, it possibly could affect the airliner materials during or after the decontamination process. Hence, to enable return to service after decontamination it is desirable to be able to predict the effect of this chemical on the aircraft's flightworthiness at least qualitatively and ideally quantitatively.

The present research, based on the main idea outlined previously, actually does not yet address the entire goals, especially with respect to the prediction of effect of the chemical used as the decontaminant agent on the aircraft's flightworthiness. However, what has been performed in the present project is a necessary precursor step. Thus, future work that needs to be done to accomplish all of these goals is presented in section 7, "Suggestions for Future Work".

Although the use of high-performance polymer-matrix fiber composites in aircraft structures has grown, for example, the Boeing 787 aircraft has a polymer-matrix fiber composite fuselage, aluminum alloys will continue to be used widely for the foreseeable future [36]. The main reason for this is the high fabrication cost of composite materials compared to those of metallic materials. In addition to this fabrication cost, certification of new aircraft components, require a long time and high costs. Metallic materials, on the other hand, have been proven to be reliable for decades. Up to the present time, metallic materials still have the advantages of being superior over composite materials in terms of

resistance to mechanical damage, high strength, and relatively high temperature limitation. Furthermore, even composite materials are being developed; however, there are also ongoing developments in structural metallic materials that still make metallic structures relatively more affordable than composite structures, at least for the time being, in terms of financial aspect [37]. Thus, metals will continue to be used widely and still the materials of choice for many airframe applications in the near future. For those reasons, in the present research, the focus is only on the airliner metallic structural materials.

2. LITERATURE REVIEW

The main objective of this present research is to find out if there is any immediate loss or degradation in aircraft metallic structural materials properties and hence performance after on-the-ground airliner decontamination has been performed. At the same time, it is also to consider whether there is incipient damage that raises the possibility of degradation during long term service. In this chapter, therefore, it is of interest to seek the background of the work and several other factors that would be likely to be involved in the process, including review of the materials used, processing procedures, and materials characterization. Some other factors that would likely affect the materials used in the near future but have not been investigated in the present research are also presented. There are three different topics that have been carried out in this study, i.e. bacterial attachment behavior onto surfaces, effect of decontamination on the microstructure and mechanical properties of aircraft metallic structural materials, and dissolution of copper into liquid hydrogen peroxide. The following sections provide literature reviews on each of these topics. The information given and reviewed in this chapter is then used in subsequent chapters for experimental design and implementation.

2.1 Factors Affecting Bacterial Attachment to Surfaces

The attachment of spoilage and/or pathogenic bacteria to a surface has always been troublesome and has serious implications in terms of safety within the food industry, domestic area, institutional locations such as hospitals, and public transportation such as aircraft [38, 39]. In general, it has been recognized that bacteria become attached to surfaces with several factors influencing the attachment. However, explanations on the mechanisms governing the attachment are rarely available and have not been fully understood [40]. Because of this, a number of studies have been performed by many investigators to more clearly define, explain, and evaluate factors affecting bacterial attachment to surfaces. Several factors that have been considered in the studies included electrolyte, surface charge differences, hydrophobicity, wettability, and surface roughness [40-49]. Results of these studies were quite different from study to study, mostly because of differences in experimental techniques, materials being used, and wide range of factors in consideration. However, in general, the results have shown that both materials and bacterial surface properties have an influence on the way bacteria attached to surfaces. Many attempts also have been made by investigators to explain the mechanisms behind the attachment process. Some explanations of the mechanisms that have been described including passive Van der Waals attractive forces, electrostatic interactions, dipole interactions, chemical bonding, hydrophobic interactions, steric forces, and in terms of bacterial properties itself including external appendages and extracellular polymer [50-53].

In terms of surface roughness, it has been reported that surface roughness affects bacterial ability to attach to a surface; the increase in surface roughness increases the

number of bacteria attached to a surface [49]. It was believed that increase in surface roughness accounted for higher wettability, while higher wettability of the surface allowed bacteria to distribute to a larger area. At the same time, it was found that surface of higher wettability had lower contact angle than that of surface of less wettability. By this fact, it can be considered that surface roughness has an important influence on the wettability and thus to the way bacteria attached to surfaces. Hence, surface roughness could be used as an initial indicator whether or not bacteria would be easily attached to a surface.

In this dissertation, the effect of surface roughness on bacterial attachment and its likely impact on the civilian aircraft decontamination process is discussed. The discussion is based on our two previous results on the effect of different surface roughness of austenitic stainless steel 304 on bacterial attachments [47, 48]. The first is related to the effect of surface roughness resulting from welding and accelerated corrosion and the second is related to the effects exerted by different types of surface finish commercially available on bacterial attachment.

In its relation to the decontamination process development for civilian aircraft, the effects of surface roughness on bacterial attachment are particularly interesting. The most important reason for this is because surface roughness could impact the decontamination process. However, at the time this work was performed, it was originally thought that this bacterial attachment research would be most relevant to the food industry area. Later on, as the work progressed to decontamination development for civilian aircraft, there arose a need to understand how bio-contaminants would behave on attachment to aircraft material surfaces. This understanding is needed especially in relation to the

decontamination process itself. In this regard, different surface properties might impact the way bacteria attach to a surface[1], and thus could require modification of the decontamination process, or it might influence the efficacy of any given decontamination setup. For that reason, this part of the bacterial attachment work was also included in this dissertation.

2.2 Surface Roughness and Bacterial Attachment

2.2.1 Surface Roughness

Surface roughness is a term used to describe the smoothness of a surface finish or irregularities of a surface texture. The term has been widely used for both practical and scientific purposes. In general, irregularities of a surface texture account for surface roughness. Surface texture itself can be repetitive or random patterns that are usually developed as inherent actions during manufacturing procedures, finishing processes, or as a result of surface damage due to say corrosion [54, 55].

There are many different parameters due to the differences in a wide variety of machining operations and need. For examples, roughness average (R_a) and root mean square roughness (R_q) are calculated based on the roughness amplitude parameter; while mean spacing of profile irregularities (S_m) and average wavelength of the profile (λ_a) are calculated based on the spacing parameter [56]. The roughness average is one of the most widely used terms, which is calculated based on the roughness amplitude parameter, and is used to indicate roughness value of a surface; the larger the value, the rougher surface of a material.

---

[1] In this regard, different surface properties might affect bacterial ability to attach to a surface due to a different mechanism of attachment and/or due to a different of the bond strength between the bacterial cells and the surface.

The value of a roughness average comes from the integral area within the average center line between top and valley of a surface topography, the shaded area in Figure 1, and the evaluation length of measurement; which is why sometimes it also called center line average. In mathematical expression this gives [54, 56]:

$$R_a = \frac{1}{L}\int_0^L |y(x)|\, dx$$

Equation 1

where:

R_a = value of the roughness average

y = ordinate of the profile

L = length of the measurement
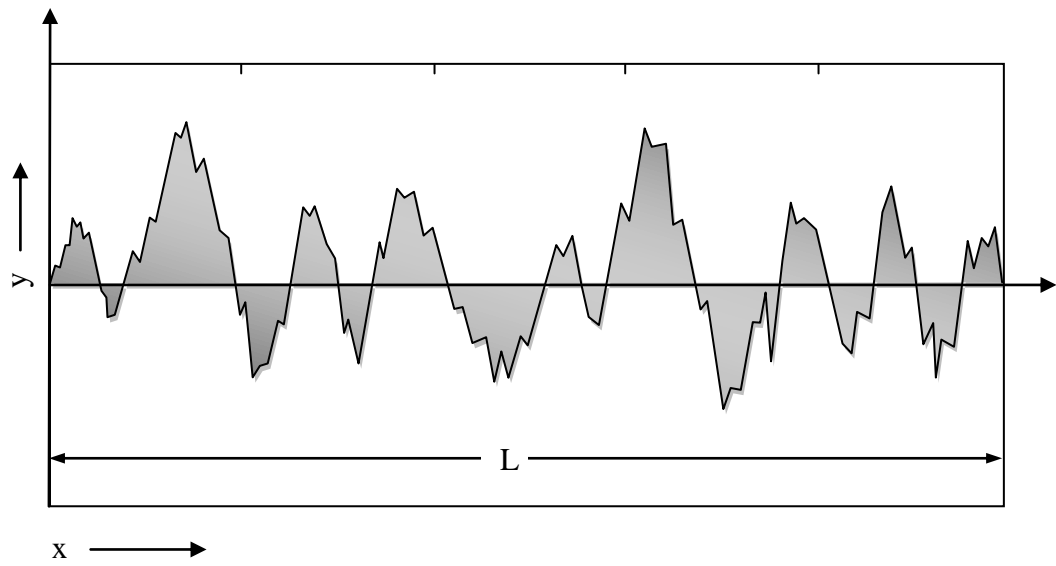
Figure 1−Schematic of surface texture profile from where the surface roughness average (R_a) is derived [54].

In many applications, surface roughness plays an important role in the performance of material itself. For examples, surface roughness greatly affects fatigue and creep life in terms of mechanical properties of a component bearing a load [54]. In the food industry area, surface roughness is of great importance in terms of the hygiene of food contact surfaces because of easiness of certain foodborne pathogens to attach to certain type of surface roughness [57].

The influence of a surface roughness on spreading of a liquid, thus microorganisms within the liquid, and how it could influence the decontamination process or efficacy of any given decontamination setup in civilian aircraft is discussed in the next section.

2.2.2 Wettability and Adhesion

Wettability is a term that refers to the ability of a liquid or fluid to wet or coat a surface. A more applicable definition is given by US Environmental Protection Agency (EPA) as "the relative degree to which liquid or fluid will spread onto or coat a solid surface in the presence of other immiscible fluids" [58]. Sometimes the term of wetting is used instead of wettability. In this regard, two or more dissimilar materials need to be in contact, either directly or through an interlayer, creating a new interface. In order to be able to predict the equilibrium wetting condition on the interface between these two dissimilar materials, the thermodynamic and kinetic implications of wettability and several other factors affecting this wettability, such as interfacial energy, adhesion, and tension, need to be considered [59-61].

A useful scientific foundation for this interfacial studies, wettability, adhesion, and spreading phenomena basically comes from the application of Young's equation [61-64]:

$$\gamma_{sv} - \gamma_{ls} = \gamma_{lv} \cos \theta$$

Equation 2

where:

θ = contact angle

γ_{sv} = interfacial tensions at the boundaries between solid - vapor

γ_{ls} = interfacial tensions at the boundaries between liquid - solid

γ_{lv} = interfacial tensions at the boundaries between liquid - vapor

The equation is used to predict the equilibrium contact angle values at the interface in terms of thermodynamic consideration. In the Young equation, the equilibrium contact angle is obtained from a balance of interfacial tensions for a liquid droplet on a solid surface, in which a low interfacial energy between liquid and solid yields a lower value of contact angle. In this regard, wettability of a liquid over a solid substrate surface can be characterized in terms of contact angle that the liquid makes on that solid surface; lower contact angles imply higher wettability.

The Young's model, however, can only be applied to an ideal surface, i.e. perfectly smooth, and the substrate should not have any internal stress that causes substrate deformation. Lester [62] has shown that when a solid has deformability within a

certain range, the experimentally measured contact angle would change inducing change of the interfacial energy in consideration. Young's model also neglects a number of factors, which in fact may alter the extent of wettability in real surfaces [63]. In real surfaces, the extent of wettability may be influenced by gravitational effects, substrate deformation, chemical inhomogeneity, contaminants present on the surface such as oxide film formation, mixing between the phases involved, and formation of second phases at solid-liquid interfaces or ahead of the spreading front [59, 63]. Because of that, a number of attempts have been made by many investigators to refine the Young's approach [59, 64]. Nevertheless, as has been mentioned, Young's approach had given a useful scientific foundation for wettability, adhesion, and spreading phenomena of a liquid over a substrate surface.

2.2.3 Wettability and Bacterial Attachment

As has been implied in the previous section, wettability and adhesion have an important influence on the bacterial attachment behavior onto surfaces. At the same time, wettability and adhesion are governed by the surface properties, including surface roughness and its combined properties with liquid and vapor phase, which basically can be characterized in terms of contact angle [63, 65]. It has been recognized that surface physical properties, in this regard surface roughness, have an important impact on bacterial attachment. Several attempts have been made by investigators to explain the effect of surface roughness on the bacterial attachment behavior. For example, Wenzel [66] has proposed that the effect of surface roughness on wettability is simply proportional to the surface area and thus to the wettability behavior on that surface. Even this proposition seems to simplify the matters; however, he has given the basic idea on

how to solve the wettability phenomena. This proposition was later elucidated by Johnson and Dettre, who studied contact angle hysteresis of specific geometry on idealized, rough, and real surfaces [67-68]. Their results implied that surface roughness was not the only factor to account for the wettability phenomena. They further suggested that factors such as surface roughness direction and liquid pressure on the surface, which might increase the spreading of the liquid according to the surface roughness direction, also need to be considered. In this case, liquid pressure parallel to the surface roughness direction will reduce the contact angle and enhance the liquid spreading and thus the wettability. In contrast, perpendicular to the surface roughness direction, the local contact angle changes as a liquid spreads over a surface and a series of metastable contact angles are established, thus results in a barrier to further spreading [67-68].

In terms of biological decontamination, the effects of surface roughness are particularly interesting, especially in relation to the adhesion and wettability phenomena of bio-contaminant/bacterial attachment. As has been mentioned previously, a low interfacial energy between liquid and solid give the implication of higher wettability and thus promotes wetting. In this case, when a drop of liquid containing bacteria spreads over a surface, surfaces of higher wettability will distribute the bacteria suspension over larger area than that of the surface of lower wettability. Therefore, surface roughness would affect the decontamination process according to which bacteria attach to that surface. In this regard, physical and chemical properties of a surface at one side and bacterial properties on the other side will have a big impact on the bacterial attachment and thus to the decontamination process that needs to be performed. On the other hand, these two factors need to be considered carefully in designing an effective

17

decontamination process. In this regard, Rogers *et al*. has found that different surface properties result in different viability of bacterial cells attached to surfaces [69]. Even though Rogers' work on different surface properties focused on differences in the materials used, it is likely that attachment of bacterial cells to the different surface properties of the same materials still affect their viability during decontamination because of different mechanisms and/or strength of the bond between bacterial cells and surface as has been mentioned earlier.

2.3   Decontamination Technology

Decontamination[2] may be defined as the destruction or complete elimination of any form of harm contaminants from a material, environment, and/or area under consideration to a safe level. Decontamination has been developed as a new discipline since Charles Chamberland invented the steam autoclave in 1879 [70]. Since then, much effort has been made by many researchers to improve the decontamination technology so it can be used for many specific purposes such as in military, medical and health care facility, and food industry [71, 72]. Several decontamination technologies, especially in the area of pharmaceutical, medical, food technology, and packaging, have been developed and are available commercially in the market nowadays. However, there is no decontamination technology that is specifically built for the civilian aircraft available up to the present time. At the same time, there is an urgent need in developing decontamination technology for civilian aircraft, especially with the lately elevated

---

[2] In many publications, the terms of decontamination, sterilization, sanitization, and disinfection are often considered from different point of perspective and thus defined differently. In this dissertation, however, all of these terminologies are referred to as decontamination.

tension of terrorist activities and the ongoing threat of epidemic and/or pandemic in which civil aviation would likely represent a key potential vector.

The available decontamination technologies in the market nowadays can be divided into several categories: physical processes such as heat and ionizing radiation, physicochemical processes such as steam and glow-discharge plasma, and chemical processes such as hydrogen peroxide and chlorine dioxide [72-77]. Other methods use combination of the different processes to achieve a synergetic effect, such as combination of low-temperature steam and formaldehyde or combination of chemical and thermal processes [73]. All of these categories, in general, are based on the characteristics of the decontamination process and response of decontaminant agents with bio-contaminants. Among these categories, the most promising candidate for the civilian aircraft decontamination is a chemical method. The main reason for this is that the other processes most likely cannot be used for the purposes of aircraft decontamination because of their incompatibility issues. For example, physical processes involve thermal or ionizing radiation. In thermal decontamination process, the temperatures for moist heat and dry heat need to be 121-134°C and 160-180°C respectively [73]. This range of temperatures would likely be not suitable to be used in aircraft, especially the heat involving moisture, because it would damage the electronic devices within aircraft. In the case of ionizing radiation, the method involves generating of radiation for the decontamination process. For example, γ-rays use radioactive isotope or high speed electron beam as a source of radiation [74]. It would be impractical, if not impossible, to generate the source of radiation to be used for such a large aircraft fuselage. This physical process is usually used as decontamination method in small product designs, food

packaging, and pharmaceutical or medical products. One of the methods in physicochemical processes involves generating a plasma from a chemical that is used for decontamination process [75]. In this case, to achieve a low temperature plasma, the enclosure needs to be in high vacuum; a process that would be impossible to achieve with a large fuselage aircraft. In the chemical methods, however, not all of the processes can be applied for aircraft decontamination purpose. Many of them are either too toxic and environmentally unsafe or too aggressive in terms of materials compatibility. In this case only the methods that are compatible with the aircraft structure and systems, without compromising safety and health in any way, can be selected and tested for further evaluation and implementation. Thus, the challenge of selecting a decontamination method requires a compromise between materials compatibility and biocidal activities of a decontaminant agent.

Several decontamination methods that are based on chemical processes and their process selection for the purpose of aircraft decontamination are discussed in the following section. The discussion will also include efficacy, affordability, and materials compatibility issues on the available chemical decontamination technologies that can be applied on civilian aircraft.

2.3.1 Chemical Methods for Decontamination

As was noted above, the potential candidate to be used for the purpose of civilian aircraft decontamination is the chemical method. As the matter of fact, the use of chemicals as decontaminant agents, which are known to have biocidal effect to the bio-contaminants, has been started long time ago even before the Federal Insecticide, Fungicide, and Rodenticide Act (FIFRA) was enacted in 1947 [78]. FIFRA, administered

by the Environmental Protection Agency (EPA), is a law that provides federal control over the constituents and use of any chemicals used as pesticides, and thus any decontaminant agents, in the United States [79]. In this regard, any chemicals to be used in the decontamination process need to follow this regulation. Up to the present time, chemicals are still widely used as decontaminant agents for many purposes [80].

The chemical methods for decontamination are basically based on either reaction of alkylating agents or oxidative compounds with the bio-contaminants [75]. Several methods involving chemicals as decontaminant agents also have been used for a long time in pharmaceutical, medical or healthcare facilities, and in the food industry. The chemicals of consideration include ethylene oxide, peracetic acid, chlorine dioxide, hydrogen peroxide, and formaldehyde [81-82].

2.3.2   Process Selection

There is no decontamination technology that is specifically designed for civilian aircraft available up to the present time. At the same time, there is an urgent need for using this technology because civilian aircraft could become a target of bioterrorist activities or due to the continuing threat of epidemic and/or pandemic. In this regard, if an aircraft becomes contaminated with a bio-contaminant from a terrorist attack or pandemic virus from a disease outbreak, decontamination is the only way to neutralize the incident. For example, if an aircraft becomes contaminated via either a deliberate terrorist activity or an outbreak, the worst possibility is just to dispose that aircraft. Yet, there is still a need to neutralize or to decontaminate the aircraft before disassembling the aircraft so the bio-contaminant will not spread, or at least the bio-contaminant will not harm people working with the aircraft. In case of numerous aircraft becoming

contaminated, disposing of the aircraft would not likely be an option either in terms of financial considerations or availability of numerous replacement aircraft in a short time [83]. Hence, the primary question that needs to be answered is how to decontaminate it within a reasonable time, in a financially viable manner and without compromising safety and health in any way.

There are several methods involving chemical agents that have been used for microbial decontamination in the area of pharmaceutical and medical industry for a long time. These available methods can be modified for use in civilian aircraft instead of building the decontamination technology from the scratch. For the chemical agents, the selections firstly would be based on the possible choices of what is legal according to U.S. Environmental Protection Agency (EPA), under Section 18 of the Federal Insecticide, Fungicide and Rodenticide Act (FIFRA) [84]. In this case, several chemical decontaminants are already available and have been used for specific use, i.e. for anthrax spore decontamination, such as ethylene oxide, peracetic acid, chlorine dioxide, hydrogen peroxide, and formaldehyde [85]. Unfortunately, most of these chemicals, except for the hydrogen peroxide, are either too toxic and environmentally unsafe or appear too aggressive in terms of materials compatibility to be used for aircraft decontamination purpose. Because of that, hydrogen peroxide delivered in the vapor phase [86], appears to be the most promising potential candidate to find application in civilian aircraft decontamination [83]. The reasons being are because of its excellent biocidal effect, especially in the vapor phase, and most importantly it is environmentally safe. Other advantages and disadvantages of hydrogen peroxide use can be found in sections 2.4.1,

22

Advantages of Vapor Phase Hydrogen Peroxide, and 2.4.2, Limitations of Vapor Phase Hydrogen Peroxide, respectively.

Several methods have been developed by several companies in order to deliver the hydrogen peroxide in the form of vapor phase. Most of them use the same principle of an isolator. An isolator is defined as a confined room which has a physical barrier preventing contact from outside contamination [87]. Two of those isolators are vaporized hydrogen peroxide from Steris Corporation with their product of VHP generator [71] and hydrogen peroxide vapor from Bioquell Inc. with their product the HPV generator [88]. The main difference between these two systems is the relative humidity (RH) prior to generating the vapor phase of hydrogen peroxide. The Steris VHP generator maintains a low humidity in the enclosure, i.e. below 30% RH at the start of fumigation, in an effort to keep the peroxide in the vapor phase and so to improve penetration of substrate surfaces [71]. Bioquell HPV generator, on the other hand, permits higher RH values in an attempt to achieve "micro-condensation" of a microscopic film of hydrogen peroxide over the surface to be decontaminated [88]. In this dissertation, however, all of the work was performed using the Steris VHP generator, although it is possible that at least some of the results may also be applicable to HPV.

2.3.3   Efficacy

In this dissertation, efficacy is defined as the ability of decontaminant agents through a decontamination process to reduce biological and/or chemical contaminants to a safe or assurance level without causing any degradation or detrimental effect to the aircraft structural materials and systems. A safe level is characterized as a circumstance in which the decontamination process renders the contaminant agents to a condition

where it would be of no harm to passengers entering the aircraft on the subsequent flight [89].

In a specific terminology, the efficacy of a chemical used as a decontaminant agent is usually expressed in terms of either $\log_{10}$ kills or D-values [90]. A one $\log_{10}$ kill is a term expressed to represents 90 percent efficiency of reduction or killing a contaminant population. As a reference, the criterion used in the sanitizer efficiency test as applied in the food industry is 5 $\log_{10}$, in which decontamination process will kill 99.999% in the number of *Escherichia coli* or *Staphylococcus aureus* bacteria within 30 seconds after application at 20°C [91]. Another criterion is the standard quantitative carrier test (QCT) method from ASTM International [92], which stipulates a performance of 6 $\log_{10}$ reduction or 99.9999% in the viability of a bacteria population. A D-value, on the other hand, is a term use to express the contact time required to achieve a one $\log_{10}$ kill or 90 percent efficiency. In this case, a short contact time[3] D-value is desirable [71].

In developing the efficacy standard for civilian aircraft decontamination process, in this work, the first consideration would be factors that affect the main process such as operational cycle and ambient environment within the aircraft cabin. The next consideration includes the presence of porous materials such as textiles and foams, surface roughness, and possibility of biofilm formation on the metallic surfaces. As a starting point for this efficacy development, data for any given agent that have been published or reported in the literature was sought and considered. But because not all such data are available, the efficacy for aircraft decontamination, in this dissertation, is

---

[3] For a short contact time, it is assumed that there is a linear relationship between $\log_{10}$ kill and time, which may or may not occur in practice.

then defined as being capable to render 8 $\log_{10}$ reductions[4] of a bacteria population within a reasonable time and manner. This efficacy in fact has exceeded the sanitizer efficacy test of 5 $\log_{10}$ reductions or 6 $\log_{10}$ reductions as used in the standard QCT from ASTM International. However, there is actually still the ongoing question about "How clean is clean enough?" [93]; and thus the criteria used in this killing efficiency are still debatable.

2.3.4   Affordability

In this term, affordability refers to a determination in which the decontamination cycles process is practical to deliver within financial framework of the airliner industry. Implementation of practicality is basically a function of selected technology and operator consideration, while financial aspects loop back to the efficacy and economically realistic within airliner industry acceptance. Based on the survey by Gale *et al*. [89], financial consideration would likely be more stressed in terms of routine activity instead of incidental decontamination. In terms of incident response or emergency use, as has been mentioned earlier, if an aircraft becomes contaminated by either a deliberate terrorist activity or due to disease outbreak, the cost consideration would be which one the most cost effective; disposing the aircraft or decontaminating it. However, consideration of disposing would not be an option if it were necessary to scrap numerous aircraft. Thus, it is likely that there would be little financial option in the case of emergency use but to proceed with decontamination. For routine decontamination activities, the financial aspect would be significant and need to be considered in terms of operator considerations,

---

[4] ACER's work in the field used a reduction of 6 $\log_{10}$ metal backed biological indicators (BIs) in determining the viability of bacteria population [89].

including required operator skill and how to achieve the necessary level of skill for the operator; assurance level in terms of how thorough the decontamination needs to be carried out; and the total time needed to perform the decontamination process, including cycle time and time needed for post-operational cleanup procedures. In this regard, capital cost per unit would decrease when production volumes increase, while operational cost per cycle would seem to change somewhat with process equipment parameters, which is in fact influenced by operator requirements in terms of efficacy and assurance level determination [89].

2.3.5   Materials Compatibility

As surfaces of all aircraft structural materials and systems will be exposed to the decontaminant agent, in this case vapor phase of hydrogen peroxide, during the decontamination process, the compatibility issues between the decontaminant agent and the aircraft structural materials need to be examined. In this context, compatibility issues will be referred to generally as materials compatibility, which is a measure of how aircraft structural materials or systems would stand up to the exposure of a decontaminant agent with no significant changes in physical or chemical properties. The physical consideration of this materials compatibility is measured in terms of microstructure and mechanical properties, while chemical properties is measured in terms of chemical composition changes of the aircraft structural materials. If aircraft structural materials properties are greatly affected by the decontaminant agent, either physical or chemical properties, the decontaminant agent is then considered incompatible and will not be tested and evaluated any further.

In developing the test case for materials compatibility, the starting point is from the fact that the structural aircraft are complex and consist of a number of metallic and non-metallic materials [36, 37, 94]. The first task is then to classify these materials in terms of what is important as an entire unit and would be likely the most affected by the decontamination process. In this regard, the consideration would be aircraft as a complete unit such as structure, frame, stringers, fuselage, wings, and the systems inside the cabin such as wires, electronic devices, and all of the accessories within the aircraft. However, there will be a long list of these materials. Thus, as the initial point, the selection will be down to the main structural aircraft materials, i.e. the materials that are used to build the skin, frame, longerons or stringers, ribs, and wings. Up to the present time, these parts still consist of metallic materials, mostly aluminum alloys. For that reason, the test case within this dissertation will be only on those metallic structural materials; in this regard the materials were represented by 2024-T3 and 7075-T6, with the addition of austenitic stainless steel 304 as used in lavatory and galley surfaces.

Initial data on the relative compatibility issues of various materials with hydrogen peroxide can be obtained from several sources [95, 96]. It needs to be stressed that these data are not sufficient, especially in terms of whole effect of decontamination and its subsequent impact on the materials properties due to the different, and often very crude, method in determining the compatibility issues and purposes. Data from these sources, however, can be used as initial guidelines since published references in this subject are very limited.

In order to determine materials compatibility with the decontaminant agent, in this case aircraft metallic structural materials and hydrogen peroxide respectively, the

following data are needed as the starting point [89]. The first is the immediate effect of decontaminant agent on the material's structure properties. This immediate effect can be evaluated by performing a tensile testing after exposure, which will be sufficient to reveal immediate loss on mechanical properties such as strength or ductility. However this would not be enough to reveal subtle, incipient damage that might induce subsequent degradation in materials performance. Thus, microstructure and mechanical investigation of the aircraft structural materials by using a standard method such as ASTM are needed after decontamination process has been performed. The second is the effect of multiple decontamination cycles on the material's properties. Single aircraft might encounter multiple decontamination cycles in case it needs to do numerous flights to a contaminated region, or at least to reduce the possibility of becoming a vector for spreading the disease concerned. The data needed would be the effect of cumulative damage on the aircraft structural materials after numerous decontamination processes. There are several more data needed in order to completely determine the materials compatibility after decontamination on the aircraft metallic structural materials such as fatigue strength, highly accelerated life testing (HALT), and subsequent corrosion and environmental effects; however these first two tests would likely be sufficient as the initial point. If these first two tests show an incompatibility issue, then there will be no point in pursuing further measurements.

In classifying the materials compatibility criteria, within ACER team perspectives, a change or reduction in any given mechanical materials property of up to 5 percent or more would be regarded as a significant damage [89].

2.4 Hydrogen Peroxide

Liquid hydrogen peroxide has been long use in industrial applications such as bleaching and nonpolluting agents for wastewater treatment [97]. It also has been use for a long time in household applications as an antiseptic. Hydrogen peroxide is a weak acid but one of the strongest oxidizing agents that is commercially available in aqueous solution. The use of this hydrogen peroxide, within the U.S., is controlled under EPA regulation. With the elevated tension of terrorist activities, especially with the spreading of *Bacillus anthracis*, EPA had issued a crisis exemption for the use of hydrogen peroxide as a decontaminant agent on a case-by-case basis [85].

The vapor phase of hydrogen peroxide has been well known to be used in decontaminating medical, pharmaceutical, and biological instruments in healthcare facilities and other medical equipments and products [98-101]. Several works by investigators have also shown that hydrogen peroxide is indeed effective in killing bacteria [98, 101, 102]. The use of hydrogen peroxide vapor by means of an isolator for decontamination was started in the early 1990's [87]. After the introduction of hydrogen peroxide isolator equipment, several publications in the related issues and validation techniques have been published. Following these, the use of vapor phase of hydrogen peroxide by means of an isolator has been developing and is now gaining acceptance for decontamination of larger areas such as rooms and small buildings [103, 104]. In this regard, hydrogen peroxide vapor has been proven to be effective when used for deactivating *Bacillus anthracis* spores employed in the attack at the General Service Administrations' Building in Washington D.C. and the U.S. State Department Mail Facility in Sterling, Virginia, in 2001 [90, 105].

Based on the selection process explained previously, hydrogen peroxide vapor is one of the potential candidates that have been proposed by the ACER team to be used as a decontaminant agent for treating civilian aircraft, and now is being tested and its impact on the aircraft structural materials properties is being evaluated [105]. The results of this work are expected to contribute towards a potential response to bioterrorism and epidemics/pandemics in which civil aviation would likely represent a key vector. Within the framework of ACER goals and objectives, the result of this study is also expected to provide at least part of the answer to the question whether VHP can be used as decontaminant safely in civilian aircraft.

2.4.1 Advantages of Vapor Phase Hydrogen Peroxide

Some advantages of using vapor phase of hydrogen peroxide as a decontaminant agent, for the purpose of civilian aircraft decontamination, are given in the following:

1. Hydrogen peroxide is one of the strongest oxidizing agents that produce free hydroxyl radicals. This free hydroxyl radical attacks essential cell components resulting in an excellent biocidal effect [97, 106].

2. It has been proven that the effectiveness of hydrogen peroxide is increased in the gaseous phase [71, 69] and it is also impractical to deliver in the form of liquid decontaminant to large volume spaces.

3. Hydrogen peroxide has been used as a reliable decontaminating or sterilizing agent in pharmaceutical and medical industry areas for a long time [72].

4. Vapor phase of hydrogen peroxide is a relatively low-temperature decontamination process, thus it would be potentially compatible for flight hardware [106].

5. Vapor phase of hydrogen peroxide easily decomposes into harmless byproducts of water and oxygen after decontamination process has been completed [71].

6. Vapor phase of hydrogen peroxide has been proven to be effective when used in cleaning up *Bacillus anthracis* spores [90, 105].

7. In addition to these, hydrogen peroxide also has been used effectively for neutralizing chemical G agents, such as agent GB [107].

2.4.2 Limitations of Vapor Phase Hydrogen Peroxide

Some limitations of using hydrogen peroxide vapor are given in the following:

1. As an oxidizing agent, hydrogen peroxide will be expected to have a detrimental effect on textiles and fabrics color [97].

2. Pores and highly absorptive materials will absorb hydrogen peroxide vapor leading to a reduction in the VHP concentration or trap the VHP so that it is difficult to remove during subsequent aeration. In addition, trapped, undecomposed peroxide might represent a fire hazard due to its inherent properties as an oxidizing agent. In its application, hence, surfaces must be reasonably clean and dry before the decontamination process [71].

3. Humidity will affect the decontamination process. The higher the humidity, the longer the time needed to achieve $1 \log_{10}$ kill, i.e. 90% of killing efficiency, as less peroxide can be safely injected [71].

4. At low temperatures, the reaction will be relatively slow [107].

5. Up to the present time, unless delivered by using a large generator, it is not possible to decontaminate huge spaces, such as large buildings, at one time [71].

2.5   Selected Aircraft Metallic Materials

Many modern aircraft are designed to be able to move large loads over long distances at subsonic high speed. Aircraft components for this purpose can only be satisfied by materials with a specific combination of high strength and lightweight properties. Because of that modern aircraft are built with complex structures and consist of variety of materials [94, 108]. The best materials for these aircraft components, which have the balance of lightweight and high mechanical strength, are aluminum alloys [36, 37]. Up to the present time, aluminum alloys are still the materials of choice and constitute the biggest proportion of modern aircraft, followed by steel, titanium alloys, and structural composites[5] [94]. Other components within the cabin such as overhead luggage compartments, sidewalls, and ceilings usually consist of lightweight plastics and polymers [109].

Properties of some selected aircraft metallic materials, i.e. aluminum alloys and austenitic stainless steel, are discussed in the following section.

2.5.1   Aluminum and Aluminum Alloys

Pure aluminum has the properties of lightweight and good resistance to corrosion and to environmental effect, but with low mechanical strength. Fortunately, the disadvantageous of being low strength can be overcome by alloying this pure aluminum with some elements of transition, alkali, and/or alkaline earth groups. Some transition elements that can readily form alloys with pure aluminum include copper, zinc, and

---

[5] It needs to be noted that, as development of the composite materials progresses, this is changing since the composite materials is now gaining acceptance widely. Composite materials constitute around 11% and 50% in B-777 and B-787, respectively [94, 108].

manganese, while alkali and alkaline earth that can form alloy with aluminum is lithium and magnesium respectively. These alloying elements, when combined with appropriate thermo-mechanical processing, greatly improve aluminum mechanical properties and increase its usefulness especially as materials of choice for aircraft and rockets applications [110].

In order to give a basic understanding about aluminum and aluminum alloys, in the following section, designation and temper of aluminum alloys, effect of alloying elements on the properties of aluminum alloys, mechanical properties of aluminum alloys, and corrosion of aluminum alloys are given.

2.5.1.1   Aluminum Designations and Tempers

Pure aluminum is highly ductile, but has a low strength. One of the methods to increase the strength of aluminum alloys is by alloying it with some other elements. Further improvements, depending upon composition, are possible through a cold working and/or heat treatment [111]. Different alloying elements and heat treatments would result in different mechanical properties and/or strength of the alloys. Because of that, there will be many varieties of aluminum alloys depending upon the alloying elements and/or their metallurgical conditions and heat treatments. To distinguish between these aluminum alloy varieties, several designation systems have been created by several associations and/or companies that gives the alloys a specific nomenclature in a meaningful manner. In the U.S., aluminum alloys designation and tempers are created by the Aluminum Association [112].

Basically, the systems differentiate aluminum alloys designation and tempers according to the sequences of major alloying elements, heat treatments, and other

metallurgical condition that have been performed to the alloys. The systems also distinguish between wrought, casting, and experimental aluminum alloys. The aluminum designation and temper systems developed by the Aluminum Association are explained in the following [111-114].

In general, aluminum alloy designations consist of four digit numbers. The first digit of designations indicates major alloying elements and the second digit indicates modifications of the major alloying elements in impurity limits. In this regard, if there is no special control on the individual impurities then the second digit will be written as zero. Otherwise, numbers from 1 through 9, indicate particular control of one or more individual impurities. The last two digits, which are assigned as needed, indicate specific minimum aluminum content for pure aluminum (first series), while for other series are used only to identify the different alloys in the group.

These four digit nomenclatures are used for both wrought aluminum alloys and casting aluminum alloys. The difference is stressed for casting aluminum alloys, in which the fourth digit is separated from the first three digits by a decimal point that indicates their form, in this regard either casting or ingot. Other nomenclature is for experimental aluminum alloys. The experimental aluminum alloy designations also use this four digit system; however the designations are prefixed by the letter X. These experimental designations only prevail during the investigational time. Once the alloys become standard and available in the market, the X number will be dropped and the nomenclature follows the regular designation system.

For wrought aluminum alloys in these designation systems, the first series, usually written in the form of 1xxx, has no major alloying element. Other series from

2xxx, 3xxx, 4xxx, 5xxx, 6xxx, and 7xxx, each of them has major alloying elements of copper, manganese, silicon, magnesium, magnesium and silicon, and zinc respectively. Series of 8xxx is used for various major alloying elements other than the previous alloying elements such as tin, lithium, and or iron, whereas 9xxx series is currently unused and reserved for future alloys. For casting aluminum alloys, the major alloying elements are the same such for wrought aluminum alloys except for 3xx.x, 6xx.x, and 8xx.x series. In this regard, 3xx.x has the major elements of silicon and other two elements of copper and magnesium, 6xx.x is unused series, whilst 8xx.x has a major element of tin.

Aluminum alloy tempers are written following alloy designations and are usually separated from the alloy designations by a dash. In general, basic temper designations consist of five individual capital letters as explained in the following. The letters F indicates as fabricated; O for annealed; H for strain-hardened; W for unstable solution heat-treated, which is applicable only to the alloys whose strength naturally changes at room temperature; and T for stable thermally-treated, sometimes with additional strain-hardening. These temper designations are further differentiated between non heat-treatable aluminum alloys and heat-treatable aluminum alloys. The H temper is used for non heat-treatable aluminum alloys, while F, O, and T are used for heat-treatable aluminum alloys. The H and T tempers are usually followed by one or more digits to indicate their particular method used to produce the tempers.

2.5.1.2   Effects of Alloying Elements

Alloying elements are usually added in certain amount to improve aluminum mechanical properties. In general, alloying elements increase the strength of aluminum

alloys through three separate mechanisms, i.e. solid solution hardening, dispersion hardening, and precipitation hardening or also called age-hardening [113]. These strengthening mechanisms basically differ in the way they were formed and depend on the alloying elements and the thermo-mechanical condition involved during the alloying process. Some impurities also will give impact on the alloys properties.

Several alloying elements and their effect on aluminum alloys properties are given in the following [111-115].

1. Copper is one of the transition metals and is one of the most important alloying elements in aluminum alloys, either as a major addition such as in 2xxx series or as an additional alloying element in other families of aluminum alloys. It considerably improves the strength of aluminum through age-hardening characteristics by forming metastable phases of θ" and θ'. Depending upon the alloy contents, the maximum strength of the alloy usually will be also influenced by the presence of other elements.

2. Manganese is one of the transition metals. Manganese actually has limited solid solubility in aluminum, but even with the amount of only up to 1% forms an important 3xxx series of aluminum alloys. Manganese forms either solid solution or fine precipitated intermetallic phase, such as Al_6Mn, in aluminum alloys and thus increases strength of the alloys.

3. Silicon is in group IV of periodic system. It is a major element in 4xxx series of wrought aluminum alloys, and along with magnesium forms important 6xxx series of aluminum alloys. Basically silicon lowers the melting point while at the same time increases the fluidity and moderate strength of aluminum alloys. In aluminum alloy, silicon forms a very small, coherent cluster in solid solution. Furthermore, from this

cluster, silicon transforms into diamond structure precipitates in the form of rods or triangular plates on several planes of the aluminum matrix. These precipitates improve the strength of aluminum.

4. Magnesium is in alkaline earth group. It is also one of the important alloying elements in aluminum alloys. Magnesium is a major element in 5xxx series of aluminum alloys. In this series, the strength is developed mainly through a work hardening. Along with silicon, magnesium forms important 6xxx series of aluminum alloys. Due to formation of rod-shaped precipitates of β'-phase, magnesium provides significant strengthening and improvement of the work-hardening characteristics of aluminum alloys, especially with the presence of other constituents such as copper and zinc.

5. Zinc is one of the transition metals and is a major element in 7xxx series of aluminum alloys. The addition of zinc itself into aluminum alloys has the drawback of hot-cracking, especially in aluminum casting. However, along with magnesium, zinc develops improvement in the strength of the alloy system through the precipitation of η'-phase. The addition of copper to the aluminum-zinc-magnesium system greatly improves mechanical properties, although with the price of corrosion resistance. But this can be overcome by the addition of small amount of chromium and zirconium.

6. Other alloying elements for different aluminum alloys properties include iron, lithium, tin, and titanium. Aluminum alloys containing these alloying elements fall into 8xxx series of aluminum alloys when these alloying elements are in the greatest proportion, but when these alloying elements are in smaller proportion than other elements, the designations follow the elements with the greatest proportion. Other

alloying elements in small amount include nickel, chromium, zirconium, indium, and lead. Sometimes these elements are found as trace elements and regarded as impurities from the aluminum process. In the case of chromium and zirconium, in small amount is needed for 7xxx aluminum alloy series in order to improve their corrosion resistance.

2.5.1.3   Mechanical Properties of Aluminum Alloys

Mechanical properties of aluminum alloys can be improved in several ways, but in general this can be done through a process of solid-solution hardening, grain-boundary hardening, work or strain hardening, aging or precipitation hardening, and/or a combination of these processes [113]. The basic principles of these methods are given in the following.

Strengthening from solid-solution comes from the fact that solute and solvent atoms may have differences in atomic size. The differences in this atomic size might cause misfit and induce elastic interaction between strain fields of the solute atoms and dislocations present in the lattice such as edge and screw dislocations [116]. In this regard, solute atoms act to hinder dislocation motion, and thus will affect edge and screw dislocations to some extents contributing to a solid solution strengthening [117].

In grain-boundary strengthening, the grain boundary acts as a barrier for dislocations. Most of the time, a dislocation cannot cross a grain boundary because of slip plane orientation and direction differences between the two neighboring grains; instead the dislocation will pile up near the grain boundary [117]. Hall and Petch have shown that grains size plays a major role in the deformation and thus in strengthening the alloys according to [118-120]:

$$\sigma_y = \sigma_f + \frac{k}{\sqrt{d}}$$

Equation 3

where:

σ_y = yield strength

σ_f = frictional stress

k = constant

d = average grain size

On the basis of this equation, the smaller the grain size the smaller the distance that can be travelled by a dislocation before encountering a grain boundary, and thus the more barriers that will hinder the dislocation resulting in higher strength. However, this assumption does not work well for extremely small grain size because it predicts unrealistic strengths [121]. In this case, key consideration is grain diameter versus grain boundary area on which dislocations pile up, and the yield strength (σ_y) is given by Li's equation [119]:

$$\sigma_y = \sigma_f + \alpha G b \sqrt{\rho}$$

Equation 4

where:

σ_f = frictional stress

α = constant, in the order of 0.4

G = shear modulus

b = Burgers vector

ρ = dislocation density

Strain or work hardening is a strengthening mechanism that results from an increase in dislocation density due to dislocation-dislocation interactions [121]. In this case, deformation occurs by the motion of existing dislocations and/or by the creation of new dislocations through mechanisms of dislocation multiplication, such as a Frank-Read source or a Bardeen-Herring climb source [117]. During the deformation process, the dislocation density increases. This increasing in dislocation density, along with dislocation-dislocation interactions, causes further deformation to become more difficult thus strengthening the alloy through strain hardening. The common way to achieve this strain hardening is by applying a cold-work such as in cold-rolled and/or cold-drawn to the alloys. Solute atoms from alloying elements in aluminum alloys can also enhance strain hardening through a process of precipitation during deformation, increasing the rate of dislocation multiplication, and/or reducing the rate of recovery [122].

Precipitation hardening occurs when the solute concentration in the alloys exceeds the limit of solubility [121]. Precipitation hardening is achieved by a heat treatment process, which involves the process of solution treatment at high temperature followed by a rapid quench to room temperature to form a supersaturated solid solution (SSSS). The

40

strength can then be increased by the aging process, which may involve several stages including formation of the metastable phases of Guinier-Preston (GP) zones, named after the scientists who separately revealed them [123, 124]. The effect of precipitation hardening, and thus the strength of the alloy, depends on several parameters such as time, alloying elements involved, and temperature of the precipitation heat treatment [125]. In Al-Cu alloys for example, precipitates other than equilibrium of θ-phase ($CuAl_2$) can be produced during the aging process. In this regard, three metastable precipitates of GP-I, GP-II (θ"-phase), and θ'-phase can be produced in addition to the stable θ-phase. In general, the process takes place according to the sequence of GP-I zone $\rightarrow$ GP-II zone (θ"-phase) $\rightarrow$ θ'-phase $\rightarrow$ θ-phase [126]. GP zones of the first kind (GP-I) are platelike arrays of copper layers oriented parallel to {100} planes in the aluminum matrix, while GP zones of the second kind (GP-II) consist of an ordered tetragonal structure of aluminum and copper layers arrangements [125, 126]. During deformation, depending on the size, spacing, and degree of coherency, these precipitates are either sheared or looped and bypassed by the dislocation motion. This mechanism of dislocation motion is called Orowan bypass [114, 121, 127].

2.5.1.4   Corrosion of Aluminum Alloys

In general, corrosion is a chemical process due to interaction between a metal and its environment that may cause deterioration to the properties of the metal. Pure aluminum has low strength but has high corrosion resistance due to its continuous oxide film on the surface. This oxide film obstructs further reaction of aluminum with environment as long as the film covers its surface; otherwise corrosion will take place

41

[112]. As has been mentioned previously, to improve mechanical properties of pure aluminum, especially for an application that needs high strength components; other elements are added to pure aluminum. The addition of these alloying elements followed by heat treatments, in principle, will promote formation of solid solution and/or small solid hard precipitate to the alloys but in the form of heterogeneous microstructure. Thus, the heterogeneous microstructures are intentionally developed to achieve the high strength and especially to optimize mechanical properties of the alloys. Unfortunately, this heterogeneous microstructure in some extent might interrupt the oxide film protection on surface of the aluminum, and thus renders the alloys vulnerable to localized attack. This vulnerability comes from the fact that microflaws due to the nature and discontinuity of oxide scale in the surface oxide film might exist, especially within the heterogeneous microstructure. Heterogeneous microstructure also presents galvanic issues between matrix and precipitates. In this regard, potential difference between intermetallic particles and the matrix might also exist, which causes galvanic couple, and further renders the alloys to be more susceptible to localized corrosions such as pitting and intergranular corrosions, particularly when the alloys are exposed to environment during service. It has also been found that transport, such as proton migration, through the oxide film induces deterioration of the oxide film and thus would also render the alloys to become vulnerable to corrosion attack [128-130]. This corrosion would result in deterioration and damaging effect to the properties of aluminum alloys, especially for load bearing components [131].

Several types of corrosion might occur to aluminum alloys, depending on the condition of the alloys and environments where the alloys are being used. In general,

corrosion of aluminum alloys may be divided into uniform corrosion, localized corrosion, and combination with other processes such as environmentally assisted corrosion and/or mechanically assisted corrosion [111]. The first type, uniform corrosion of aluminum alloys, occurs in the presence of acidic or alkaline solutions and/or relatively high chloride concentration. The presence of acidic or alkaline solutions and/or high chloride concentration basically will destroy aluminum oxide film on the surface and thus uniform attack will form on the aluminum alloys surface [131]. Localized corrosion can be divided further into several sub types of pitting, intergranular, crevice, filiform, galvanic, exfoliation, and biologically induced corrosion [111, 132]. The other forms of aluminum alloys corrosions are environmentally assisted and/or mechanically assisted corrosions. The corrosion forms include abrasion, erosion, or fretting corrosions for mechanically assisted corrosions, while for environmentally assisted corrosions, the forms include stress corrosion cracking (SCC) and corrosion fatigue [131, 133].

Localized corrosions have always been troublesome for aluminum alloys used in structural materials, particularly in the form of intergranular and pitting corrosions. It has been found that intergranular and pitting corrosions occur in commercial aluminum alloys used in aircraft such as 2024 and 7075 aluminum alloys [112, 134].

While intergranular corrosion occurs at the grain boundary, pitting mostly occurs on the surface and/or at the intermetallic constituent particles [112, 135]. Intergranular corrosion takes place when large intermetallic precipitates form at the grain boundary from a supersaturated solid solution. Formation of these large intermetallic precipitates causes copper-depleted regions at the adjacent area close to the grain boundary. Large intermetallic precipitates and copper-depleted regions then develop a potential difference

43

resulting in galvanic processes and further pronounce intergranular corrosions [112]. Although the initial localized attack might be minute and regarded as least damaging, however the rates of attack can be significant and lead to subsequent stress corrosion cracking [132].

Pitting corrosion occurs when the oxide film that forms on the surface of aluminum alloys breaks down locally causing subsequent dissolution of the substrate material [112, 136]. The dissolution of substrate materials leads the creation of small holes on the surface of aluminum alloys. This hole has a tendency to bury in the alloy matrix resulting in lacking of oxygen and become anodic. At the same time, areas with excess of oxygen become susceptible to cathodic reduction. These two areas then develop an electrochemical potential leading to pitting corrosion; see the sketch in Figure 2 for more detail. The primary cause of oxide film breakdown can be from environmental effects such as high concentration of chlorides and/or from electrochemical potential between the intermetallic constituent particles of aluminum alloys [137, 138]. Furthermore, even a single pit, if it were on a critical point, will cause a great deal of damage and result in premature catastrophic failure [112].
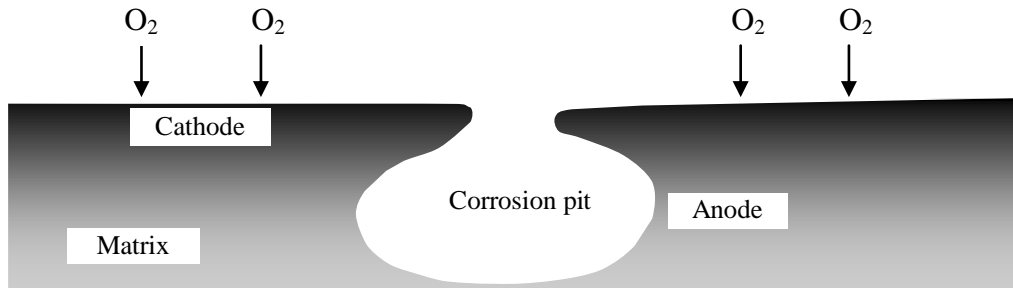
Figure 2–Illustration of corrosion pit buried into the mass of the metal, not drawn to scale.

Pitting corrosion also has been found to occur at intermetallic constituent particles in aluminum alloys [137-145]. Gao *et al.* [137] have investigated pitting corrosion on 2024-T3 and 7075-T6 aluminum alloys and further divided the constituent particles into two types, i.e. type A for anodic particles and type C for cathodic particles. Anodic particles tend to dissolve preferentially while cathodic particles tend to promote dissolution of the neighboring matrix. For 2024-T3 aluminum alloy, anodic particles are those that emphasize the content of Mg with an Al_2CuMg nominal composition. Whereas cathodic particles are those that emphasize the content of Fe and Mn with more complex and varying compositions, but they are principally $(Cu,Mn,Fe)Al_6$ or Cu_2FeAl_2 [137]. These two types of intermetallic particles, especially Al_2CuMg particles (also known as S phase), are the main source for pitting corrosion on 2024-T3 aluminum alloy [139, 140]. For 7075-T6 aluminum alloy, anodic particles are those that emphasize the content of Mg such as $MgZn_2$; whereas cathodic particles are those that emphasize the content of Fe and Mn [138, 145] such as Al_7Cu_2Fe [136].

Because the particles are important in promoting corrosion, characterization of their crystal structure, chemical composition, and electrochemical behavior is needed to better understand the particle-corrosion relationship in commercial aluminum alloys. To provide a more complete understanding of the interactions of constituent particles and the matrix during corrosion, which is usually initiated by pitting-type corrosion, it will be useful to use analytical electron microscopy (AEM) technique [146]. This technique can be used to study the major constituent particles in aluminum alloys, both structurally and chemically. The phases are determined according to the crystal structural information from convergent beam electron diffraction (CBED) and selected area electron diffraction

46

(SAD) analyses. The chemical compositions of the particles can be analyzed by using EDS and are then compared with the stoichiometric compositions of known compounds [147]. By using this technique, Gao *et al.* [137] have been successfully identified crystallographic properties of several particles in 2024-T3 and 7075-T6 aluminum alloys (see Table I). Some other particles and or phases, including their stoichiometric composition and structure, however, are still unclear and require further study [137, 138]. This technique will be also useful to determine the nature and extent of their interactions following exposure to hydrogen peroxide. However, this work falls beyond the scope of the present dissertation, which focuses on the specific effect of decontamination on aviation materials, rather than on the general mechanisms of corrosion of aluminum alloys.

Table I. Crystallographic properties of particles found on 2024-T3 and 7075-T6 aluminum alloys that have been identified so far [137, 138]. The crystallographic parameters of a, b, and c are in pm, whilst α is in degree.

Alloys	Particles	Structure	a (pm)	b (pm)	c (pm)	α (deg)
2024-T3	Al_2CuMg	Orthorhombic	431	956	747	90
	Al_2Cu	Tetragonal	607		488	90
	$(Fe,Mn)_x\text{-}Si(Al,Cu)_y^*$	Rhombohedral	1,598			75
7075-T6	$Al_{23}CuFe_4$	Orthorhombic	759	666	884	90
	SiO_2	Amorphous				

* Composition of this particle does not conform to any of the known compounds; hence further study is needed.

2.5.2   2024 and 7075 Aluminum Alloys

2024 aluminum alloy has a major alloying element of copper with a concentration of up to 4.9 wt.%   [148]. Other alloying elements include silicon, iron, manganese, magnesium, chromium, and zinc. This alloy was developed in 1931 due to the increasing demand in aircraft industry and was the first exclusively used to build the DC-3. This was then followed by more general use by Boeing in the late 1970s. Nowadays, the most common application of this alloy, beside aircraft, is for other aerospace and industrial applications needing the lightweight and high strength components [149]. The work that is still ongoing about this alloy in today research is due to the vulnerability of this alloy to corrosion, especially to localized corrosion. The susceptibility of this alloy to corrosion is due to the nature and discontinuity of oxide scale in the surface as has been explained in the previous sections. For that reason, many efforts have been made by investigators to increase the corrosion resistance of 2024 without losing its high strength [145, 150].

7075 aluminum alloy has a major alloying element of zinc with the concentration of up to 6.1 wt.%   [148]. Some other alloying elements include silicon, iron, copper, manganese, magnesium, chromium, and titanium. This alloy was first introduced in Germany in 1920s and then was further developed in the U.S. for use in airplane wings. Like 2024 aluminum alloy, 7075 aluminum alloys is also susceptible to localized corrosion; however, compared to 2024 aluminum alloy, this alloy has more corrosion resistance due to its chromium content while at the same time containing less copper. Nowadays, the main use of this alloy is for aircraft application including circumferential frames, stringers, lower wing spars, and upper wing skins.

2.5.3   Other Metallic Materials Used in Airframes and Cabin Fittings

There are several metals alloys used in aircraft materials for specific use other than aluminum alloys mentioned in the previous sections. One of them is austenitic stainless steel 304 as used in lavatory and galley surfaces. Stainless steels are basically ferrous-base alloys with a minimum content of 10% chromium [151]. This minimum content of chromium is the amount needed to prevent the corrosion of the alloys, which is basically where the term of stainless comes from. There are actually many types of stainless steels depending on their compositions, treatments, and/or metallurgical condition. Austenitic stainless steel can be divided into two types: chromium-nickel based alloys and chromium-manganese-nitrogen based alloys. Austenitic stainless steel 304 belongs to austenitic chromium-nickel based stainless steel group with a chromium content of up to 20 wt.%. Other alloying elements include carbon, manganese, silicon, phosphor, sulfur, and nickel [152]. It has high ductility, excellent drawing, forming, and spinning properties. In aircraft, as has been mentioned previously, austenitic stainless steel 304 is used for lavatory and galley surface applications. Other common uses are in the applications of tubing, flexible metal hose, food processing equipment, kitchen sinks, refrigeration equipment, and sanitary fittings [153].

2.6   Copper Dissolution in Hydrogen Peroxide

Copper is one of important alloying elements in aluminum alloys. In 2xxx aluminum alloys, copper is a major element alloying element with concentration of up to 4.9 wt.%. In 7xxx aluminum alloys, copper is one of the alloying elements with the concentration of up to 2.0 wt.%. Several investigators have investigated the dissolution

of pure copper and its properties in several acidic solutions such as sulfuric acid [154, 155], hydrochloric acid [156, 157], and ethylene diamine tetra acetic acid/ethylene diamine (EDTA/EDA) base solutions [158]. Several others have investigated the copper dealloying and or nucleation and growth behaviors in aluminum alloys in the presence of sodium chloride [159-162]. No data have been found, however, to the best of the author's knowledge, about the dissolution of copper or alloys containing copper into hydrogen peroxide solution. To better understand the mechanism involved during the reaction, identification, separation, and kinetic quantification of the reactions are needed. It would be a challenge to resolve all of these problems since most of the processes are complicated, especially when more than apparent rate data are sought. For this reason, copper dissolution rate into hydrogen peroxide is investigated in the present work to help understanding the corrosion process.

The dissolution of a solid is often of great interest for both natural and industrial purposes. Dissolution occurs when the bonding within a solute material breaks down into ions, atoms, or molecules due to heterogeneous process of chemical reactions [163]. The heterogeneous chemical reactions may take place in several stages depending on the reactions involved. However, in general, the reactions involve the processes of detachment of atoms from the solid at the solid-liquid interface and the mass transfer from this interface into the solution. Most of dissolution processes are controlled by the second process, which is basically a diffusion process [164]. From chemical point of view, the chemical reaction kinetics is of great interest, while diffusion control is the usual situation in the majority reactions of industrial importance [165]. However, despite the importance of the reactions, the kinetic theory for diffusion in liquids has not been as

well developed as that for dilute gases, and thus it has been always difficult to give analytical predictions of diffusivities in the dissolution process [166].

The basic diffusion model was firstly enunciated by Fick in 1855 [167]. Fick's model has been used and applied by investigators for solving diffusion problems in many areas. In 1897, Noyes and Whitney developed a diffusion model for a substance that dissolves into its own solution [168]. Noyes and Whitney's model has been applied by many investigators to measure the rate of diffusion of a substance into a solution, and several improvements have been made by several other researchers such as Nernst and Brunner [169, 170] and King [171].

Diffusion model of a plate specimen into a solution can be solved by using a rotating disc/cylinder technique, where a solid sample is rotated in a liquid capable of dissolving the solid. The basic theory for a diffusion of a plate specimen into a liquid comes from an empirical equation [172]:

$$\frac{m}{t} = k(C_s - C_t)A$$

<div align="right">Equation 5</div>

where:

m = amount of the material dissolved

t   = time

k   = constant

C_s = concentration of the saturated solution

C_t = concentration of the solution at time t

A = surface area of the dissolving body

Nernst [172] has shown that, in this empirical theory, the constant k is proportional to D, the diffusion coefficient, or:

$$\frac{m}{t} = D \frac{(C_s - C_t)}{\delta} A$$

Equation 6

where δ is another constant, which represents the thickness of the diffusion layer. Diffusivity of a static solid in a liquid is very small [172]; because of that, the constant need to be resolved in a moving media. The experiment for this purpose can be performed by using a rotating disk. In a rotating disk experiment, in order to obtain the thickness of this diffusion layer, the equations for the tangential, radial, and axial contributions to the fluid flow near the surface of a rotating disk need to be firstly solved by applying a boundary condition. The equation for this model was derived by Cochran

in 1934 [173]. In 1962, Levich [172], with the use of Cochran equations, obtained the equations for boundary layer thickness of a solute species dissolving from a rotating disk:

$$\delta = 0.5 \left(\frac{D}{\nu}\right)^{\frac{1}{3}} \delta_0$$

where:

δ_0 = thickness of hydrodynamic layer, and $\delta \leq \delta_0$

ν = kinematic viscosity

$$\delta_0 = 3.6 \left(\frac{\nu}{\omega}\right)^{\frac{1}{2}}$$

where:

ω = angular velocity

On the basis of powder particles, three diffusion control models have been developed: the cube-root law derived by Hixson and Crowell [167, 174], the two-thirds-root law derived by Higuchi and Hiestand [175, 176], and the square-root law derived by Niebergall *et al.* [177]. Wang and Flanagan [178, 179] have shown that the cube-root

54

model is the most suitable for the long range diffusion when the particle size is much larger than the thickness of the diffusion layer; the two-thirds model is the most suitable for very fine particle; while the square-root model is the most applicable for particulate with different particle size. Nevertheless, the cube-root model has been the most used by many investigators because of its simplicity and applicability to a wide range of dissolution process [180-184]. The cube-root model is also called the surface reaction control shrinking core model and has been widely used in hydrometallurgy processes [185-188]. In this dissertation, the rate of copper dissolution by hydrogen peroxide was calculated by using the cube-root law. In order to use this model, the reaction of copper with hydrogen peroxide is assumed to be homogeneous and isotropic with a constant diffusion layer thickness. It is also assumed that in the solution there will be Cu^+ and/or Cu^{2+}, but these two ions are not differentiated; i.e. the concentration measured is the total concentration from these two ions.

Reaction of copper and hydrogen peroxide is basically an oxidative reaction. According to the table of standard electrode reduction and oxidation, half reactions that involve metallic copper and hydrogen peroxide are as follows [189]:

$$Cu_{(s)} = Cu^{2+}_{(aq)} + 2e^-$$

Equation 9

$$H_2O_{2(aq)} + 2\ H^+_{(aq)} + 2e^- = 2\ H_2O_{(l)}$$
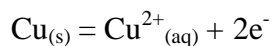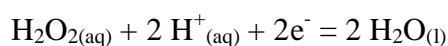
Equation 10

Adding the two half reactions together then gives the overall reaction:

$$Cu_{(s)} + H_2O_{2(aq)} + 2\ H^+{}_{(aq)} = Cu^{2+}{}_{(aq)} + 2\ H_2O_{(l)}$$
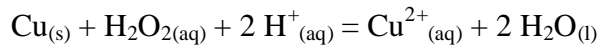
Equation 11

Because the reaction involves powder particles, it is also assumed that the rate of copper diffusion at the particle surface away into the bulk liquid as the controlling step; therefore is proportional to the instantaneous surface area. In this regard, the rate will be given by [180, 185]:

$$\frac{dm}{dt} = -nkA$$

Equation 12

where:

m = mass of the undissolved copper particle

n = number of the particle

k = dissolution rate constant

A = instantaneous surface area

Surface area of a sphere is $4\pi r^2$. Substitution of $4\pi r^2$ into Equation 12 and then solving it by integration gives the straight forward cube-root law [180, 185]:

$$1 - \left(\frac{m_t}{m_0}\right)^{\frac{1}{3}} = \frac{kt}{r_0 \rho}$$

<div align="right">Equation 13</div>

where:

m_0 = total mass of the undissolved particle at time zero

m_t = total mass of the undissolved particle at time t

r_0 = initial size of the particle at time zero

ρ = copper density

    The dissolved copper is measured in terms of Cu^{2+} concentration, in this case the dissolution product based on the reaction in Equation 11. Based on this dissolution product, Equation 13 can be rewritten in the form [181, 185]:

$$\left(1 - \frac{[C]_t}{[C]_\infty}\right)^{\frac{1}{3}} = 1 - \frac{kt}{r_0 \rho}$$

<div align="right">Equation 14</div>

where:

$[C]_t$ = copper concentration at time t

$[C]_\infty$ = copper concentration at infinite time

As has been mentioned previously, this straight forward cube-root law can be applied when the powder suspension disperse homogeneously in the solution; in this regard plot of $1- (1- [C]_t/[C]_\infty)^{1/3}$ vs. t will be linear with a gradient of $k/(r_0\rho)$. Activation energy for the dissolution of copper can be determined by plotting ln k vs. 1/T from Arrhenius equation [185]:

$$k = A \exp\left(\frac{-Q}{RT}\right)$$

Equation 15

where:

k = rate constant

A = pre-exponential factor

Q = activation energy

R = gas constant

T = temperature in Kelvin

In practice, however, when the powder suspension disperses heterogeneously, the observed kinetics for the dissolution will deviate from the simple cube-root law.

2.7   Effect of Hydrogen Peroxide on Fatigue Life

The majority of service failures are due to fatigue. It has been well known that corrosion pits have a detrimental effect on fatigue life [190-194]. Different from high-cycle fatigue that usually occurs without any prior macroscopic symptoms; in corrosion fatigue pits are usually found as the crack origin [194]. This implies that introduction of pits on the surface components bearing load would trigger fatigue crack initiation. Because of that, establishment of life prediction after decontamination on the aircraft structural materials would be desirable. Hence, to get a quantitative understanding on the nature of crack growth after a decontamination process, fatigue testing is also needed, especially to reveal subtle, incipient damage that could induce subsequent degradation in the airliner structural materials performance [89].

Several other works on fatigue properties that involve corrosion process on aluminum alloys have been done by several researchers. Du *et al*. [195] have investigated the damaging effect of sequential exposure to fatigue, corrosion and fatigue in 2024-T3 aluminum alloy. In their work, 2024-T3 aluminum alloy was intermittently subjected to sequential corrosion and fatigue process where the specimens were first subjected to various degrees of fatigue damage in air, then immersed in a corrosive solution of 3.5 wt% NaCl and 10v% H_2O_2 for a fixed amount of time, and subsequently further fatigued in air to failure. Bystritskii *et al*. [196] also have studied the change in tensile and fatigue properties of 2024 and 7075 aluminum alloy samples modified using plasma-enhanced ion beams. The bending fatigue test was carried out both in air and in a 0.5 M NaCl aqueous solution which acted as a corrosive media. Interestingly enough, their results showed that exposure to the corrosive media after an initial fatigue increase the sum of

fatigue life of aluminum alloys specimens as compared to that of the sample without corrosion treatments. However, no studies or sufficient explanations on the mechanism have been performed so far. Some explanations of the mechanisms behind the increase of this fatigue life that still need to be tested experimentally are the blunting of fatigue-generated microcracks, oxide induced closure, which would be significant with short cracks, and the removal of other mechanical surface micro-damage by the corrosion process, such as intrusion or extrusions [195] created at the initial stage of fatigue.

3. OBJECTIVES OF THE RESEARCH

In general, the objective of this present research is to find out if there is any immediate loss or degradation in materials properties and hence performance after the decontamination process has been applied to the airliner, and if there is any possibility of cumulative damage from multiple decontamination cycles following either deliberate or unintentional incidents of biological on-the-ground airliner decontamination. This study was focused on the evaluation of airliner metallic structural materials; i.e. aluminum alloys that cover around 80% on Boeing 747 or around 70% on Boeing 777 and austenitic stainless steel as used for galley and lavatory surfaces [94].

There are three specific objectives of this present research. The three specific objectives are associated with three distinct but related works that have been done and explained as following:

❑ The first objective is to study the effect of surface roughness and wetting phenomena on bacterial attachment and its likely impact on the decontamination process. Within the framework of the study, the work is divided into two parts; the first part is aimed at investigating the effect of welding and subsequent corrosion on bacterial attachment, while on the second part is aimed at investigating the effect of different types of surface finish on the bacterial attachment.

❑ The second objective is to evaluate the effect of decontamination, at the same time the effect of chemicals used as decontaminants, in this case hydrogen peroxide, on the airliner metallic structural materials after a decontamination process has been applied to civilian aircraft.

❑ The third objective is to assess the dissolution rate of copper induced by hydrogen peroxide. Copper is the main alloying element in the 2024-T3 aluminum alloy and one of alloying elements in the 7075-T6 aluminum alloy; thus, any effect to this main alloying element would likely have an impact on the properties of the two aluminum alloys.

4. MATERIALS AND METHODS

4.1   Bacterial Attachment Behavior to a Surface

4.1.1   Specimens Preparation

There were two activities that have been performed in an effort to assess the behavior of bacterial attachments to a surface. The first was the attachment of *Listeria monocytogenes* to an austenitic stainless steel surface after welding and accelerated corrosion treatments. *L. monocytogenes* is a Gram-positive bacterium that may cause listeriosis with the dose of about 1000 total organisms; however, the exact pathogenic dose would vary with the strain and the victim's susceptibility [197]. The main purpose of this work was to investigate the effect of welding and subsequent corrosion on the bacterial attachment. For this work, pieces of 300 mm by 300 mm and 2-mm thick austenitic stainless steel 304 sheet and fillers with the same composition (McMaster-Carr, Atlanta, GA., USA) were subjected to four different welding protocols of heat input and travel speed. Welding was performed in Auburn University Engineering Shop with tungsten inert gas (TIG) equipment with current of 40~190 A, orifice diameter of 1.6 mm (1/16 inch), shielding gas Ar with the rate of about 0.92 ml/s (14 cup/hr), a standoff distance of about 3.2 mm (1/8 inch), and the welding parameters are listed in Table II. The weld treatments were high heat input at low speed (L1), low heat input at low speed

(L2), high heat input at high speed (S1), and low heat input at high speed (S2). The size of the weld metal and the microstructure of the entire weld (i.e., weld metal plus the unmelted HAZ surrounding it) are affected by a combination of the welding current and the welding speed (i.e., how fast the welding rod is moved along the weld seam) [198-199].

After the welding, the plate was cut into smaller parts with an electric discharge machine (EDM HS-300, Brother, Inc., Bridgewater, N.J., USA), and coupons of 24 mm by 9 mm containing a portion of weld, HAZ, and base metal were sectioned with a ISOMET 2000 Precision Saw (Buehler, Lake Bluff, IL, USA). Base metal coupons that were not subjected to welding were included as controls. All welded coupons were final polished to a mirror surface finish by using 40 nm colloidal silica suspension on a TegraForce-1 attached to a TegraDoser-5 system (Struers, Westlake, OH, USA). The coupons were divided into two categories of uncorroded and corroded. To prepare the corroded coupons, the welded-polished coupons were electroetched for 60 seconds in 20% nital (nitric acid and ethanol) solution at 5 V and 0.5 A prior to the corrosion test, which consisted of exposure to 60% nitric acid at 90°C for 1 week.

Table II. Parameters for the TIG welded austenitic stainless steel 304

Coupon Series	Description		Welding Parameters		
	Bead Size	Heat Input	Bead width (mm)	Time (s)	Speed (mm/min)
L1	Large	High (190 A)	7.5	25	62
L2	Large	Low (40 A)	5.0	25	62
S1	Small	High (190 A)	5.5	15	104
S2	Small	Low (40 A)	3.0	15	104

After the corrosion treatment, the coupons were prepared for bacterial attachment, which was done by Ms. Tam Mai in the Auburn University Poultry Science Department. The procedure is as follows: Following the corrosion process, the acidic coupons were neutralized ultrasonically 10 successive times for 2 minutes each in a saturated solution of sodium bicarbonate. All coupons were cleaned with acetone and then with 10 successive changes of deionized water for 2 minutes each in a sonicator (Cole-Parmer, Vernon Hills, IL, USA). The coupons were autoclaved at 121°C for 15 minutes, aseptically transferred onto sterile petri dishes containing a layer of Whatman No. 2 filter paper, and dried in a desiccator at 42°C for 24 hours. The coupons were then ready for bacterial attachment process.

A second activity was a study of the attachment of *L. monocytogenes* to an austenitic stainless steel with three different types of commercially available surface finish. The main purpose of this work was to investigate the effect of different types of surface finish on the bacterial attachment. For this work, sheets of austenitic stainless steel type 304 of 305 mm by 305 mm and 1 mm thick with a No. 2B finish, a No. 4 satin finish, and a No. 8 mirror finish were obtained from McMaster-Carr (Atlanta, GA, USA). All of the surfaces except for No. 2B finish were covered with a plastic film. These sheets were sectioned into coupons of 24 mm $\times$ 9 mm by using a Buehler ISOMET 2000 Precision Saw (Lake Bluff, IL, USA). For No. 2B finish, coupons were cleaned with acetone twice, for 10 minutes each time, in a sonicator (Cole-Parmer, Vernon Hills, IL, USA). The coupons were sonicated twice in deionized water, for 10 minutes each time, and then were autoclaved at 121°C for 15 minutes. The coupons were then aseptically transferred onto sterile Petri dishes matted with a layer of Whatman No. 2 filter paper and

dried in a desiccator at 42°C for 24 hours before exposure to bacteria. For No. 4 satin finish and No. 8 mirror finish, the plastic films were removed from coupons, which were then soaked for 3 hours and then sonicated (Cole-Parmer, Vernon Hills, IL) twice, for 10 minutes each time in Mötsenböcker Lift Off[®6] Tape Remover liquid (Mötsenböcker Advanced Developments, San Diego, CA, USA) to remove any residual glue on the surface. The coupons were soaked for 1 hour and sonicated twice for 10 minutes each time, in hot hand soap solution (70°C). After being rinsed with deionized water to eliminate soap, coupons were soaked in acetone for 15 minutes and then sonicated twice, for 10 minutes each time, in deionized water. The coupons were autoclaved and then ready for bacterial attachment process, which was done by Ms. Tam Mai in the Auburn University Poultry Science Department.

4.1.2 Surface Roughness and Contact Angle Measurements

Surface roughness measurements were performed by using a profilometer Alpha Step 200 model (KLA-Tencor, San Jose, CA, USA) available in Electrical Engineering Department. For contact angle measurements, the sterilized and dried coupons were positioned on a light microscope stage. A drop consisting of 10 µl of brain heart infusion (BHI) containing 107 CFU/ml of *L. monocytogenes* was deposited on each coupon test surface. Surface contact angles were evaluated at 23°C with a 4-megapixel digital camera (Nikon USA, Melville, N.Y., USA) attached to a stereo microscope (Olympus America, Melville, N.Y., USA) oriented to permit a side view of the inoculum droplet, see Figure 3 for detail. Photographs were taken 30 seconds after the droplet deposition, and a direct

---

[6] Mötsenböcker Lift Off is a registered trademark of and distributed by Mötsenböcker Advanced Developments Inc., San Diego, CA 92169, USA.

contact angle measurement was made from the recorded image. Each surface roughness and contact angle reported in this work was the average of six measurements.

4.1.3 Attachment of *L. monocytogenes*

For the bacterial attachment, *L. monocytogenes* ATCC 19111 was used. The bacteria was inoculated into brain heart infusion (BHI) and incubated for 24 hours at $37^{o}C$ to obtain a stationary-phase cell culture of about 109 cells per ml. The testing suspension was prepared by diluting 1 ml of this *L. monocytogenes* culture in 49 ml of BHI. Bacterial attachment was performed by using a drop technique. A drop consisting of 10 µl of BHI containing 107 CFU/ml was placed on each tested surface of the coupon. After incubation under saturated humidity conditions for 3 hours at $23^{o}C$, the samples were washed three successive times for 2 minutes each with 200 ml of sterile water at 100 rpm. As has been mentioned previously, this bacterial attachment process was done by Ms. Tam Mai in the Auburn University Poultry Science Department. After washing, the coupons were treated with a fixative agent, which consisted of 2 ml of 2% osmium tetroxide (OsO_4), for 45 minutes. The clean and dried coupons were then coated with gold using a sputter coater (ESM 550X, Hatfield, PA, USA.) and examined with a scanning electron microscope (JSM 840, JEOL, Peabody, MA, USA) to determine the number of *L. monocytogenes* cells attached to each of the test surface.

A total of 18 different surface types were tested. For each type of weld, four different surfaces were tested, i.e. HAZ-uncorroded, weld-uncorroded, HAZ-corroded, and weld-corroded. Uncorroded and corroded base metal coupons were included as controls.

68

 Figure 3–Stereo-light microscope setup oriented to permit a side view of the inoculum droplet.

4.1.4   Statistical Analysis

For each surface treatment, six coupons were tested, and 60 fields of view were evaluated to determine bacterial concentrations. The number of bacteria attached to each of the surfaces under the field of view was counted by Ms. Tam Mai. All concentration data were normalized to account for differences in the surface area of the inoculum due to differences in interfacial energy as reflected in the differences in measured contact angle. For statistical purpose, the SAS System package (SAS Institute Inc., Cary, NC, USA) was used to run the ANOVA and Duncan's test analyses to determine the significant differences, if any, between the treatments.

4.2   Effect of Decontamination on Aircraft Structural Materials Properties

On the effect of decontamination process, as has been mentioned previously, the main purpose is basically to examine the effect of the decontamination process and the chemical used as the bio-decontaminant, in this case hydrogen peroxide, on the properties of aircraft structural materials. The selected metallic structural materials were two aluminum alloys and an austenitic stainless steel 304 as used for galley and lavatory surfaces. Thus, because the focus was on the materials properties, there were no bacteria or bio-contaminant involved during the process.

4.2.1 Specimen Preparation

The airliner structural metallic materials are represented by 2024 aluminum and 7075 aluminum sheets, each with dimensions of 610 mm x 610 mm (24"x24") and 1.27 mm (0.050") thick and with a heat treatment that conforms to T3 and T6 temper respectively, and an austenitic stainless steel 304 sheet W/#8 mirror finish with dimension of 610 mm x 610 mm (24"x24") and 1.22 mm (0.048") thick that conforms to ASTM A240 [151]. The austenitic stainless sheet is used as a stand in for galley and lavatory surfaces. All of these materials were obtained from McMaster-Carr (Atlanta, GA, USA). In addition to these materials, to ascertain the effects of composition versus heat treatment, some of the 2024-T3 aluminum alloy specimens were reheat-treated into 2024-T6 aluminum alloy. As-received 2024-T3 aluminum alloy was re-annealed at 493°C for 3 hours and then water quenched (15°C). This as-quenched condition is called the O-temper. For the T-6 temper, the O-tempered material was artificially aged at 190°C for one day, and then air cooled to room temperature. All of the heat-treated materials were kept in freezer at -22°C to prevent natural aging before the treatments. Except for the tensile specimens, the large sheets were cut into smaller parts in the Auburn University Engineering Shops and then into 12.7 mm x 25.4 mm (½" x 1") coupons by using Buehler ISOMET 2000 Precision Saw. Tensile specimens, both in the longitudinal and transversal direction, were prepared from the sheets in accordance to ASTM standard E8M-00b [200].

4.2.2 Metallographic Preparation

All of the aluminum metallographic specimens were polished by using non-water based polishing materials followed by final polishing of 1:1 40 nm colloidal silica suspension and ethanol. Non-water based polishing materials were used because copper tends to accumulate on the intermetallic particle grooves when the specimen was polished using water based materials. Austenitic stainless steel 304 was polished by using 4000 grit silicon carbide followed by final polishing of 40 nm colloidal silica suspension. All of polishing activities were performed on a Struers TegraForce-1 attached to a TegraDoser-5 system. After polishing, the specimens were ultrasonically cleaned using ethanol and dried by using compressed air and then kept in desiccators for 24 hours. Metallographic samples were compared before and after exposure. In case of etching, the etchants used were Keller's reagent (2.5 ml HNO_3, 1.5 ml HCl, 1 ml HF, and 95 ml H_2O) and mixed acids (2.5 ml HF, 10 ml HNO_3, 10 ml HCl, and 27.5 ml H_2O) for the two aluminum alloys and the austenitic stainless steel 304 respectively. The metallographic samples were characterized by both light microscopy and using JEOL JSM 7000F field emission scanning electron microscope (FE–SEM) operated at 15 kV for imaging, together with energy dispersive x-ray spectroscopy (EDS) employing an ultrathin window (UTW) detector and Princeton Gamma-Tech (PGT) analyzer operated at 20 kV.

4.2.3   Vaporized Hydrogen Peroxide (VHP) Exposure

A Steris VHP[®7] 1000ED unit from Steris Corporation, operated using cycle parameters explained in the following paragraph was used to introduce the hydrogen peroxide into a test chamber. The test chamber, containing the test samples, consists of a glove box, from Purified Micro Environment (a division of Germfree Labs., Inc., Miami, FL, USA) with a total volume of approximately 0.38 m^3 (13.4 ft^3) and modified by the vendor to include inlet and outlet ports to connect to the Steris unit. The objective of this test is to evaluate the materials compatibility to hydrogen peroxide by comparing the materials after exposure and control (non-exposure).

There are four phases that are performed automatically by Steris VHP 1000ED unit to carry out one cycle of decontamination process, namely (see Figure 5 for detail):

1. Dehumidification phase. At this stage, relative humidity in the enclosure was reduced up to 10-30%; the lower the humidity, the better to minimize the probability of unintended condensation of the hydrogen peroxide. During this dehumidification phase, the temperature inside the enclosure and hoses will also warm up and so to allow higher H_2O_2 vapor concentrations. For the enclosure size of 0.38 m^3 and air flow rate of 0.37 standard cubic meters per minute, SCMM (13 standard cubic feet per minute, SCFM), the time needed for this phase was around 10 minutes.

2. Conditioning phase. At this stage, hydrogen peroxide was flash vaporized by the VHP 1000 ED from 35% liquid hydrogen peroxide (VAPROX[®8] Sterilant, STERIS

---

[7] VHP is a registered trademark of STERIS Corporation, 5960 Heisley Road, Mentor, Ohio 44060-1834 USA.

[8] VAPROX is a registered trademark of STERIS Corporation, 5960 Heisley Road, Mentor, Ohio 44060-1834 USA.

Corporation, Mentor, OH, USA) and then was injected into the chamber at a rate of 60 mg s^{-1} to establish an inlet concentration of 2,000 ppm and a chamber concentration of 450 ppm.

3. Decontamination phase. After a concentration of vapor phase of 450 ppm inside the enclosure was achieved, the phase was then held for 4 hours and 48 minutes to achieve 8 log$_{10}$ kill by injecting 21 mg s^{-1} steady vapor phase concentration. Hydrogen peroxide concentrations in the vapor phase were monitored using ATI sensors (ATI Inc, Collegeville, PA, USA), which are capable of sensing concentrations above around 50 ppm with a nominal accuracy of ± 0.1 ppm, at the hydrogen peroxide inlet and outlet inside the chamber.

4. Aeration phase. After 4 hours and 48 minutes, in which the decontamination has been done, the next phase is to remove the H_2O_2 vapor from the enclosure by breaking H_2O_2 down catalytically into non-harmful by-products of water vapor and oxygen (see the reaction in Figure 6). With the enclosure size of 0.38 m^3, it took approximately 75 minutes to complete this aeration phase. At the end of the run, after the hydrogen peroxide concentration in the chamber was below 1 ppm, as measured using a Dräger CMS sensor and Dräger tubes (Dräger, Luebeck, Germany), supplemented by peripheral monitoring via a Dräger accuro$^{®9}$ detector, the water and oxygen byproducts were then vented safely into the lab atmosphere.

---

[9] Dräger accuro is a registered trademark of Drägerwerk AG, Moislinger Allee 53-55, D-23542 Lübeck, Germany.

During the process, temperature was monitored by putting 8 thermocouples at 8 different locations inside the chambers chosen so as to represent the entire enclosure. This was done to ensure that the temperature inside the chamber was homogenous and no condensation occurs during the decontamination process. Time, pressure, relative humidity, and hydrogen peroxide concentrations was adjusted by using the Steris unit and data collected with respect to the parameters can be printed by the Steris unit. In order to examine the effect of multiple decontamination processes on a given aircraft, up to 25 VHP exposure cycles were performed.
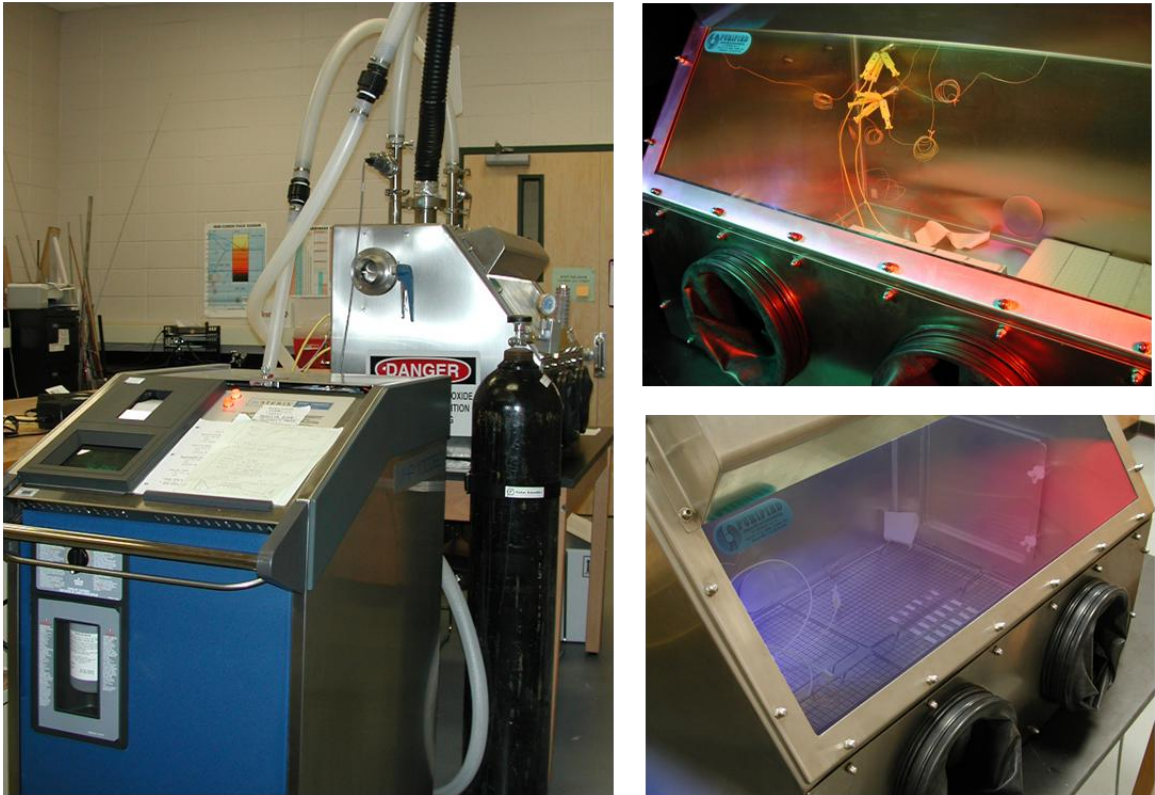
Figure 4–Equipment set up for vapor hydrogen peroxide exposure; left side is the Steris VHP 1000ED unit with the hoses into the test chamber. The test chamber (right side) containing the test samples, consisted of a glove box from Purified Micro Environment (a div. of Germfree Labs., Inc., Miami FL) modified by the vendor, and the sensors.
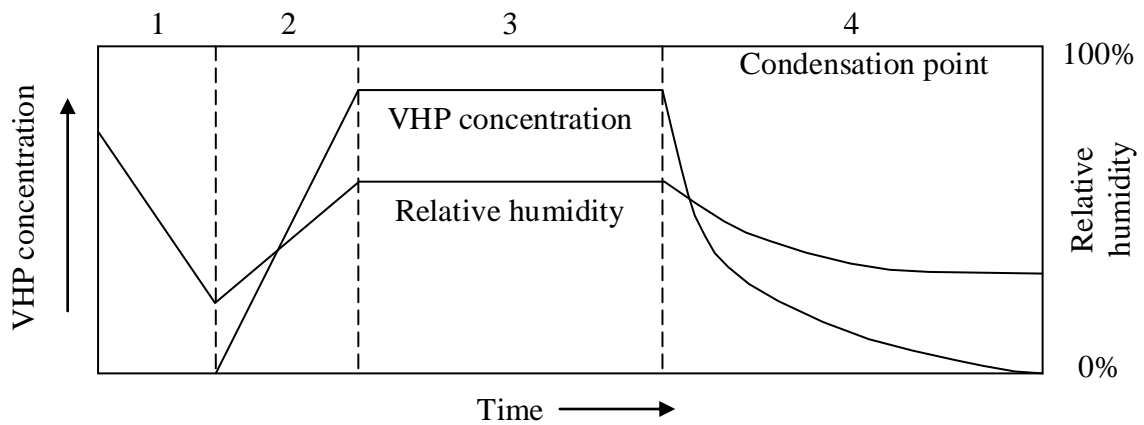
Figure 5–Typical Steris VHP 1000ED bio-decontamination cycle [71].
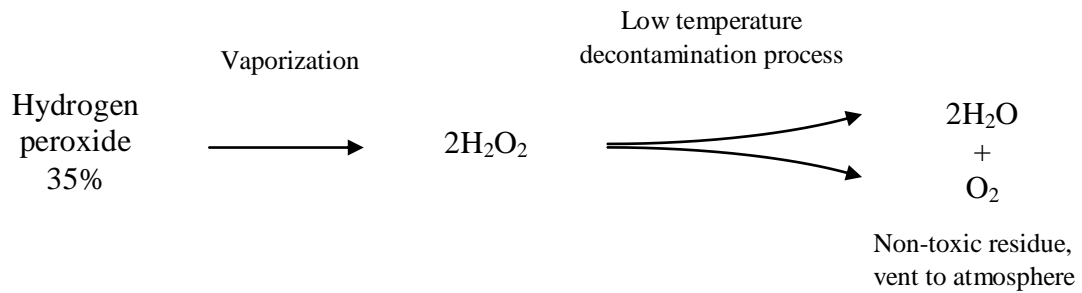
Figure 6–Decomposition of hydrogen peroxide into harmless by-products of water and oxygen [71].

4.2.4   Dip-Testing Using the Liquid Peroxide Feedstock

Dip testing is immersion of a specimen into a liquid, in this case the submergence of metallic specimens into hydrogen peroxide for a certain time. In most cases, the decontamination process was done using hydrogen peroxide vapor with a concentration of approximately 2000 ppm in the inlet and 450 ppm inside the chamber. However, dip testing employing the liquid hydrogen peroxide feedstock with a concentration of approximately 35% is needed to simulate the worst possible case, i.e. spillage of the liquid concentrate due to the operator abuse, or conditions where large-scale condensation of the peroxide takes place due to failure of the decontamination process control. Since hydrogen peroxide decomposes photochemically under light, dip testing was done in opaque containers (NALGENE HDPE, Nalge Nunc International, Rochester, NY, USA) containing 250 ml of analytical grade 35% hydrogen peroxide solution (Fisher Scientific, Fair Lawn, NJ, USA) for short time of 24 hours and longer time of 168 hours. Dip testing was conducted at both room temperatures ($\sim 22^{o}$C), at which the hydrogen peroxide would be expected to be relatively unstable but any reaction with the metallic samples relatively rapid, and refrigeration temperature (0 to -2 ℃), at which hydrogen peroxide would be expected to be relatively stable but any reaction with the metallic samples would be slower. After dip testing the samples were ultrasonically cleaned in high purity water (ARIES High-Purity D.I. Loop, ResinTech, West Berlin, NJ, USA).

4.2.5 Weight Change and Surface Roughness

Those chemicals that oxidize biological agents will also tend to oxidize exposed metal surfaces and metallic components of the electronic equipment. The direct exposure to an oxidizing agent will cause metal to oxidize and/or to undergo aqueous corrosion. It may not cause immediate problems or failures; however, since hydrogen peroxide is a strong oxidizing agent, then it will be a wise consideration to measure the weight change of the metals after the exposure as well as its surface roughness. The main reason for this is that during exposure the materials could be affected by the hydrogen peroxide. An increasing weight change could indicate that there is some oxidation on the surface, while a decreasing weight change could indicate some dissolution or leaching of particles from the surface.

For the purpose of weight change and surface roughness, the samples were ultrasonically cleaned in acetone and ethanol before the exposure to remove any residual debris from machining or polishing that would affect the measurements and then dried in a desiccator for 24 hours. Weight change was measured by using a Fisher Scientific analytical balance (accuSeries 124, Arvada, CO, USA) with a nominal accuracy of $\pm$ 100 µg. After the exposure the samples were cleaned in high purity water and dried in a desiccator for 24 hours and weighed again. The same cleaning procedure was done on the specimens for the surface roughness measurement. Surface roughness was measured by using an Alpha Step 200 profilometer (KLA-Tencor, San Jose, CA, USA). It needs to be mentioned that weight change work on the VHP exposure was performed by Mr. Mobbassar Hassan SK of the Auburn University Materials Research and Education Center.

4.2.6   Microstructure and Mechanical Properties

Microstructural characterization was performed through visual inspection by using light microscope (Olympus PME3, Melville, N.Y., USA) and/or scanning electron microscope (JEOL JSM 7000F FE–SEM, Peabody, MA, USA), and observations were recorded before and after the exposure. At the same time, chemical composition change on the surface before and after treatments were also observed by using an energy dispersive X-ray spectrometer (EDS) on a JEOL JSM 7000F FE–SEM employing an ultrathin window (UTW) detector and Princeton Gamma-Tech (PGT) analyzer operated at 20 kV. For mechanical purposes, the properties were observed through changes in microhardness (LECO DM-400 Hardness Tester, Lakeview, MI, USA), nanoindentation (NANO Indenter XP, MTS System, Eden Prairie, MN, USA), and tensile testing (Q Test 100 universal testing machine, MTS Systems, Eden Prairie, MN, USA) in accordance with ASTM standard E8M-00b [200] before and after treatments. The specimen geometry for this tensile testing is shown in Figure 7.

4.2.7   Statistical Analysis

For statistical purposes, whenever needed, the SAS System package from SAS Institute Inc., Cary, NC, USA, was used to run the ANOVA and Dunnett's test analyses for determining the significant differences, if any, between the treatments.
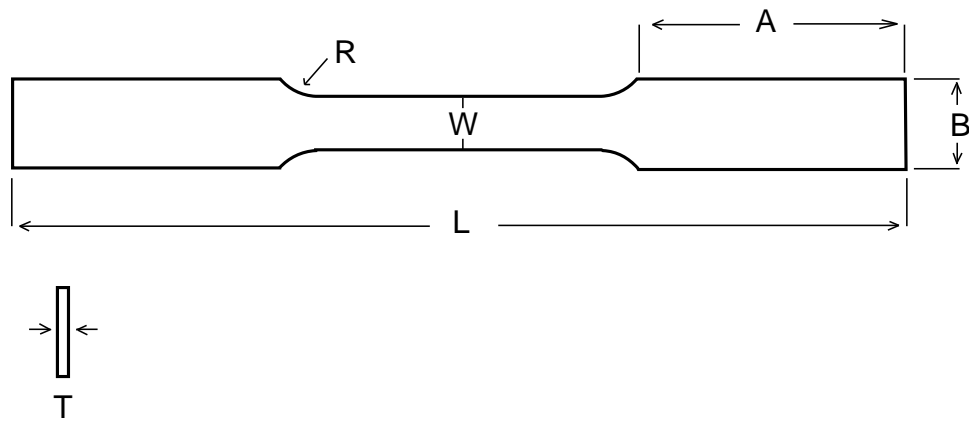
L – Total length, 100 mm

W – Width, 6 mm

A – Length of grip section, 30 mm

B – Width of grip section, 10 mm

R – Radius of fillet, 6 mm

T – Thickness, 1.27 mm for aluminum and 1.22 mm for stainless steel

Figure 7–Schematic of tensile test specimen with nominal dimensions.

4.3 Copper Dissolution in Hydrogen Peroxide

The copper dissolution rate into hydrogen peroxide was determined after an initial study of the impact of decontamination on the properties of aircraft structural materials, in which some leaching of copper into hydrogen peroxide during the dip testing was observed. Dip testing is immersion of a specimen into liquid hydrogen peroxide for a certain time. This was done to simulate the worst possible condition, i.e. spillage of the liquid concentrate due to operator abuse or conditions where large-scale condensation of the peroxide takes place due to the failure of decontamination process control. This leaching was expected because of copper dissolution into hydrogen peroxide. Since copper is one of the important alloying elements in the aluminum alloys, to get the idea how fast the process takes place and so to help understanding the subsequent corrosion process, if any, this work was also performed. For this purpose, an atomic absorption spectrometer (Varian AA240, Varian Inc., Palo Alto, CA, USA) was used to analyze the copper concentrations at different stirring speed, times, and temperatures.

4.3.1 Specimens Preparation

A 325 mesh copper powder with a metal basis grade (99%) from Alfa Aesar (Ward Hill, MA, USA) was used as a reference material. For the aluminum alloys, a 3 mm diameter circular specimen was cut from the sheet using EDM and ultrasonically cleaned in acetone and ethanol each for 5 minutes, dried up, and then kept in desiccators for 24 hours. All of the aluminum alloys surfaces were coated (Micro-Shield from SPI-Chem, West Chester, PA, USA) except at one side on which copper dissolution measurement was carried out.

4.3.2 Testing Procedures

An amount of 20 mg of copper powder was weighed on an analytical microbalance (Mettler Toldeo AT20, Mettler-Toledo GmbH, Laboratory & Weighing Technologies, CH-8606 Greifensee, Switzerland) with a nominal accuracy of $\pm$ 1 µg. The specimen was then put into small glass bottle containing 20 ml of 35% hydrogen peroxide solution (Fisher Scientific, Fair Lawn, NJ). The bottle containing the specimen was put into water bath on a plate (Corning Stirrer /Hot Plate model PC-420, Acton, MA, USA) and stirred at a certain speed, time, and temperature. Thereafter the sample was removed from the bottle and the solution was filtered using a Whatman No. 2 filter paper. Copper concentration in the hydrogen peroxide solution, in this case indicating the dissolved copper, was analyzed by using AAS with a copper standard diluted from copper standard solution 1000 ppm (Copper standard solution 1000 ppm, Fisher Scientific, Fair Lawn, NJ). The same testing procedures were applied to both 2024-T3 and 7075-T6 aluminum alloys.

4.3.3 Data Analysis

Data from the dissolution studies were grouped into three different categories of stirring speeds, reaction times, and temperatures. Each of the categories was statistically analyzed using ANOVA to find any difference within the groups, while Dunnet's test was using to find the difference among the groups. Results from this analysis were then used as an input for a simple theoretical model of the dissolution rate.

4.3.4 Modeling

The objective of this task is basically to study the kinetics of copper dissolution into hydrogen peroxide. Result from this work was then compared to those of two aluminum alloys of 2024-T3 and 7075-T6 in order to get deeper understanding of reaction step and so to provide basis knowledge on how the subsequent corrosion of those two aluminum alloys occurs in the presence of hydrogen peroxide. For this purpose, the dissolution of copper powder hydrometallurgically dissolved in hydrogen peroxide solution was measured. The dissolution rate was obtained from the dissolving of copper in the solution analyzed by atomic absorption spectrometer.

5. RESULTS AND DISCUSION

This section provides results and discussion for the three different topics explained in the previous section. The first part will discuss the effect of surface roughness and wetting phenomena on bacterial attachment, and its likely impacts on the decontamination process. The second part will present the effect of decontamination and thus the decontaminant, in this case hydrogen peroxide, on the microstructure and mechanical properties of aircraft metallic structural materials, which covers 2024-T3 aluminum alloy, 7075-T6 aluminum alloy, and austenitic stainless steel 304 as used in lavatory and galley surfaces. The third part deals with copper dissolution rate into hydrogen peroxide. Based on the copper dissolution rate into hydrogen peroxide, this third part will also discuss the possibility of two aluminum alloys of 2024-T3 and 7075-T6 becoming corroded in the presence of liquid hydrogen peroxide.

5.1 The Impact of Surface Roughness and Wetting Phenomena on Bacterial Attachment

Several other studies that have been performed by other investigators used an immersion technique to examine bacterial attachment behavior onto surfaces. In this technique, samples are immersed fully in a bacterial suspension. As has been mentioned earlier, wettability is a characteristic of a given surface-liquid combination and can be

measured as the contact angle. At the same time, the problem with doing this immersion technique is that the liquid wetting aspect will be masked and thus the problem may not be examined correctly; in this case contact angle and thus wetting phenomena cannot be investigated. For this reason, in order to reveal the wetting phenomena, in this study, the investigation of bacterial attachment to the surfaces was not done by using the immersion technique; instead the liquid containing bacteria was deposited onto the surface by the drop technique. In this technique the effect of wetting phenomena would be clearly apparent. Results from this study are given in the following section.

5.1.1 Surface Roughness and Contact Angle

Surface roughness (Ra) values obtained by surfaces treatments on the as-polished samples were about 40 nm, indicating similarities in the surface areas for all of the as-polished samples. This value of surface roughness is consistent with the use of 40 nm colloidal silica suspension, which was used for the final polishing. However, Ra values obtained from the polish-corroded samples ranged from 450 to 480 nm, indicating small differences in the surface topography according to the specific surface treatments. It is clear that after being exposed to corrosive media, the surface roughness values of the corroded samples were much higher than those of the uncorroded samples. More detail on this surface roughness can be seen in Figure 8. At the same time, contact angles measurements for the as-polished samples were about 72 degree, while for the polish-corroded samples ranged from 41 to 54 degree.
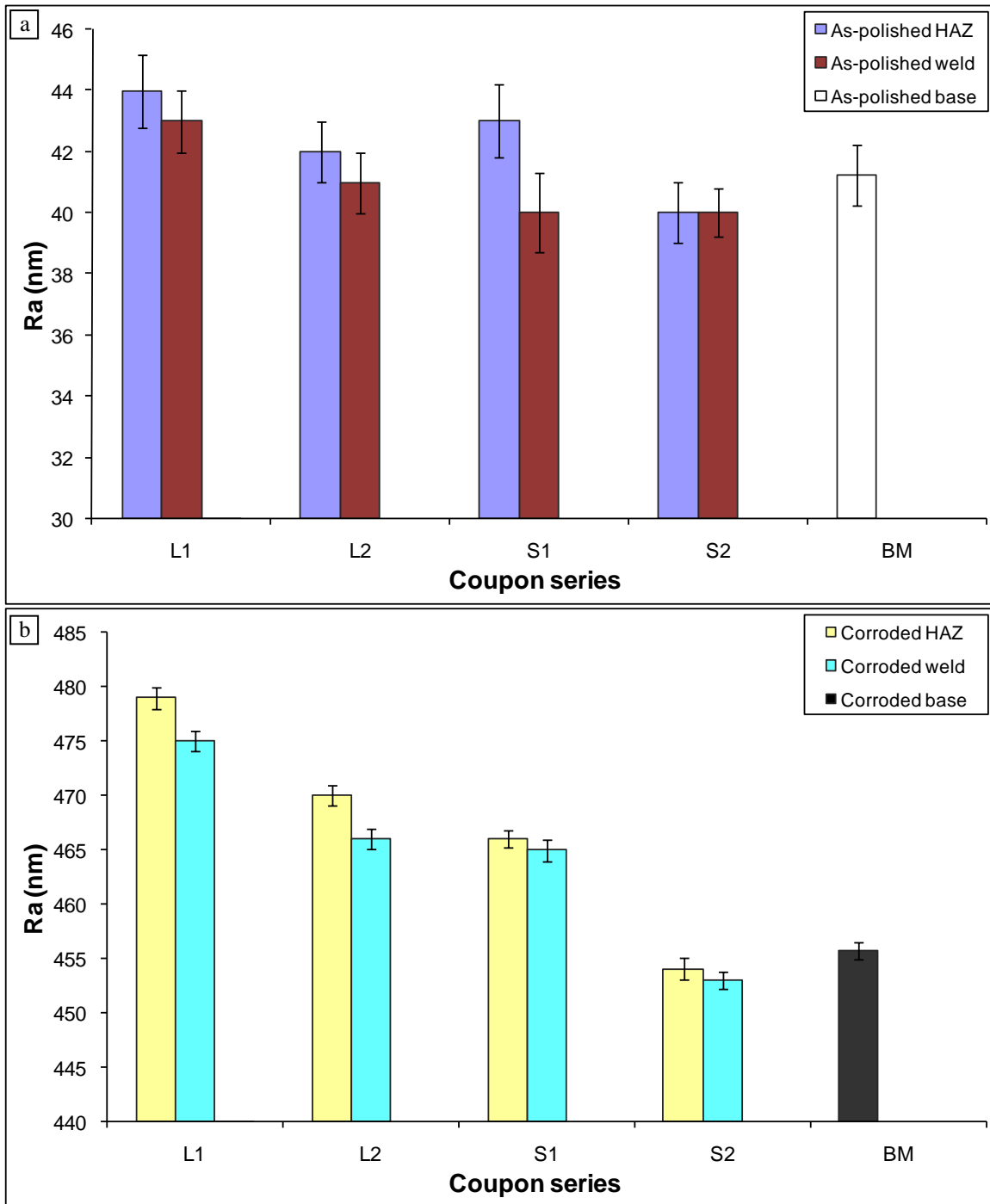
Figure 8–Surface roughness measurements for the as-polished (a) and polish-corroded (b) surfaces; see Table II for coupon series detail. Error bars show standard deviation.

There was a strong negative correlation between surface roughness and contact angle values, which was about -0.97. In this case, it is suspected that the increase in surface roughness may have accounted for a decrease in contact angles. Even there was no difference in contact angle measurements of the three surface zones of the uncorroded samples statistically; however, on the corroded specimens, the corrosion treatment seemed to substantially reduce the contact angle. The results showed that contact angle measurements of the corroded HAZ and weld zone of the large bead and high heat input sample were the lowest. The contact angle difference between the as-polished and polish-corroded coupons that results in surface area differences can be seen clearly in the representative pictures in Figure 9 (a) and (b) respectively, while quantitative results on this contact angle can be seen detail in Figure 10.

Although in the corroded samples, it was not always consistent that the higher values of surface roughness lead to the lower values of contact angle, however, in certain extent, the increases of surface roughness seemed to play a role on the decreases of the contact angle measurements of the samples in this work. Nevertheless, a direct correlation between surface roughness and wettability cannot be precisely determined in this work since a detailed statistical analysis of the correlation of surface roughness to wettability was not included. As has been mentioned in the previous section, the work involved the acceleration of corrosion process, which would likely entail other factors as a result of the corrosion induced product(s). Thus, more investigation is actually needed to fully determine the direct correlation between surface roughness and wettability, independent of other factors associated with corrosion, for example potential reduction in

solid-vapor interfacial energy which may be induced by the formation of corrosion products.

Effect of different surface roughness of three different zone of TIG welding that results from the corrosion treatment on the bacterial attachment are discussed more detail in the following section.
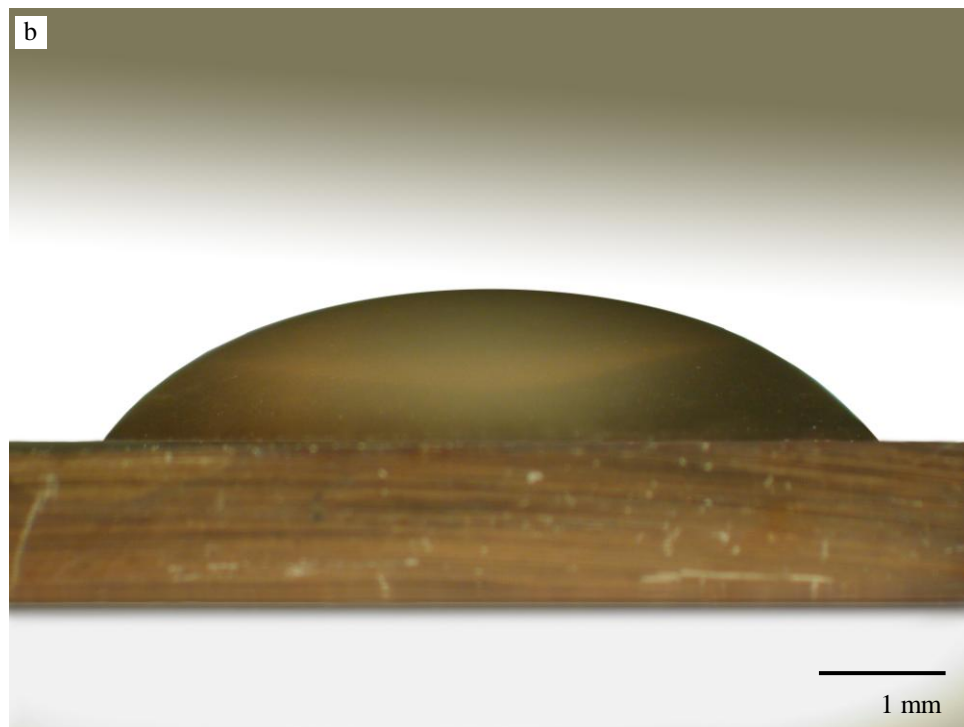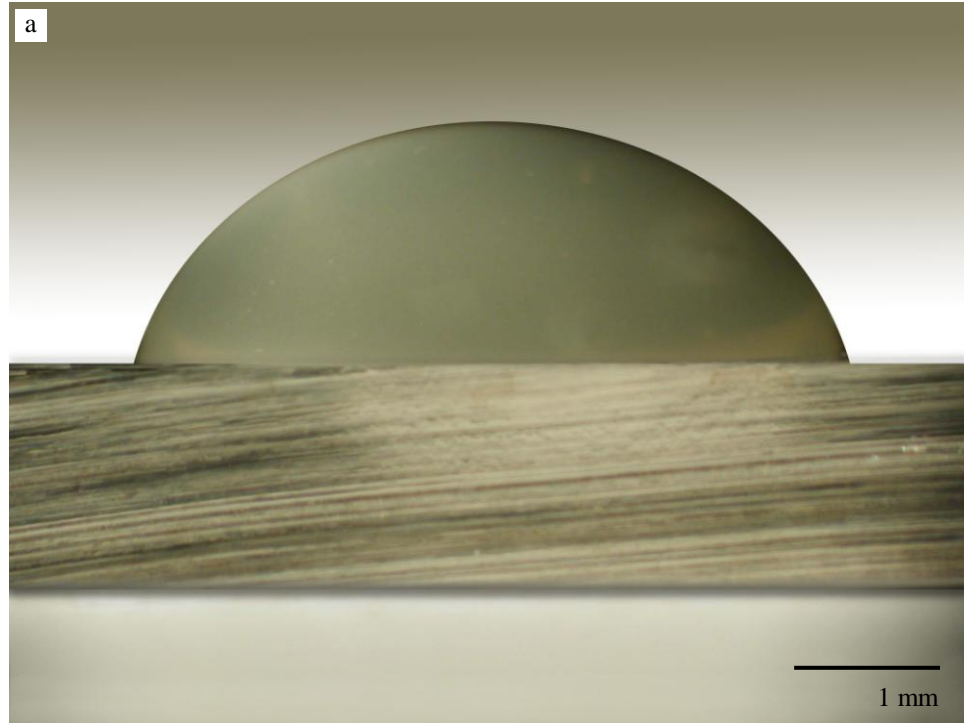
Figure 9–Sessile drop of 10 µl BHI containing 10^7 CFU/ml of *L. monocytogenes* on the as-polished (a) and polish-corroded (b) surfaces that results in different contact angles.
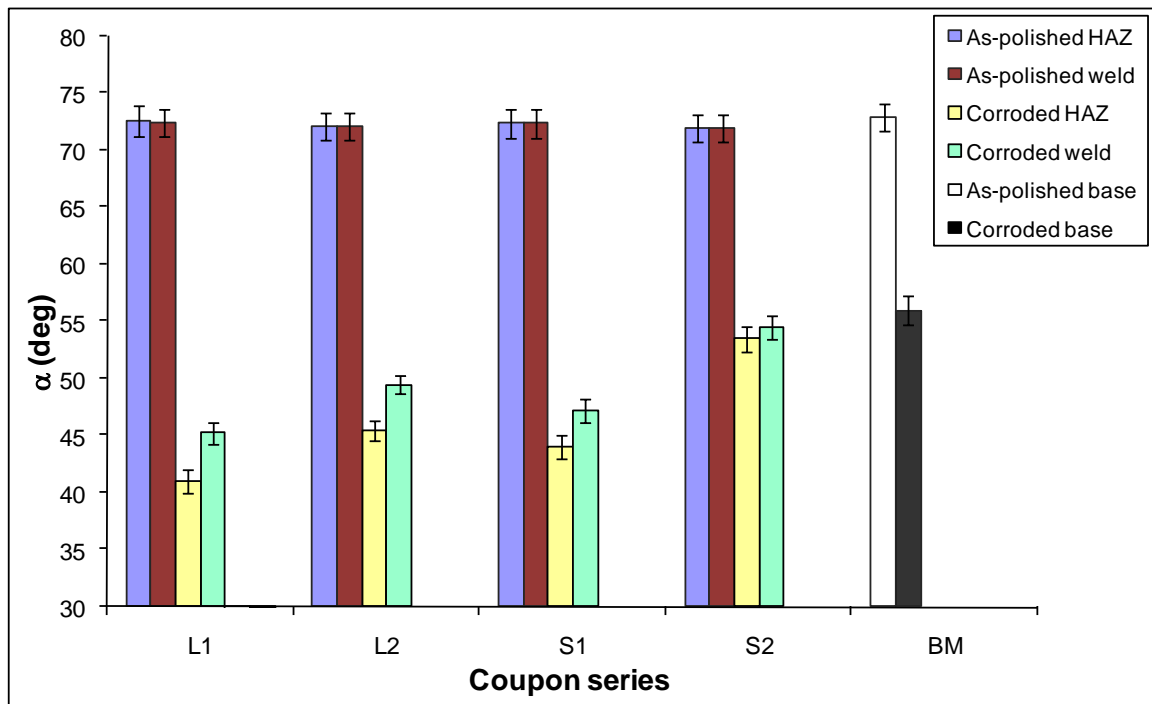
Figure 10–Contact angle measurements for the as-polished and polish-corroded surfaces; see Table II for coupon series detail. Error bars show standard deviation.

5.1.2 Wettability Phenomena

The wettability phenomena underlying the spreading of a liquid over a surface comes from the fact that the higher the surface wettability due to the effect of surface roughness, the more area covered and thus the more distribution of *L. monocytogenes* over the surface area and vice versa. Therefore, in order to investigate the influence of differences in contact area, normalization of bacterial counts was needed. This normalization was also required especially to account for differences in the surface area of the inoculum due to differences in interfacial energy as reflected in the differences in measured contact angle. The equation was formulated with the assumptions:

1. There was no bio-film formation

2. The solution and thus bacteria spread homogenously

3. The substrate and thus the surface laid over a flat area

For this purpose, the normalization equation was derived based on spreading of a liquid drop over surface area on the substrate, in which the term of wetting is sometimes used to describe the propensity instead of wettability [201], and is explained in the following section.
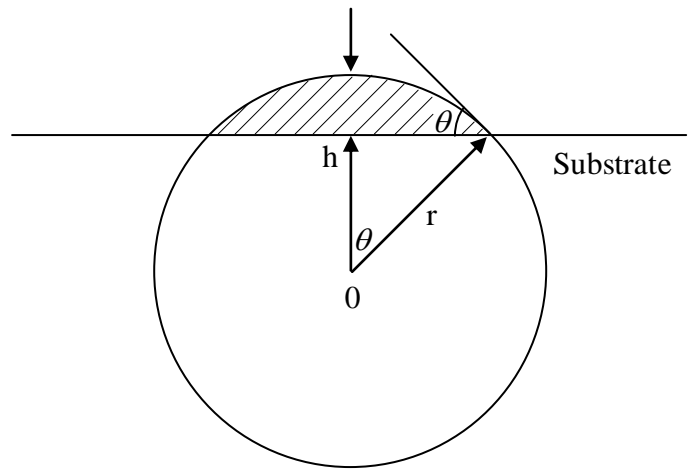
Figure 11–Derivation of normalization equation was based on spreading of a liquid drop on the surface of a substrate [201].

Volume of the cap, V_c, the shadow area in the Figure 11, is the volume of the sessile drop and is given by:

$$\int_0^{dh} dV_c = S\, dh$$

Where S, the surface area under the cap, is equal to:

$$S = \pi(r^2 - h^2)$$

Combination of Equation 16 and Equation 17 gives the equation of:

$$V_c = \int_{r\cos\theta}^{r} \pi\,(r^2 - h^2)\, dh$$

Since S is also given by:

$$S = \pi r^2 \sin^2\theta$$

Combination of Equation 18 and Equation 19 will give the surface area of:

$$S = \pi \left[\frac{V_c \sin^3 \theta}{\frac{2}{3} - \cos \theta + \frac{\cos^3 \theta}{3}} \right]^{\frac{2}{3}}$$

Equation 20

Solving this equation will then give the solution for normalized bacterial count as following:

$$X = \left(\frac{\sin \alpha}{\sin \theta} \right)^2 \left(\frac{2 - 3 \cos \theta + \cos^3 \theta}{2 - 3 \cos \alpha + \cos^3 \alpha} \right)^{\frac{2}{3}} Y$$

Equation 21

where:

X = normalized bacterial count

Y = bacterial count on the field of view that needs to be normalized

α = contact angle of the inoculum that need to be normalized

θ = contact angle of the inoculum that is used as standard for the normalization

5.1.3 Wettability and Bacterial Attachment

Number of bacteria attached to each of the surfaces before and after normalization is given in Table III and Table IV, respectively, and the accompanying graph with Duncan's grouping is shown in Figure 12. Representative SEM micrographs of the attachment on the base metal, HAZ, and weldment surface areas are given in Figure 13, Figure 14, and Figure 15, respectively. Although the results showed that there were no differences ($P > 0.05$) in the numbers of bacteria attached on the three surface zones of the uncorroded samples; however, the numbers of bacteria detected on the three zones of welds exposed to the corrosive media were higher ($P < 0.05$) than those on the corresponding three zones of the uncorroded surfaces. Among the corroded surfaces, attachment to the HAZ surface was consistently higher than that of the weld region, while the highest attachment occurred on the HAZ corroded sample, which was welded with a large bead and high heat input (L1). Furthermore, the amount of bacteria on the base metal was lower ($P < 0.05$) than those on HAZ and weld regions.

Table III. The average number of bacteria attached to each of the surfaces before normalization. Standard deviation is given in parenthesis.

Coupon series		As-polished		Polish-corroded	
		HAZ	Weld	HAZ	Weld
High heat	Large bead	160 (60)	153 (47)	208 (72)	160 (69)
	Small bead	154 (63)	156 (51)	163 (55)	130 (45)
Low heat	Large bead	147 (64)	159 (56)	161 (59)	120 (39)
	Small bead	148 (64)	147 (72)	149 (50)	143 (52)
Base metal		148 (40)		131 (37)	

Table IV. The average number of bacteria attached to each of the surfaces after normalization. Standard deviation is given in parenthesis.

Coupon series		As-polished		Polish-corroded	
		HAZ	Weld	HAZ	Weld
High heat	Large bead	142 (53)	135 (42)	351 (121)	250 (108)
	Small bead	137 (56)	138 (45)	254 (86)	188 (66)
Low heat	Large bead	131 (56)	141 (50)	257 (94)	181 (59)
	Small bead	131 (57)	131 (64)	202 (68)	190 (69)
Base metal		131 (36)		170 (48)	
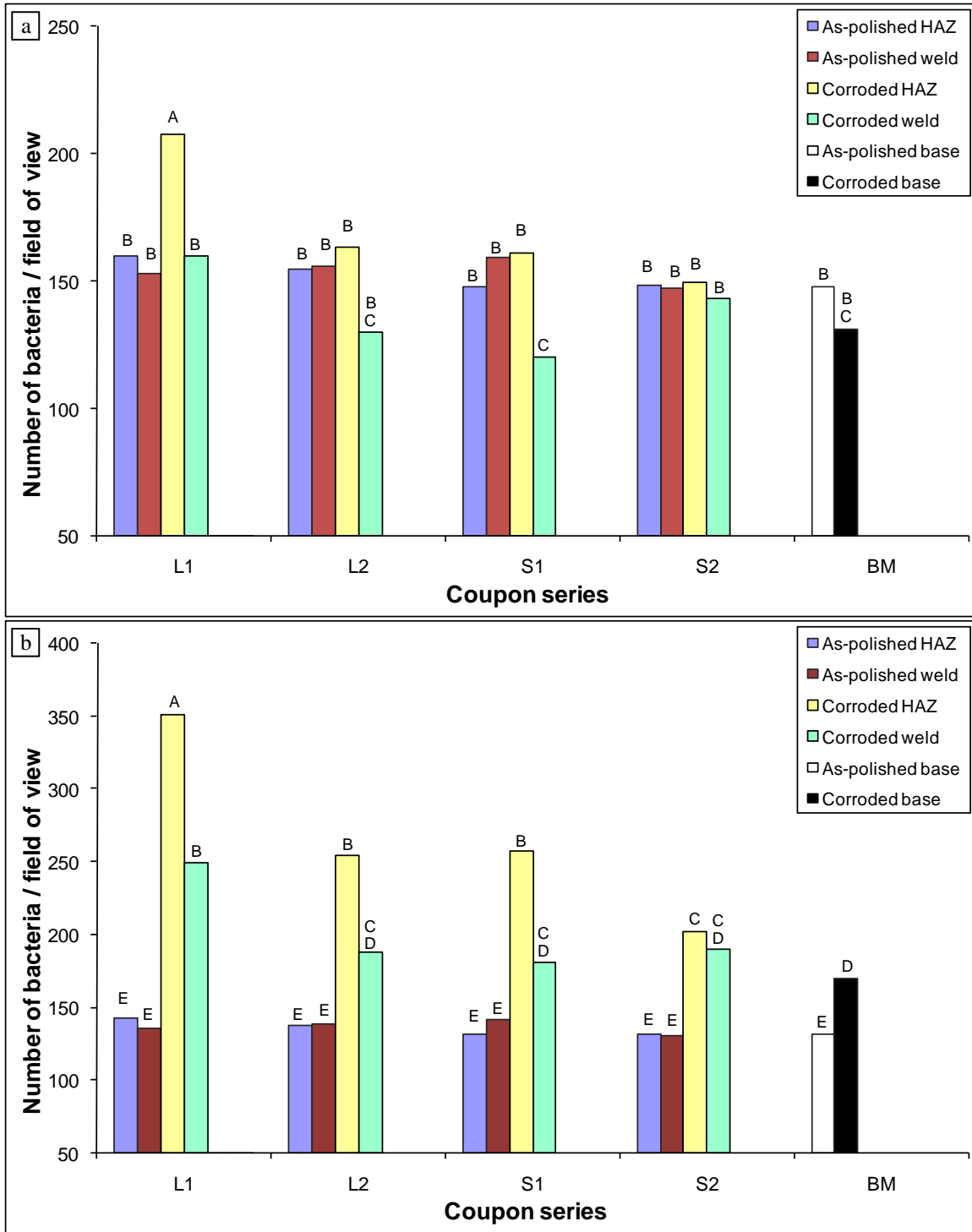
Figure 12–Means of bacterial counts before (a) and after (b) normalization on the field of view of tested surfaces; see Table II for coupon series detail. Different letters indicate significant differences (P < 0.05) in number of bacteria on the surfaces.
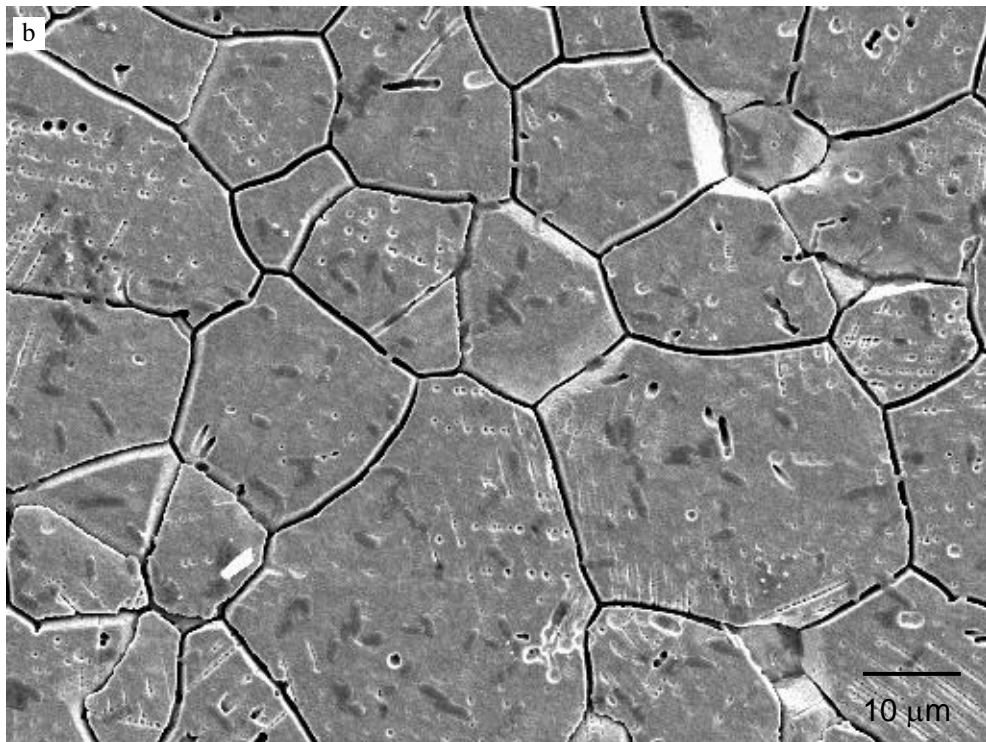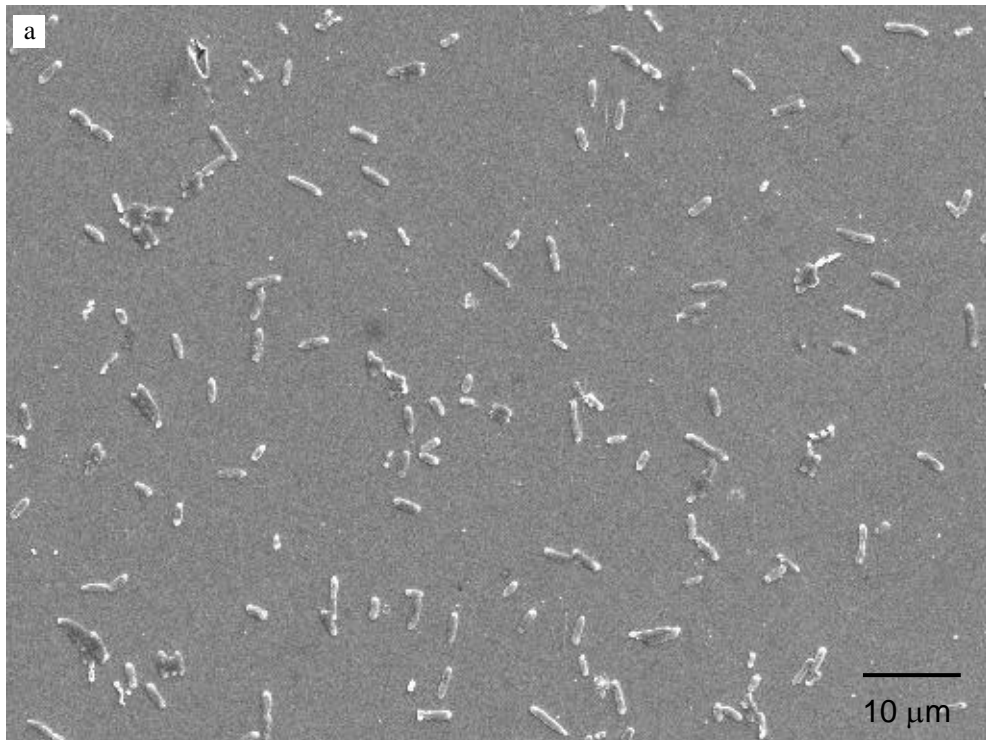
Figure 13–Secondary electron images of the attachment of bacteria on the as-polished base metal (a) and polish-corroded base metal (b) coupons.
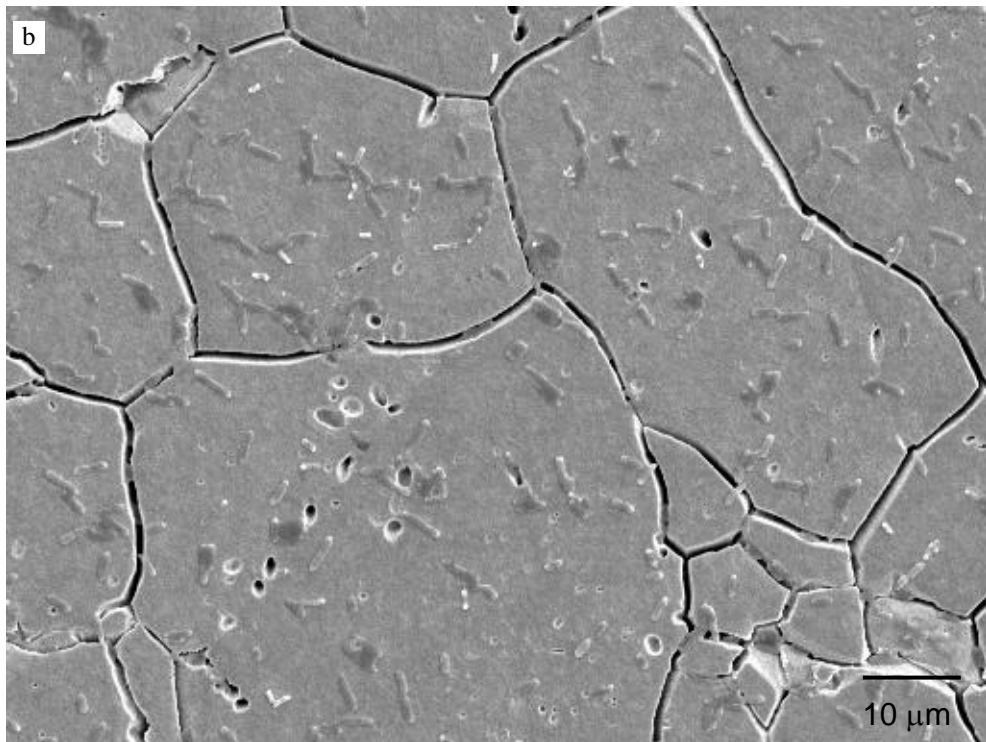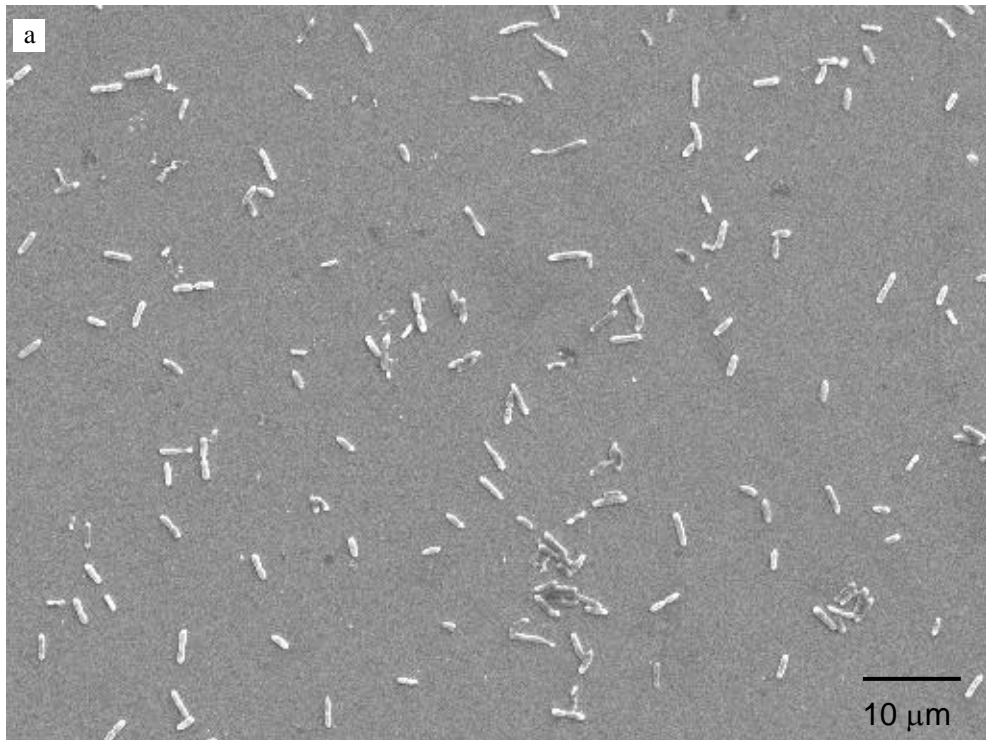
Figure 14–Secondary electron images of the attachment of bacteria on the as-polished HAZ (a) and polished-corroded HAZ (b) coupons.
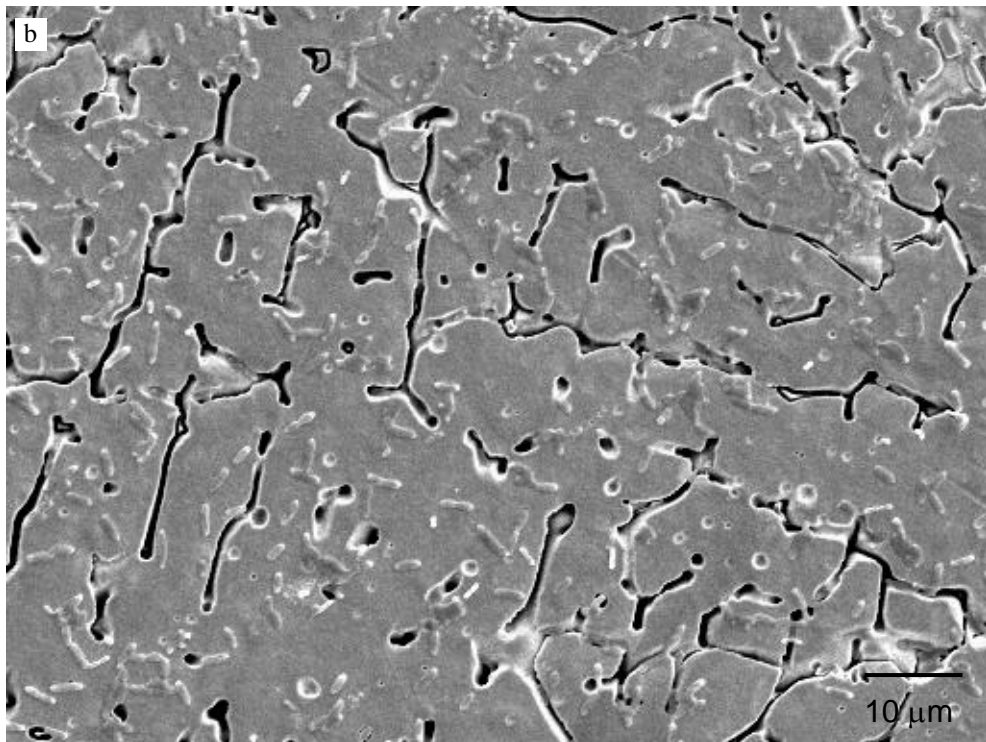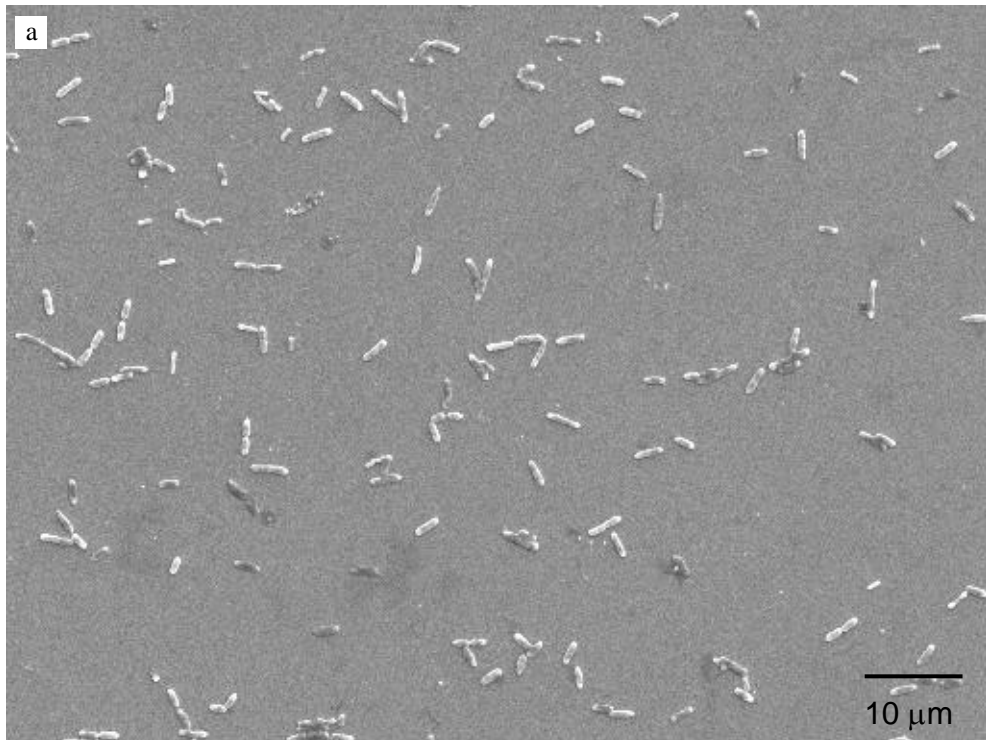
Figure 15–Secondary electron images of the attachment of bacteria on the as-polished welded (a) and polished-corroded welded (b) coupons.

In context of bacterial attachment due to the spreading of liquid containing bacteria onto a surface and its relation to decontamination, the effects of surface roughness are particularly interesting. As has been mentioned previously, one of the factors affecting bacterial attachment onto surfaces is wetting and adhesion. In this regard, the distribution of bacterial cells over the surface of the substrate is affected by those factors that govern the wetting of the surface, in this case by the factor affecting the liquid carrying the bacterial cells. Results from this work showed that surfaces of higher roughness distributed the *L. monocytogenes* suspension over larger area than the surface of lower roughness. However, in this work there were several variables that could result from the material treatment itself, such as surface roughness, wettability, microstructural changes, and other factors that might be induced by the corrosion process. These variables unfortunately were not independently controlled. Thus, the dominant parameter could not be identified precisely; it could be due to increased in surface area, increased in wettability, microstructural changes or a combination of these variables. Nonetheless, in this work, the overall wettability of the surfaces appeared to be a primary determinant of the results. In its relation to the decontamination process, the more the spreading of bacteria over a surface, the more it likely prevents or at least affects the decontamination process; and hence, this corrosion site should get more attention than the other surface areas because it might become a harborage after either incident or intentional release of bio-contaminant agents.

As can be seen in the selected photomicrographs in Figure 13, Figure 14, and Figure 15 for the base metal, HAZ, and welded surface areas, respectively, SEM analysis revealed that bacteria that attached to the surfaces were randomly distributed. It needs to

be noted that, however, due to the large contact area under inoculum, only the selected area within the field of view was considered for the bacterial count purpose.

Comparison of bacterial counts prior to normalization of the data showed that there were no differences ($P > 0.05$) in bacterial counts among the different surfaces, except for corroded HAZs of high heat input at low speed. This zone, as has been mentioned before, had the highest number of bacteria ($P < 0.05$), while corroded weld metal of high heat input at high speed had the lowest number of bacteria ($P < 0.05$). However, when the data were normalized, differences in numbers of bacteria on the surface were apparent as can be seen in Figure 12 (b).

The results of this first study indicate that welding of austenitic stainless steel 304 followed by mirror polishing does not affect the ability of *L. monocytogenes* to attach to the surface under the conditions examined; however, corrosion of the welded stainless steels does promote the attachment of *L. monocytogenes* with the largest effect occurring in the HAZ. In its relation to the decontamination process, results of this work would likely indicate that corrosion site, especially on the austenitic stainless steel 304 welded joining and its surrounding HAZ should need more attention because it could become a source or a harborage after either incident or intentional release of bio-contaminant agents.

On the second work, a comparison of surface roughness and contact angle values for the three different types of surface finish tested is shown in Table V, while representative SEM micrographs of the attachment of bacteria on those three different surfaces are given in Figure 16. As has been mentioned before, wettability is a characteristic of the combined properties of a surface, a liquid and a vapor phase and is

measured as the contact angle, in which lower contact angle corresponding to better wetting [63, 65]. Thus, when investigating bacterial attachment with non-immersed exposure, such as drop contact, which was also used in this work, surface wettability needs to be considered because it can play an important role in the initial events that will lead to attachment of bacteria to the surface [47]. In this case, the surface area covered by droplets of equal composition and volume would vary according to the surfaces wettability characteristics, i.e. contact angle.

Results of this work showed that the surfaces of higher wettability or lower contact angle (as observed on a No. 2B surface) allowed distribution of the *L. monocytogenes* suspension over a larger area as compared to surfaces of lower wettability (No. 4 and No. 8 surface finishes). To investigate the influence of differences in contact area, bacterial counts were also normalized (Equation 21) to account for differences in the surface area of the inoculum due to differences in interfacial energy as reflected in the differences in measured contact angle. However, given the small differences in contact angle, this normalization of the data did not significantly affect the results. As with normalized data, bacterial counts differed among the different surface finishes, with the lowest count occurring on the No. 2B finish and the highest count on the No. 8 finish.

It is generally accepted that roughness of surfaces strongly affects the measured contact angle [202, 203], as also has been supported by the previous work on the weld corroded surface; however, as can be seen from the values in Table V, the influence of surface roughness on the measured contact angle was not clear in this second work. The coupons No. 4 satin and No. 8 mirror finish had the highest and lowest value of surface roughness respectively, but No. 8 mirror and No. 2B finish had the highest and the lowest

value of contact angle, respectively. The number of bacteria attached to No. 8 finish was significantly greater than those of No. 4 satin and No. 2B finishes, while the lowest number of bacteria was found on the No. 2B finish.

Table V. Surface roughness, contact angle measurements, and means of bacterial counts per field of view (FOV) before normalization (BN) and after normalization (AN). Different letters indicate significant differences (P ≤ 0.05). Standard deviation for surface roughness and contact angle is shown.

Steel Surface Finish	Surface roughness (nm)	Contact angle (deg)	BN/FOV	AN/FOV
No. 2B	425 ± 2	72 ± 1	70 (A)	79 (A)
No. 4	439 ± 3	79 ± 1	108 (B)	109 (B)
No. 8	39 ±1	80 ± 1	132 (C)	132 (C)
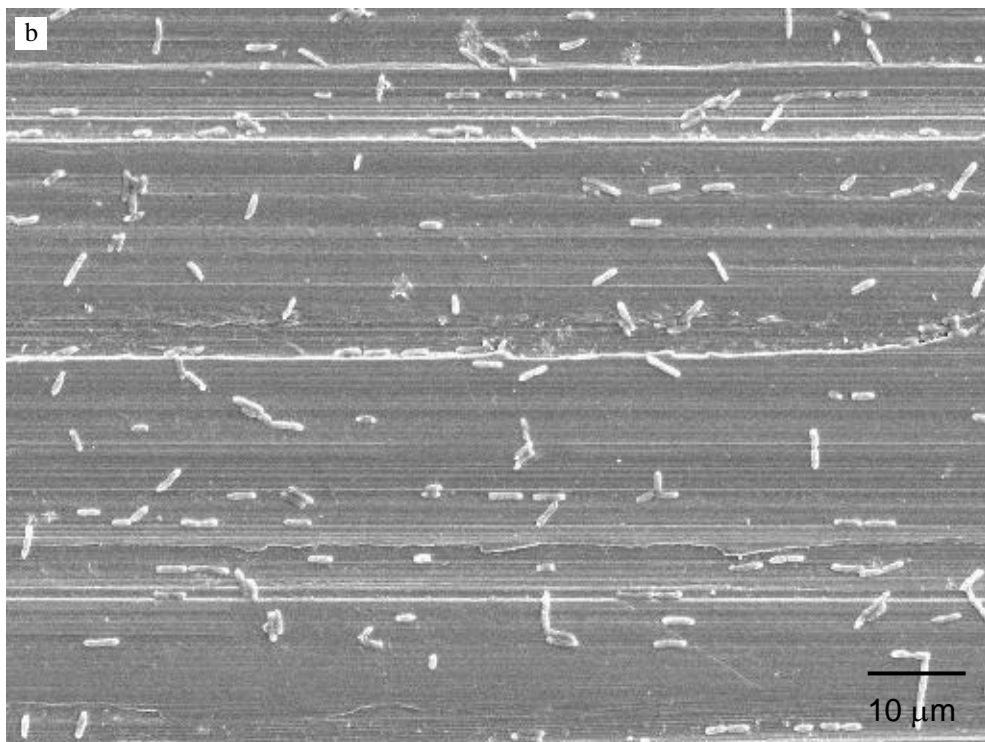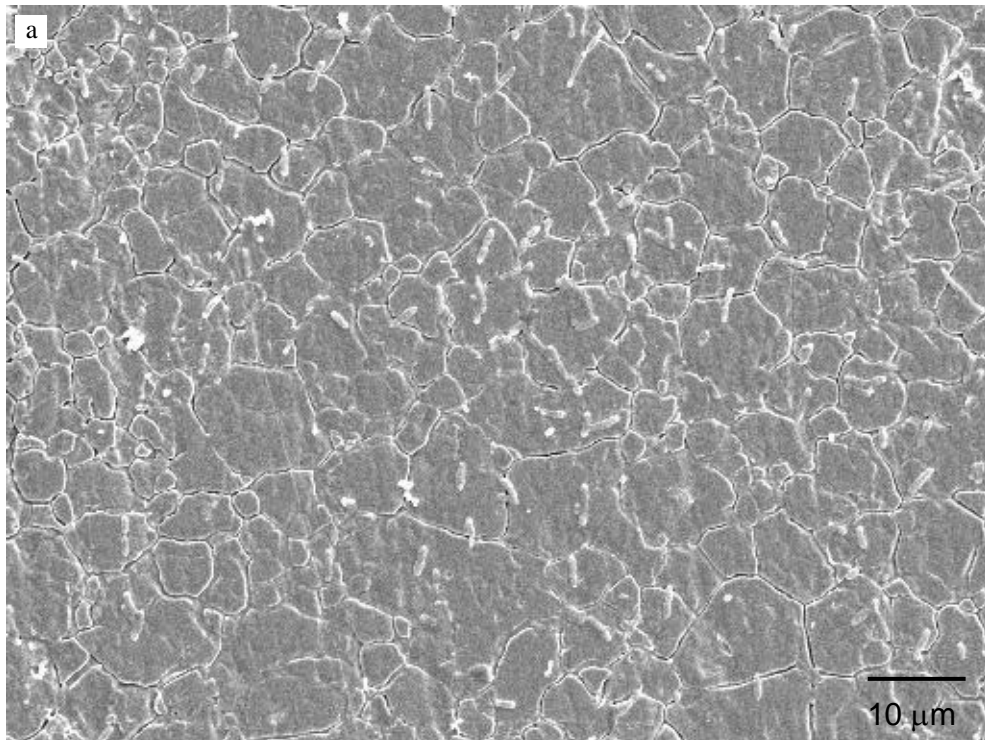
Figure 16–Secondary electron images of surfaces following the application of bacterial suspension drop on No. 2B finish (a), No. 4 satin (b), and No. 8 mirror (c, see next page) coupons.
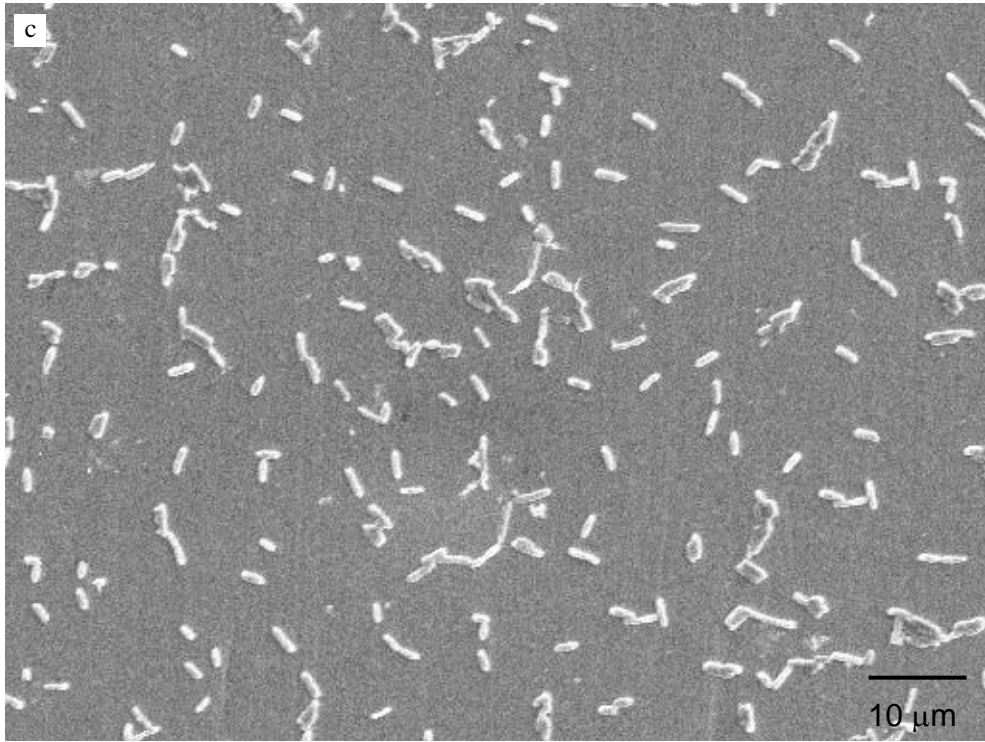
Continued

Investigating the sole effect of surface finish on the initial attachment of bacteria is challenging since it is difficult to separate surface finish from other variables such as surface roughness, surface wettability, and surface charge if materials of differing electrical properties are also considered. In terms of solely surface roughness, the result of this work does not fully agree with the previous results in which more bacterial attachment occurred on surfaces with higher wettability or lower contact angle. In this work, it appears that there was a correlation between the value of contact angle and the number of bacteria attached to the surface; the greater value of contact angle of the surface, the greater number of bacteria on the surface. However, it is hard to draw conclusions as to an effect due solely to the surface roughness since each surface roughness represents a different surface finish. This would likely explain why result of this work does not fully agree with the previous results. The discrepancy could also be explained further by the fact that when the contact angle of a surface increased to a certain degree, detachment of bacteria on that surface was observed to become more difficult.

In its relation to the decontamination, the major finding of this second work is that polishing an austenitic stainless steel 304 surface to a certain smoothness, which would influence wettability, may give rise to more adhesion of bacteria on the surface. Thereby, it might take more time to decontaminate bio-contaminant on that type of surface finish compared to other certain type of surface finish. On the other hand, certain type of surface smoothness might impact the ability of decontamination treatments to remove or inactivate attached cells. In terms of surface finish, a certain type of surface finish might be better than the other in terms of the easy of decontamination; thus there would be a

need to find an optimum surface roughness. Furthermore, these two works were done only on an austenitic stainless steel 304; however, since the work concentrated on fundamental aspects, much of the knowledge obtained herein could possibly also be applied to other aircraft metallic structural materials.

5.2 Effect of Decontamination on Materials Properties

The effect of decontamination and thus decontaminant agent on material properties is discussed in this section of the work. The discussion will be divided into several parts: effect of decontamination on surface chemical composition change, effect of decontamination on weight change and surface roughness, effect of decontamination on surface microstructural change, and effect of decontamination on mechanical properties of aircraft metallic structural materials.

5.2.1 Effect of Decontamination on Surface Composition Change

The nominal chemical composition and the chemical composition determined by EDS analysis (JEOL JSM 7000F) of the aircraft metallic structural material surfaces is shown in Table VI, Table VII, and Table VIII for 2024-T3 aluminum alloy, 7075-T6 aluminum alloy, and austenitic stainless steel 304, respectively. In general, the average surface chemical compositions of 2024-T3 and 7075-T6 aluminum alloys were almost unaffected by VHP exposure and liquid hydrogen peroxide dip testing. However, an apparent effect on the surface chemical composition change of large intermetallic particles containing copper was found on 2024-T3 aluminum alloy after 168 hours of dip testing as can be seen in Table VI. This copper is the main alloying element in 2024 aluminum alloy. It is suspected that redeposition and/or dissolution of copper might occur

during the dip testing since the composition decreases by around 29% as compared to the as-received sample. For 7075-T6 aluminum alloy, there was no significant statistical difference. However, a small change in the composition of intermetallic particles containing copper was also observed as can be seen in Table VII. However, almost there was no effect in the zinc composition, the main alloying element in this 7075-T6 aluminum alloy.

As has been mentioned in the previous section, in general, these two age hardenable aluminum alloys are much less corrosion resistant than pure aluminum. This would be understandable since microflaws due to the nature and discontinuity of oxide scale in the surface oxide film, induced by alloying elements, might exist. Furthermore, it needs to be noted that the two main alloying elements, copper and zinc, on the large intermetallic particles behave differently with respect to the hydrogen peroxide, in which copper seems to be more vulnerable to hydrogen peroxide as compared to zinc. This difference might be explained by the fact that copper and zinc differ widely in terms of their solid-state solubility in aluminum: solid solubility of copper is much smaller than that of zinc [204]. This solid solubility difference would affect the formation of intermetallic particles in the alloys. In this case, within aluminum alloys, copper would be more likely to form intermetallic particles as compared to zinc. At the same time, the electrochemical potential reduction of these two elements also differs: copper has +0.34 volts while zinc has –0.76 volts [112, 189]. In terms of elemental properties, based on this electrochemical potential value, zinc is basically more reactive than copper. However, with this reactivity, zinc reacts readily with oxygen to form an adherent oxide film on its surface, thus protect it from further corrosion attack [205, 206]. Thus, it would

be understandable that copper seems to be more susceptible to hydrogen peroxide compared to that of zinc. For austenitic stainless steel 304, as can be seen from Table VIII, almost no surface chemical change was detected. This material has excellent corrosion resistance; thus, it would be unsurprising that there was almost no change in the surface chemical composition after the treatments.

The small changes in the large intermetallics particles containing copper on this 2024-T3 and 7075-T6 aluminum alloys may not have a major effect for short time periods, especially on the alloys mechanical properties. However, in the long term, it might induce corrosion to the materials, which further trigger fatigue crack initiation resulting in catastrophic failure. Because of that there is a need for more investigation on the effect of this composition change on fatigue life after decontamination has been done (see section 7 on the Suggestions for Future Work).

Table VI. Nominal chemical compositions [141] and chemical compositions obtained experimentally using EDS analysis for 2024-T3 aluminum alloy, wt.%. Standard deviations (5 samples), given for elements of interest only, are in parenthesis.

	Al	Cr	Cu	Fe	Mg	Mn	Si	Ti	Zn
Nominal	Bal.	0.1	3.8-4.9	0.5	1.2-1.8	0.3-0.9	0.5	0.15	0.25
As-received	93(1)	0	4(1)	<1	2	<1	0	<1	0
As-polished									
Average	92(1)	0	6(1)	<1	1	1	0	<1	0
Spot on Matrix	93(1)	<1	4(0)	0	1	<1	0	<1	0
Spot on Particle	23(10)	0	68(14)	3	3	2	<1	0	0
Polished VHP 25 run									
Average	92(1)	0	6(1)	0	2	1	0	0	0
Spot on Matrix	93(1)	0	5(0)	0	1	1	0	0	0
Spot on Particle	23(9)	0	68(12)	5	1	3	1	0	0
Polished 168h Dip									
Average	91(1)	0	6(1)	<1	1	1	0	0	<1
Spot on Matrix	93(1)	0	5(0)	<1	1	1	0	<1	0
Spot on Particle	40(9)	0	48(12)	3	6	2	1	0	0
Polish-Etched									
Average	92(1)	0	6(1)	<1	1	1	0	<1	<1
Spot on Matrix	93(1)	0	5(1)	<1	1	1	0	<1	<1
Spot on Particle	88(6)	<1	9(5)	1	2	1	0	<1	<1

Table VII. Nominal chemical compositions [141] and chemical compositions obtained experimentally using EDS analysis for 7075-T6 aluminum alloy, wt.%. Standard deviations (5 samples), given for elements of interest only, are in parenthesis.

	Al	Cr	Cu	Fe	Mg	Mn	Si	Ti	Zn
Nominal	Bal.	0.18-0.28	1.2-2	0.5	2.1-2.9	0.3	0.4	0.2	5.1-6.1
As-received	89(0)	<1	2(0)	<1	3	0	0	0	6(0)
As-polished									
Average	89(1)	<1	2(0)	<1	2	0	0	<1	6(0)
Spot on Matrix	89(0)	<1	2(0)	<1	3	0	0	<1	6(0)
Spot on Particle	47(5)	3	15(10)	28	<1	<1	2	0	5(2)
Polished VHP 25 run									
Average	89(1)	0	2(1)	0	2	0	0	0	6(0)
Spot on Matrix	89(1)	0	2(0)	0	2	0	0	0	7(1)
Spot on Particle	46(3)	3	16(13)	27	0	1	2	0	5(1)
Polished 168h Dip									
Average	89(0)	<1	2(0)	<1	2	0	0	<1	7(0)
Spot on Matrix	89(0)	<1	2(0)	<1	2	0	0	<1	7(0)
Spot on Particle	47(6)	3	12(7)	31	0	<1	1	0	5(4)
Polish-Etched									
Average	88(0)	<1	2(0)	<1	2	<1	0	<1	7(0)
Spot on Matrix	89(0)	<1	2(0)	<1	2	0	0	<1	7(0)
Spot on Particle	88(0)	<1	2(0)	<1	2	0	0	<1	7(0)

Table VIII. Nominal chemical compositions [151] and chemical compositions obtained experimentally using EDS analysis for austenitic stainless steel 304, wt.%. Standard deviations (5 samples) of all the large composition elements are below 0.5.

	C	Co	Cr	Fe	Mn	Mo	N	Nb	Ni	P	S	Si
Nominal	0.08	0	18-20	Bal	2	0	0.1	0	8-10.5	0.045	0.03	0.75
As-received	0	1	18	71	1	<1	0	0	8	0	<1	<1
As-polished												
Average	0	1	17	71	2	0	0	0	9	0	0	0
Spot	0	1	17	71	2	0	0	0	9	0	0	0
Polished VHP 25 run												
Average	0	<1	17	71	2	0	0	0	9	0	0	0
Spot	0	<1	17	71	2	<1	0	0	9	0	0	0
Polished 168h Dip												
Average	0	<1	17	71	2	<1	0	0	9	0	0	0
Spot	0	1	17	71	2	0	0	0	9	0	0	0
Polish-Etched												
Average	1	1	20	68	1	1	0	<1	6	<1	0	1
Spot	1	1	20	68	1	1	0	<1	6	<1	0	1

5.2.2   Effect of Decontamination on Weight Change and Surface Roughness

Figure 17 shows the graphs of surface roughness of the materials after dip testing at two different temperatures (a) and surface roughness of the materials after VHP exposure and dip testing (b). As can be seen in Figure 17 (a), statistically there was no significant difference between dip testing at room temperature (22°C) and under refrigeration (-2°C). These two treatments at different temperatures were performed to find the effect of temperature on the decontamination. As has been mentioned in the previous section, at room temperature hydrogen peroxide would be relatively unstable and the reaction with metallic samples should be relatively rapid, while at lower temperature hydrogen peroxide would be relatively stable and the reaction with metallic samples would be slower. Technically, the treatments are also important in terms of environmental conditions. The initial ambient conditions, Alaska in the winter versus Florida in the summer, for example, could be important because the decontamination process might give different effects on the same aircraft structural materials.

At room temperature, no significant difference was observed for the surface roughness before and after treatments for both dip testing and VHP exposure; however, as can be seen from the surface roughness graph in Figure 17 (b), the 2024-T3 aluminum alloy surface roughness tends to decrease. This material also exhibits the largest weight change among the three metal alloys, as can be seen in Figure 18 (a). The change in surface roughness was interesting to note in its relation to the previous works on the attachment of *Listeria monocytogenes* to the austenitic stainless steel 304, which have shown that surface roughness at some point affected the way bacteria attached to the

surface. Thus, in its relation to the decontamination, there was a concerned that it could conceivably affect the decontamination process as well [47-48].

Figure 18 shows the graph of weight change of the materials after exposure and dip testing (a) and intermetallic coarse particle size data change for 2024-T3 and 7075-T6 aluminum alloys after dip testing (b). The horizontal lines on the weight change graph in Figure 18 (a) show the limit of measurable percentage weight changes for combination of balance and sample employed. In the case of liquid hydrogen peroxide dip testing, very small amount of changes were observed but there was no significant difference observed between single VHP exposure (4.8 hours) and 24 hours dip testing. There was also no significant difference observed between refrigeration temperature (-2°C) and room temperature (22°C); however, there was a significant difference observed between 24 hours dip-testing and 168 hours dip testing. For the 2024-T3 and 7075-T6 aluminum alloys, some weight loss was observed following dip testing to the liquid hydrogen peroxide as can be seen in Figure 18 (a). This weight loss, even it was very minor about 0.04% macroscopically, might be able to explain the change in large intermetallic particles size as can be seen in Figure 18 (b). Figure 19 shows particle size distribution for 2024-T3 (a) and 7075-T6 (b) aluminum alloys before and after dip testing. As can be seen from the figures, there is an indication that the coarse particle size indeed has changed with the shifting of Feret diameter to the left after the dip testing. Furthermore, it would be much clearer if this weight loss is also correlated with the surface chemical compositional change of large intermetallic particle containing copper as has been mentioned previously.

117

Different from the liquid hydrogen peroxide testing, which dissolved some of the elements from the surface, in the case of VHP exposure, the situation appears to be a little more complicated. As can be seen in Figure 18 (a), multiple cycles of VHP exposures result in a small weight gain around 0.01% and 0.02% for 2024-T3 and 7075-T6 aluminum alloys respectively. The increase on this weight change seems to indicate a limited amount of oxidation on the surface of aluminum alloys by the vapor of hydrogen peroxide. However, the oxidation product could not be confirmed under SEM; it may be still too thin to observe within the limit of SEM and so the validity of this indication is still uncertain at the present time. On the contrary, unlike multiple VHP cycles, a single VHP run results in a very small (< 0.01%) weight loss but statistically was insignificant. For the austenitic stainless steel 304, almost no weight change was observed for the VHP exposure; however, a very small (< 0.01%) and insignificant weight loss after 168 hours dip testing was also observed.
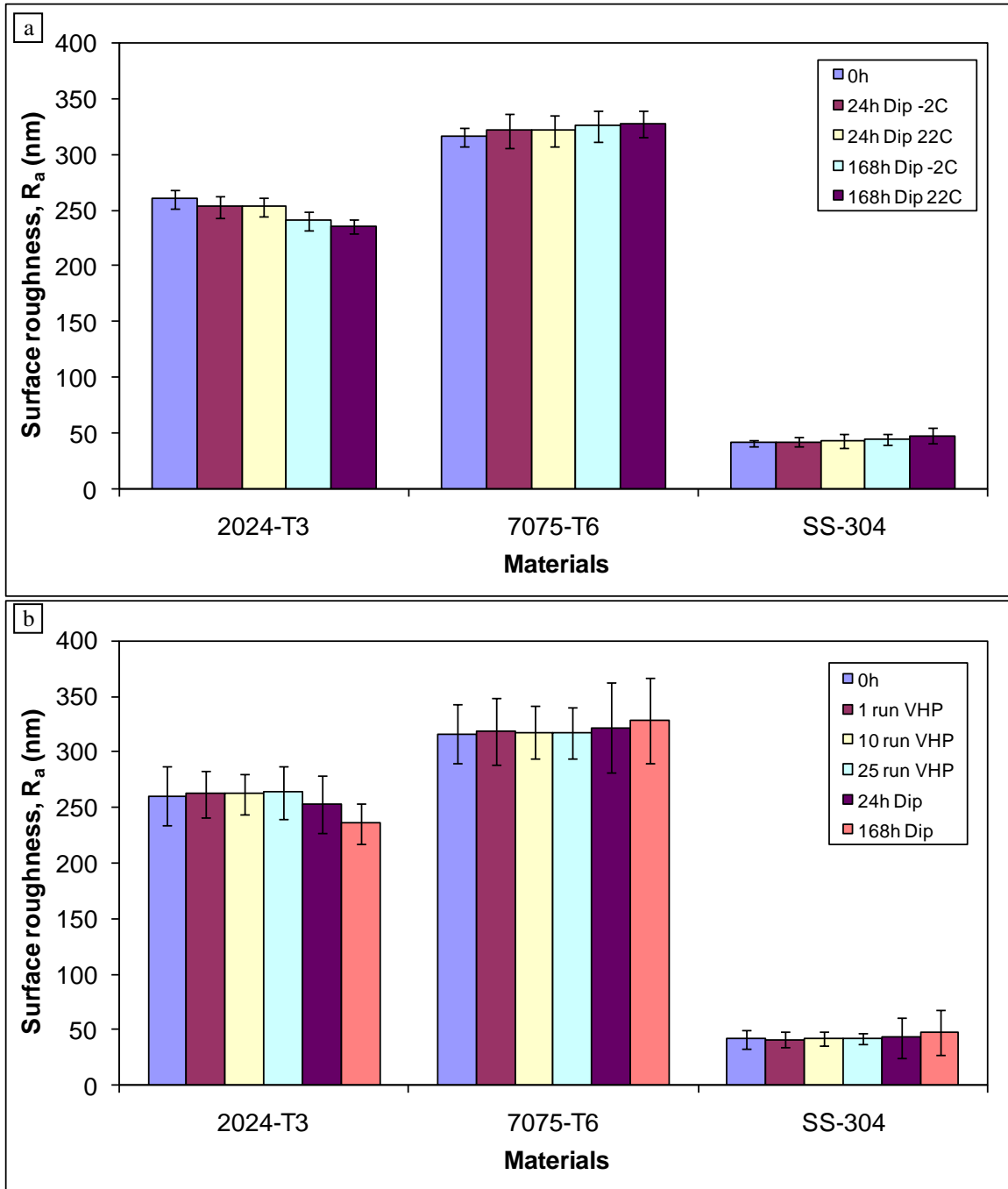
Figure 17–Surface roughness of the materials after dip testing at two different temperatures (a) and after VHP exposure and dip testing at room temperature (b). The error bar for each of the graphs shows the standard deviations from 5 samples.
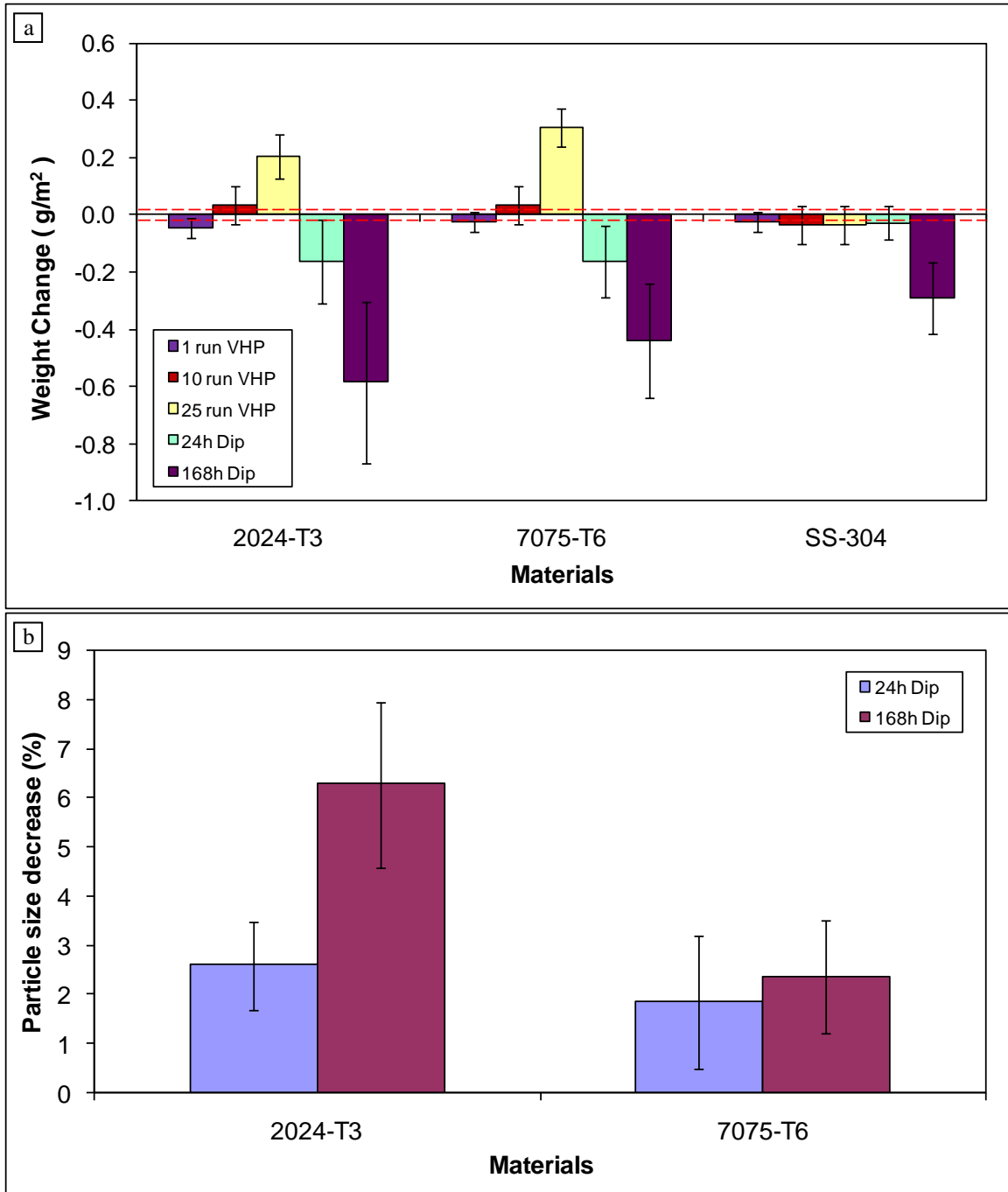
Figure 18–Weight change of the materials after exposure and dip testing (a) and coarse particle size data change for 2024-T3 and 7075-T6 aluminum alloys after dip testing (b). The horizontal lines on the weight change graph show the limit of measurable percentage weight changes for combination of balance and sample employed.The error bar for each of the graphs shows the standard deviations from 5 samples.
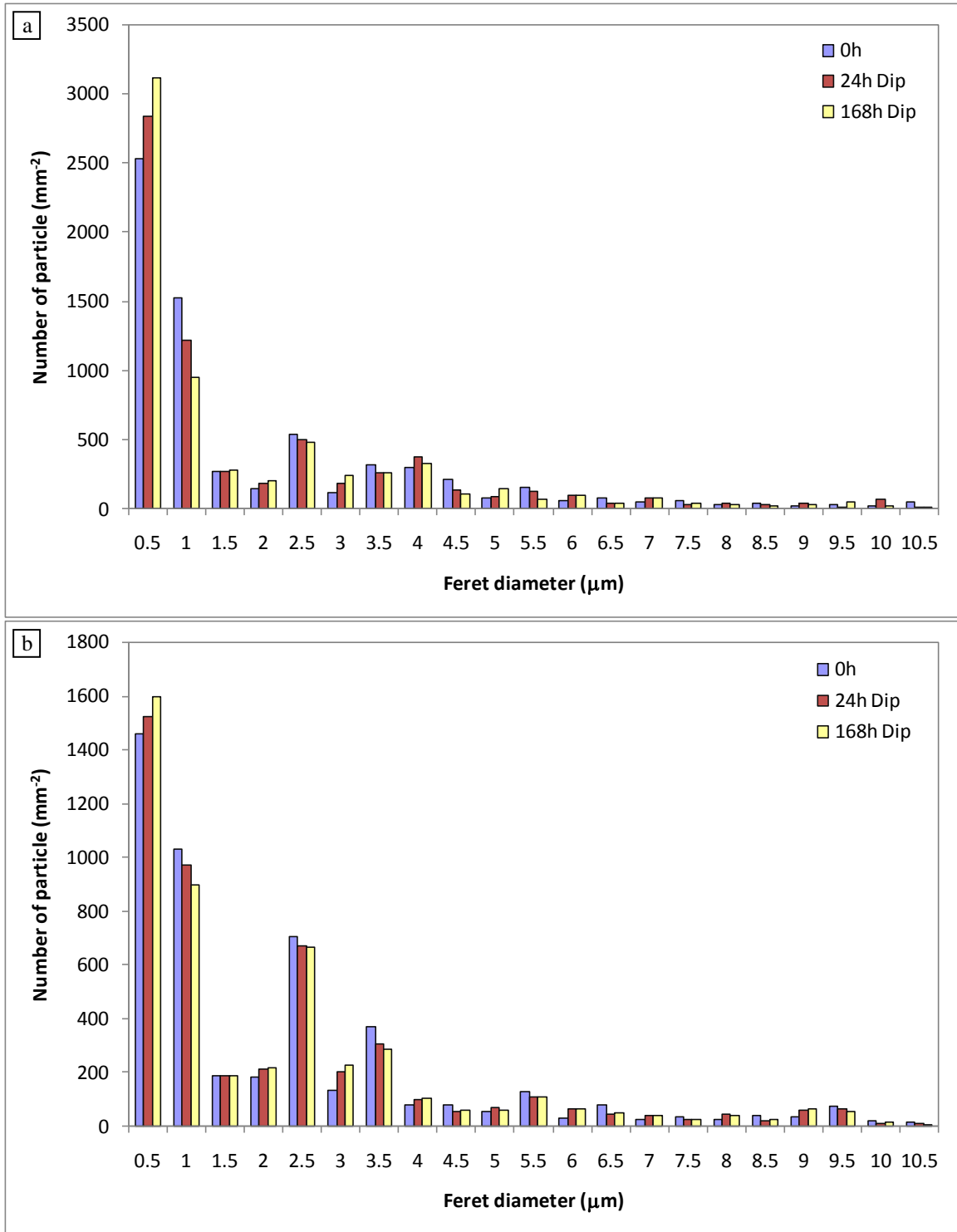
Figure 19–Particle size distribution of 2024-T3 aluminum alloy (a) and 7075-T6 aluminum alloy (b) before and after dip testing.

5.2.3 Effect of Decontamination on Surface Microstructural Change

Figure 20 shows light microscopy images of 2024-T3 aluminum alloy (top), 7075-T6 aluminum alloy (middle), and austenitic stainless steel 304 (bottom). Left to right is as-received, as-polished, and polish-etched, respectively. These figures are shown as a reference for the microstructure of the materials after treatments. Secondary electron images of the microstructure can be seen in Figure 21 that shows microstructures of the materials before and after dip testing; 2024-T3 aluminum alloy (above), 7075-T6 aluminum alloy (middle), and austenitic stainless steel 304 (below). Left to right is as-polished, dip testing for 24 hours, and 168 hours respectively. No surface microstructural changes, including grain boundaries, were apparent after VHP exposure or liquid hydrogen peroxide dip testing as can be seen in Figure 22 and Figure 23; but small change in particle size from intermetallic containing copper were observed after dip testing around 2.5-6% and 2-2.5% for 2024-T3 and 7075-T6, respectively, as can be seen in Figure 18 (b) and representative SEM pictures in Figure 23. It needs to be mentioned, however, the particles in consideration encompass only the coarse insoluble particles that have the range size from ~ 1 – 10 µm.
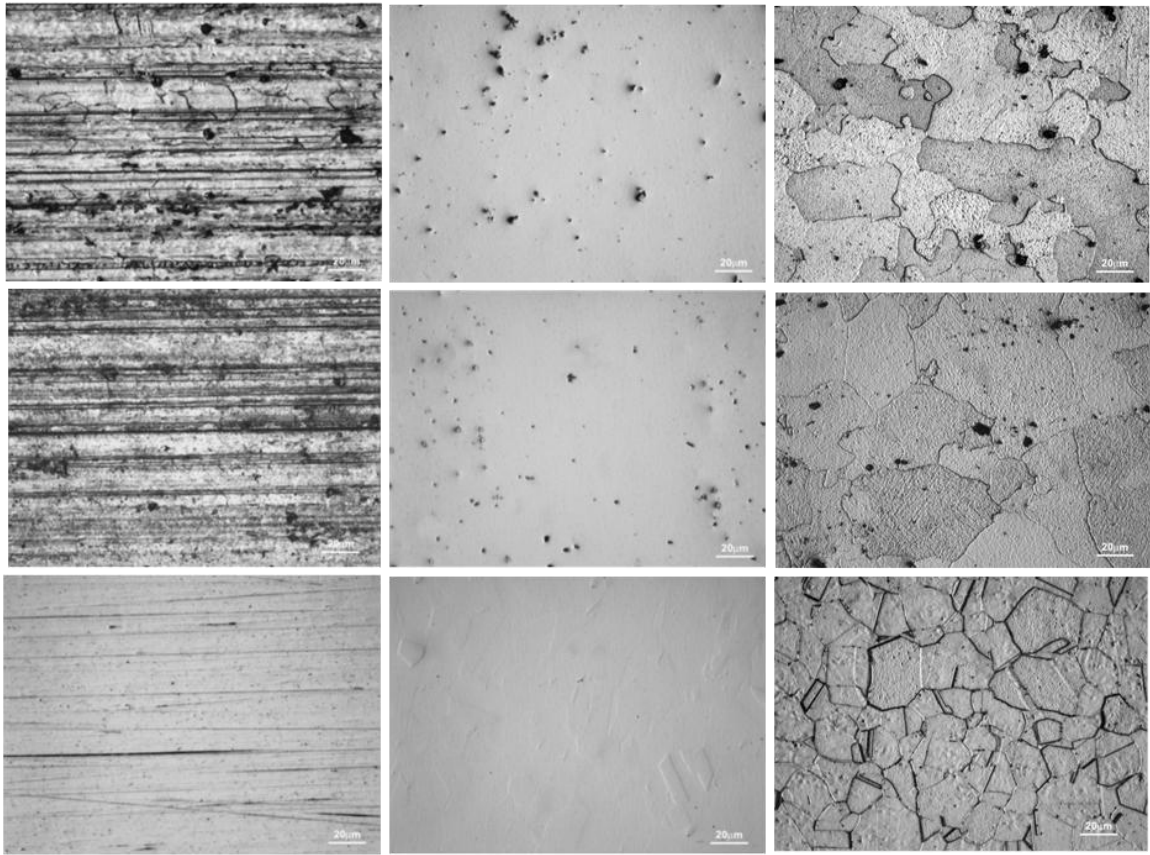
Figure 20–Light microscopy images of 2024-T3 aluminum alloy (top), 7075-T6 aluminum alloy (middle), and SS-304 (bottom). Left to right is as-received, as-polished, and polish-etched materials respectively.
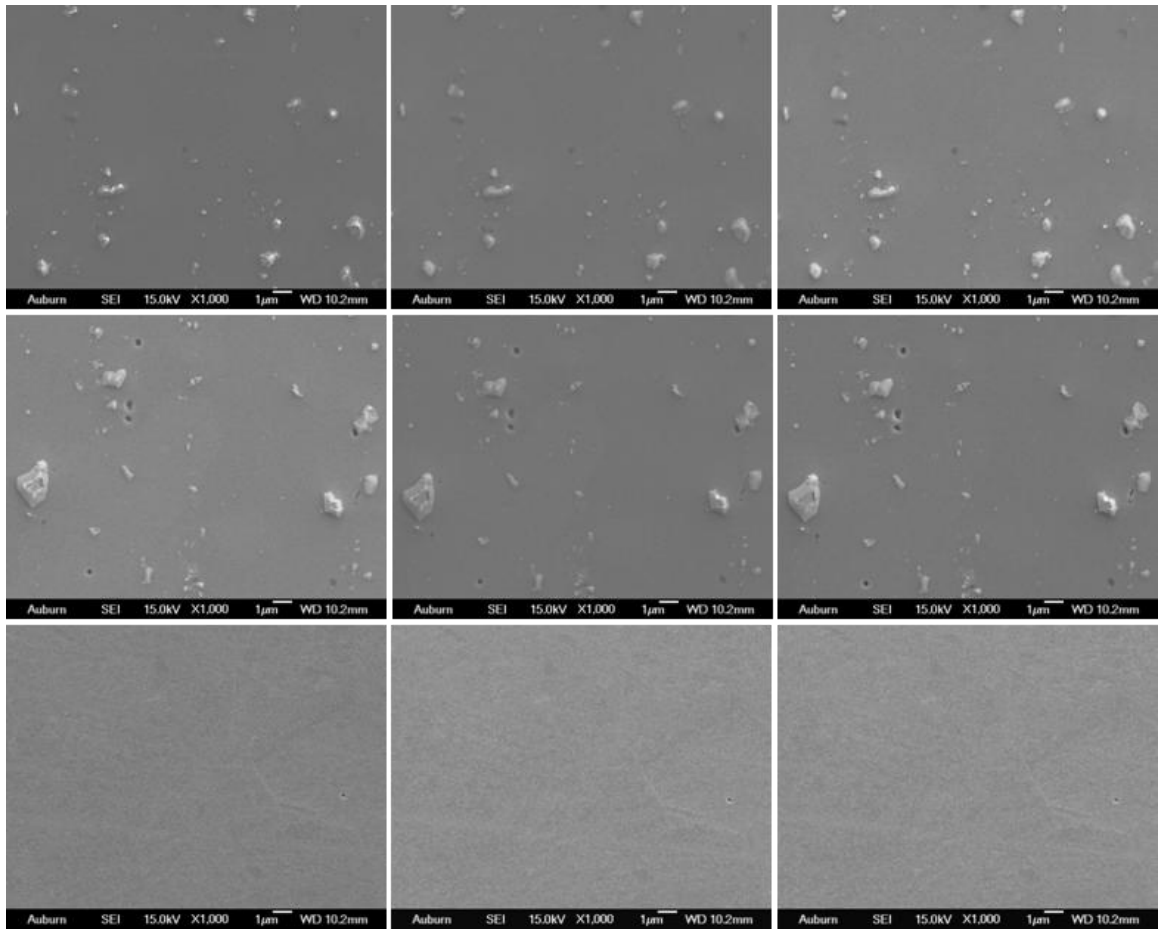
Figure 21–Secondary electron images of 2024-T3 aluminum alloy (above), 7075-T6 aluminum alloy (middle), and SS-304 (below). Left to right is as-polished, dip testing for 24 hours, and 168 hours respectively.

Figure 22–Secondary electron images of intermetallic particles on the surface of 2024-T3 aluminum alloy (top) and 7075-T6 aluminum alloy (bottom) after VHP exposure. Left to right is as-polished, 10-cycle, and 25-cycle respectively.

Figure 23–Secondary electron images of intermetallic particles on the surface of 2024-T3 aluminum alloy (top) and 7075-T6 aluminum alloy (bottom) after dip testing. Left to right is as-polished, dip testing for 24 hours, and 168 hours respectively.

5.2.4   Effect of Decontamination on Mechanical Properties

5.2.4.1 Microhardness and Nanohardness Testing

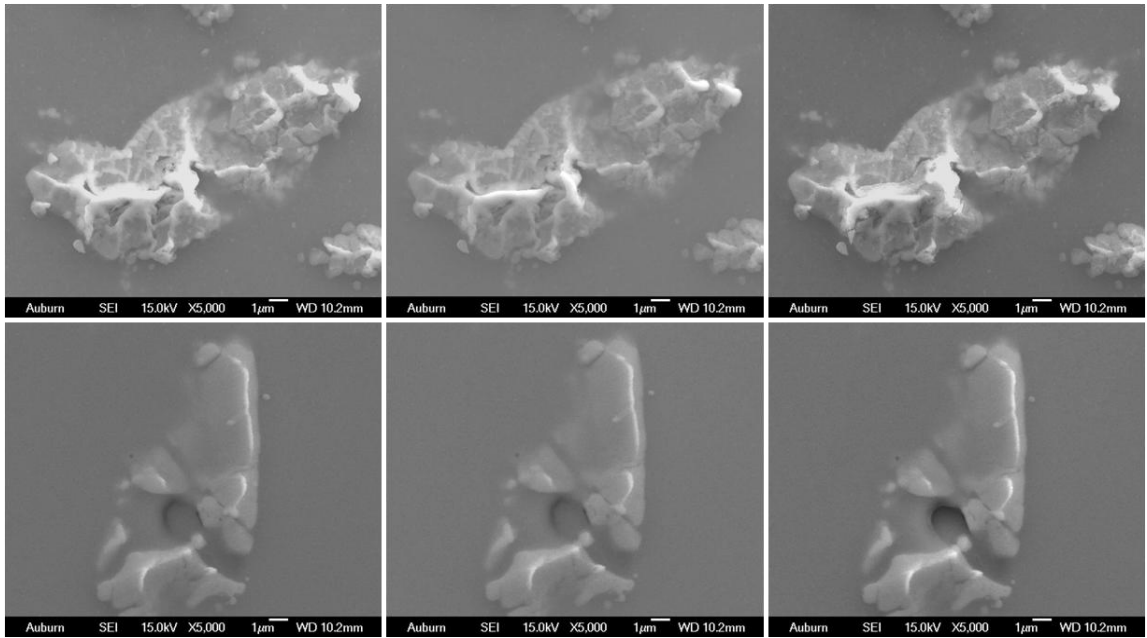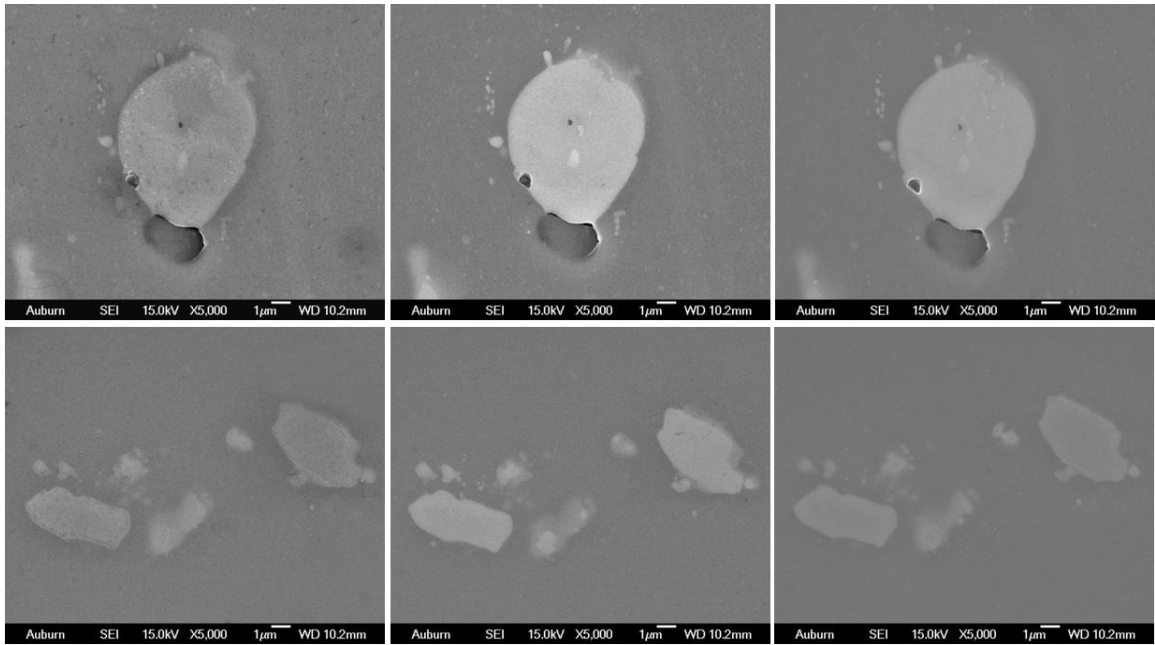Figure 24 shows graphs of Vicker's microhardness (a) and nanohardness from nanoindentation (b) of the materials before and after treatments of VHP exposure and liquid hydrogen peroxide dip testing. No significant difference was found for all of the materials; however, compared to the as-received specimen, there was a consistent decrease of hardness after dip testing observed for 2024-T3 aluminum alloy from both of the testing, but not after the VHP exposure. As can be seen from the microhardness data in Figure 24 (a), there is no apparent trend towards surface softening observed after both VHP exposure and dip testing for 7075-T6 aluminum alloy despite the fact that there was also a loss of some copper from coarse intermetallics particles on the surfaces of this material as has been mentioned in the previous part. Softening on the surface of the austenitic stainless steel 304 material was also not observed in the microhardness measurements.

In the case of nanohardness, nanoindentation testing suggested that there may be some softening on the exposed surface for 2024-T3 after dip testing as can be seen in Figure 24 (b). In this case, dissolution of copper on the surface after dip testing seems to affect the hardness very close to the surface of this 2024-T3 aluminum alloy. On the contrary, since the main alloying element in 7075-T6 aluminum alloy is zinc, which was not affected by the dip testing, it would be reasonable to say that the hardness of this 7075-T6 aluminum alloy would not be significantly affected. Furthermore, since the strength of material is usually dominated by the fine intermetallics particle produced by age hardening, it would be unsurprising that even some loss of copper from

intermetmallic coarse particles occurred; the softening close to the surface after dip testing was insignificant. For the austenitic stainless steel 304, given the corrosion resistance and high strength of this material, there was almost no effect of the dip testing to the surface hardness of this material.
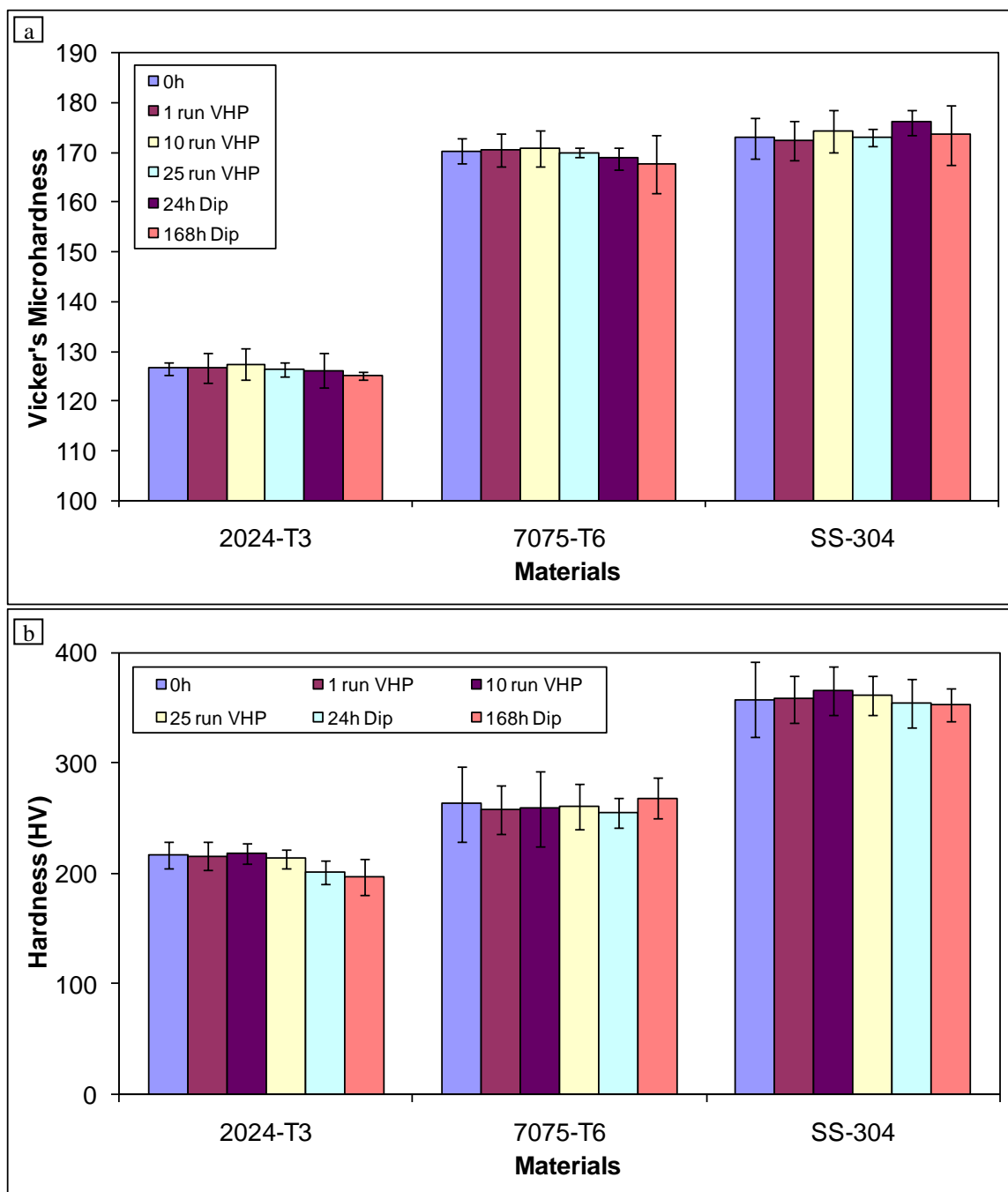
Figure 24–Vicker's microhardness (a) and nano indentation (b) of the materials before and after exposure. The error bar for each of the bar graphs shows the standard deviations from 5 samples.

5.2.4.2 Tensile Testing

Figure 25, Figure 26, and Figure 27 show 0.2% offset yield stress, ultimate tensile strength, and elongation to failure of longitudinal (a) and transversal (b) directions, respectively, of tensile test specimens before and after treatments of VHP exposure and dip testing on the 2024-T3 and -T6, 7075-T6, and austenitic stainless steel 304. Statistical results showed that there were no significant differences between the treatments and the un-exposed material for both the aluminum alloys and austenitic stainless steel 304. As can be seen from the figures, there was no pattern, systematic effect of exposure by increasing severity from single VHP exposure up to 168 hour of dip testing on the tensile properties of any of the materials under the condition examined.

If this result is correlated to the hardness, in which there was some effect on the hardness very close to the surface of 2024-T3 after dip testing; however, since the influence was only in the vicinity very close to the surface area, it would be unsurprising that there was no effect of the liquid hydrogen peroxide dip testing on the tensile properties, given the result of tensile properties would be dominated by the total load of the cross section. It would be also unsurprising that the highly ductile, corrosion resistant austenitic stainless steel 304 was also unaffected by either VHP exposure or liquid hydrogen peroxide dip testing on its tensile properties.

As has been mentioned in the previous section, to ascertain the effects of composition versus heat treatment on the mechanical properties, some of the 2024-T3 aluminum alloy specimens were reheat-treated into 2024-T6 aluminum alloy. Results of the tensile testing on this 2024-T6 aluminum alloy showed that both VHP exposure up to 25-cycle and liquid hydrogen peroxide dip testing up to 168 hours did not have any

appreciable effect on the 2024-T6 aluminum alloy. However, as can be seen in Figure 25 and Figure 26, reheat-treating of 2024-T3 into 2024-T6 lowered the ultimate tensile strength of around 7% and 5% for longitudinal and transversal direction, respectively, but increased yield stress of around 2% and 13% for longitudinal and transversal direction, respectively. Elongation to failure also decreased around 46% and 49% for longitudinal and transversal direction, respectively, as can be seen in Figure 27.

Figure 25–Charts are the 0.2% offset yield stress of the longitudinal (a) and transversal (b) direction of the materials tensile specimens before and after exposure and dip testing. The error bar for each of the bar graphs shows the standard deviations from 10 samples.

Figure 26–Charts are ultimate tensile strength of the longitudinal (a) and transversal (b) direction of the materials tensile specimens before and after exposure and dip testing. The error bar for each of the bar graphs shows the standard deviations from 10 samples.
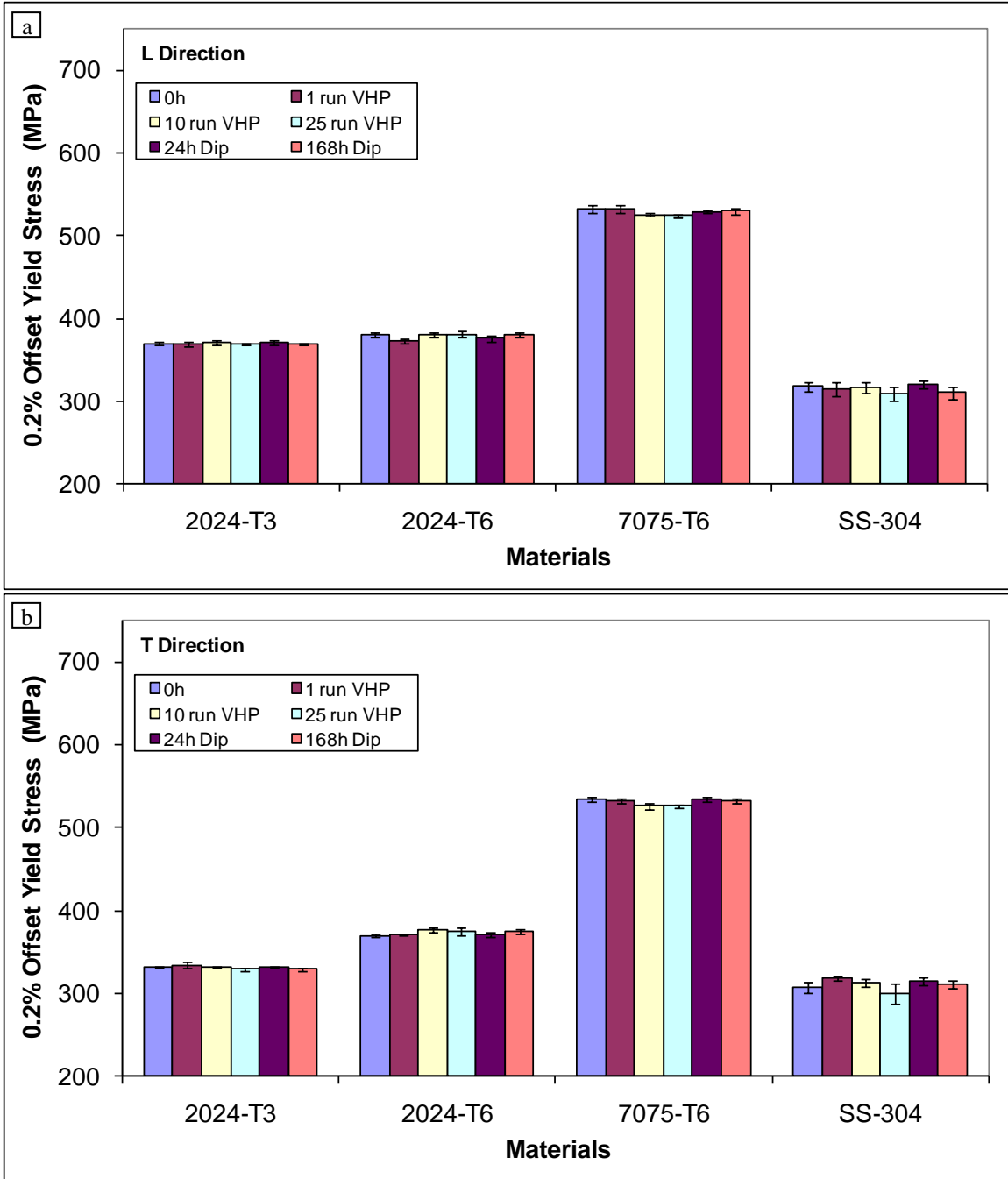
Figure 27–Charts are elongation to failure of the longitudinal (a) and transversal (b) direction of the materials tensile specimens before and after exposure and dip testing. The error bar for each of the bar graphs shows the standard deviations from 10 samples.
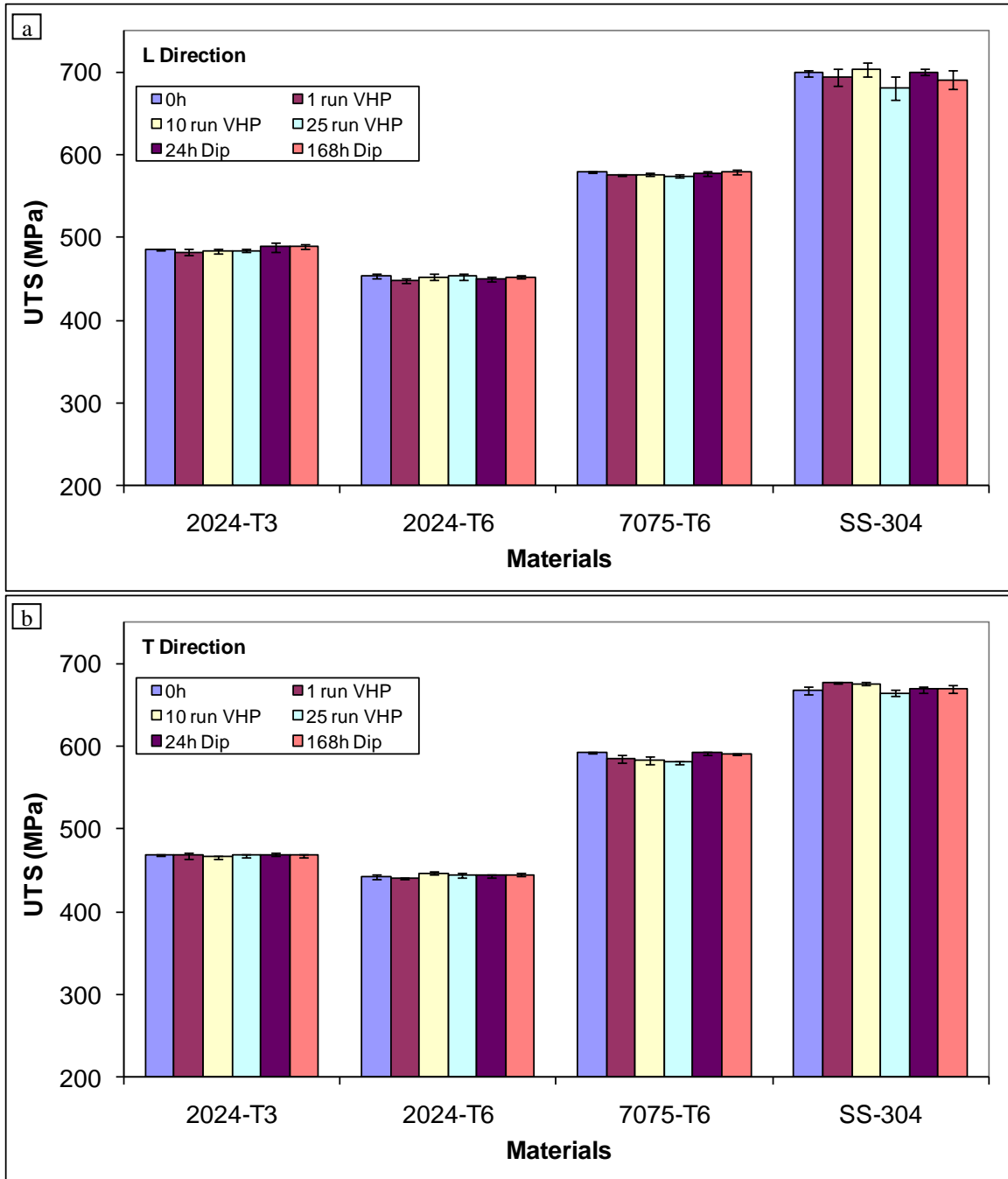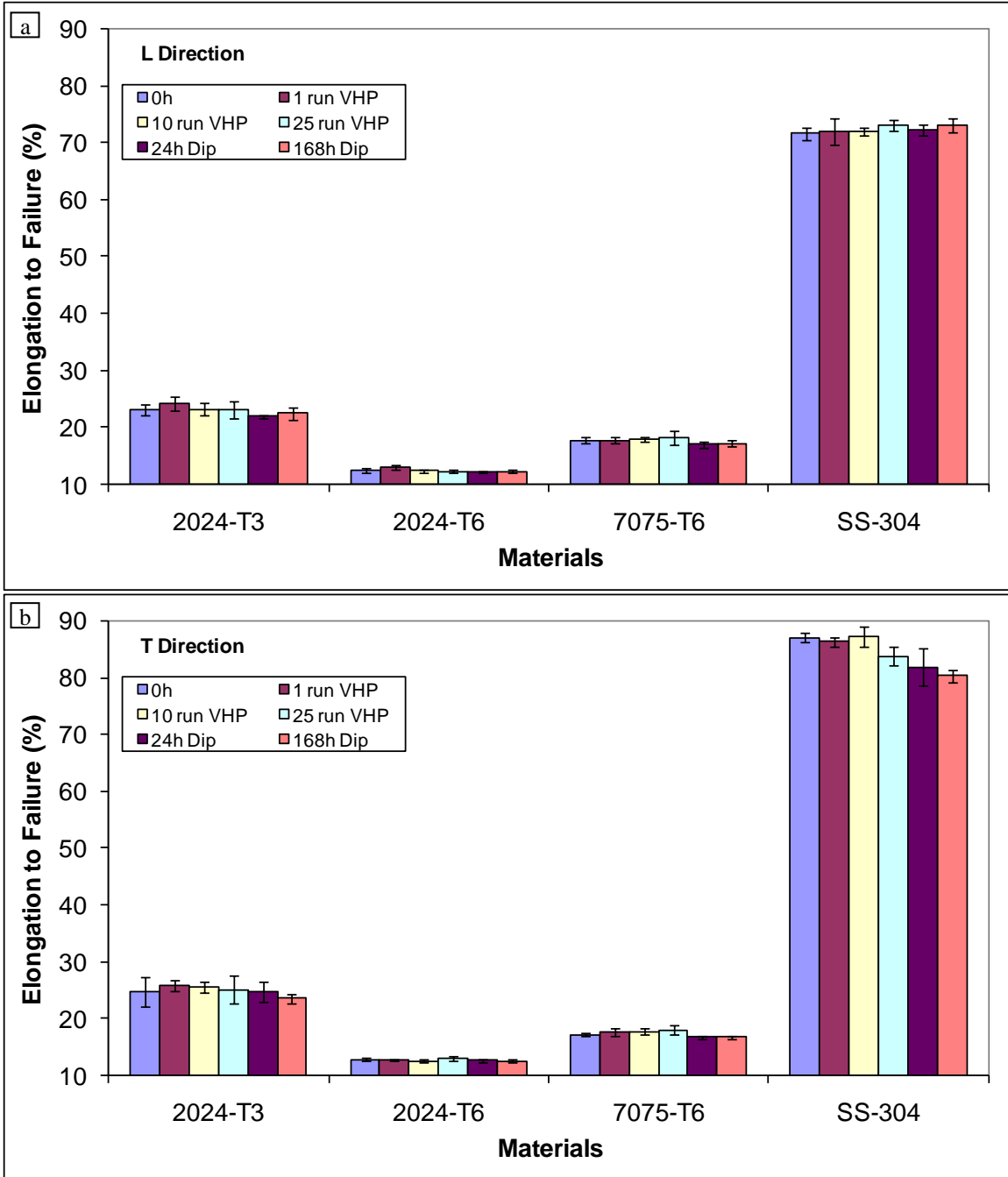
Secondary electron images of 2024-T3 aluminum alloy, 7075-T6 aluminum alloy, and austenitic stainless steel 304 in the longitudinal direction after tensile testing are given in Figure 28, Figure 29, and Figure 30 respectively. From each of the figure, top figures are machined sides; middle figures are plan-edge close to the fracture surface; and fracture surfaces are on the bottom. Left to right are the as-received, 25-cycle of VHP exposure, and 168 hours of dip testing, respectively. In a thin body, such as used in the aircraft fuselage, a condition of plane stress is much more dominant than plane strain condition. In this case, the stress through the thickness cannot vary appreciably as compared to a thick body, where the material is constraint due to the thickness resulting in a plane strain condition. Because of that, in a thin specimen, the state of stress tends to biaxial and the material fractures in a characteristic ductile manner, with a 45° shear lip being formed at each free surface [207].

For 2024-T3 aluminum alloy, as can be seen from the machined sides of the tensile specimens (top part in Figure 28), more cleavage cracks are observed the more severe the treatments from the as-received up to 168 hours of dip testing. Crack developments are also apparent on the plan-edge surfaces of the tensile specimens. However, as can be seen from the 0.2% yield stress and ultimate tensile strength in Figure 25 and Figure 26, both in longitudinal and transversal direction, there was no evident that this crack development had any effect on the mechanical properties. For the 7075-T6 aluminum alloy, as can be seen in Figure 29, like what has been found in 2024-T3 aluminum alloy, shows only a moderate ductility; however there was no trend in the crack development. Austenitic stainless steel 304, as can be seen in Figure 30 in both machined side and plan-edge, shows a classic ductile elongation of failure as expected.

135

On the fracture surfaces, as can be seen on the bottom part of Figure 28 and Figure 29, both 2024-T3 and 7075-T6 aluminum alloys showed porosity with fairly ductile fracture; however, there was not much difference that can be observed among the samples before and after treatments. Despite the fact that crack propagation of 2024-T3 aluminum alloy was observed on the machined side as mentioned previously, there was no indication that either VHP exposure or liquid hydrogen peroxide dip testing had an effect on this propagation of failure. The fracture surface of the austenitic stainless steel 304, as can be seen in the bottom part of Figure 30, again shows a classic ductile fracture as expected.

In terms of overall effects of decontamination, and thus the effect of hydrogen peroxide as a decontaminant agent, on the properties of aircraft metallic structural materials, results of the testing in general are promising. Most of the results under the condition examined including microstructure and mechanical properties, even under the most severe circumstances that could occur; in this case prolonged dip testing to the liquid concentrated hydrogen peroxide up to 168 hours, showed that only very limited damage was observed. However, as has been mentioned previously, even very small damage, with combination of fatigue and corrosion attack could result in catastrophic failure. In addition, it needs to be noted that the range of materials examined is still inadequate to cover all of complex aircraft structural materials. Thus, further work is needed as can be read in detail in section 7, "Suggestions for Future Work".
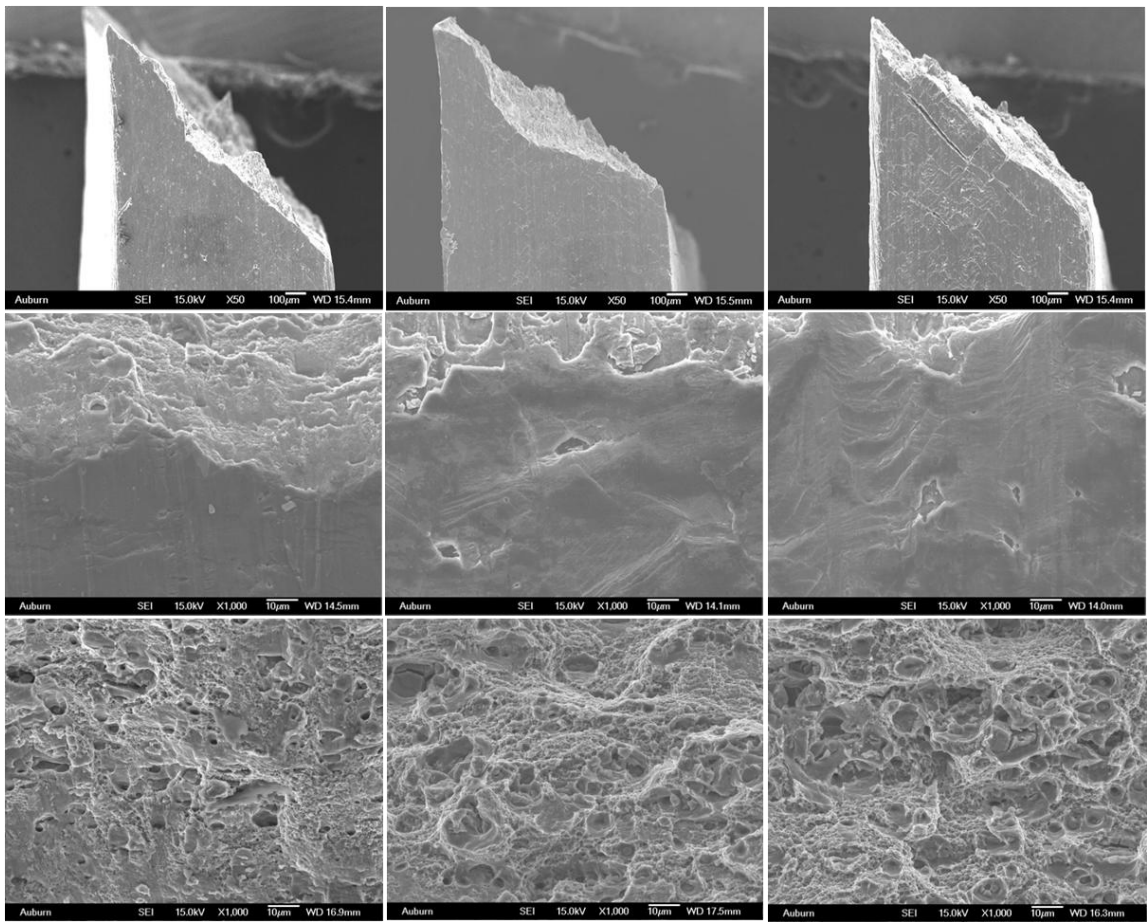
Figure 28–Secondary electron images of 2024-T3 aluminum alloy on the longitudinal direction after tensile testing: machined side (top), plan-edge (middle), and fracture surfaces (bottom). Left to right is the as-received, 25-cycle VHP exposure, and 168 hours of dip testing, respectively.

Figure 29–Secondary electron images of 7075-T6 aluminum alloy on the longitudinal direction after tensile testing: machined side (top), plan-edge (middle), and fracture surfaces (bottom). Left to right is the as-received, 25-cycle VHP exposure, and 168 hours of dip testing, respectively.

Figure 30–Secondary electron images of austenitic stainless steel 304 on the longitudinal direction after tensile testing: machined side (top), plan-edge (middle), and fracture surfaces (bottom). Left to right is the as-received (a), 25-cycle VHP run (b), and 168 hours of dip testing (c), respectively.
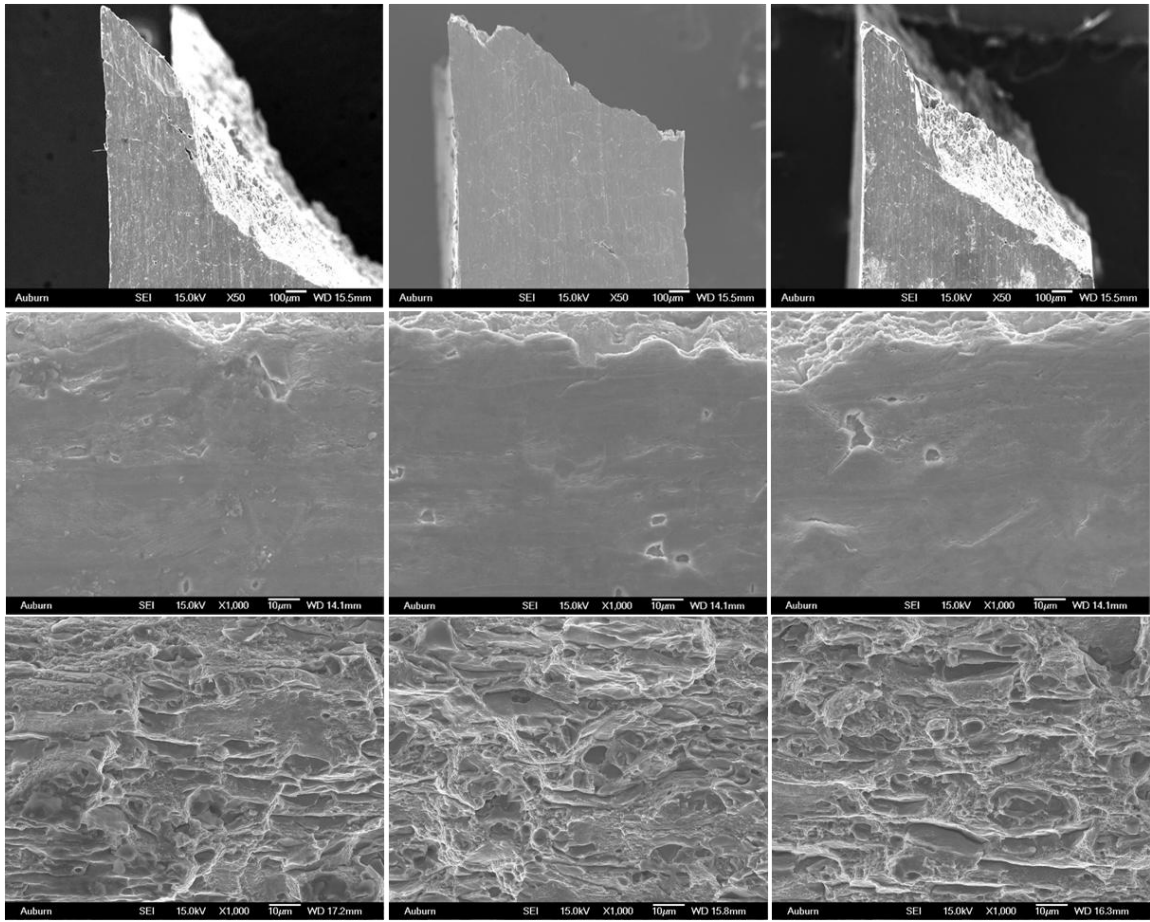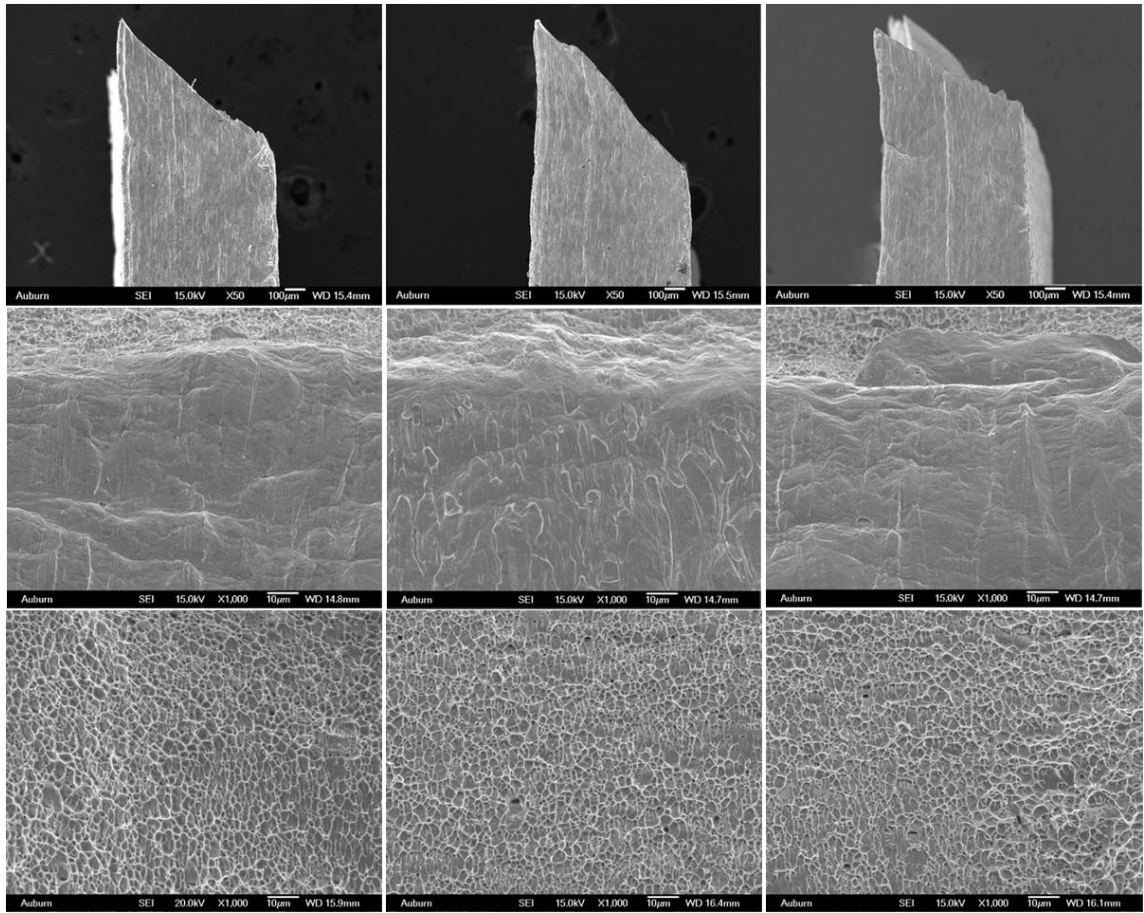
5.3 Copper Dissolution in Hydrogen Peroxide

In this work, copper dissolution was assessed by using powder method, in which copper powder particle was dissolved into 35% hydrogen peroxide. For the rate modeling, the cube-root model [180-184], which is also called the surface reaction control shrinking core model [185-188], was adopted. As has been mentioned previously, reaction of copper and hydrogen peroxide is basically an oxidative reaction. In the following discussion, the effect of stirring speed and temperature on copper dissolution into hydrogen peroxide is based on this reaction. In order to use the cube-root model, the following assumptions were made:

1. There will be Cu^+ and/or Cu^{2+} in the solution, however these two ions are not differentiated; i.e. the concentration measured is the total concentration of these two ions.

2. Owing to the slight amount of the copper dissolved, the surface geometrical change of the particles was considered to be negligible.

3. The concentration was assumed to be uniform or homogeneous throughout the solution. Because the reaction involves powder particles, it is also assumed that the rate of dissolution of powder particles at the particle surface as the controlling step; the dissolution is therefore proportional to the instantaneous surface area.

As has been mentioned previously, the straight forward cube-root law can be applied when the powder suspension disperse homogeneously in the solution, in this regard plot of $1- (1- [C]_t/[C]_\infty)^{1/3}$ vs. t will be linear with a gradient of $k/(r_0\rho)$, see again Equation 14. In this equation, k is the apparent dissolution rate constant. Activation

energy for the dissolution of copper can be derived from Arrhenius relation, see again Equation 15. In this regard, activation energy is determined by plotting ln k vs. 1/T.

5.3.1   Effect of Stirring

The effect of stirring speed on the copper dissolution was performed in 35% hydrogen peroxide. There were three different stirring speeds and a control, i.e. 250, 550, and 1100 rpm for the maximum time of 3 hours. However, as can be seen in Figure 31, the fraction of copper dissolved becomes constant after one hour of reaction time. At this point, it is suspected that the dissolution process has been limited by the formation of copper hydroxide, which was observed through a precipitation after the solution settled for some time. Because of that, the reactions shown were only for that of maximum time of 60 minutes. Even in the 60 minutes of dissolution time, the fraction of copper dissolved tends to increase with the increase of stirring speed is only of up to about 15 minutes of the reaction time. After this time, the fraction of copper dissolved becomes constant. However, because the final consumption of hydrogen peroxide was not controlled, the exact reason for this constant dissolution cannot be determined at this time. The variation of $1 - (1 - X)^{1/3}$, where X represents the fraction of copper dissolved, in this case $[C]_t/[C]_\infty$ as in Equation 14, with time for various copper dissolution at different stirring speeds is given in Figure 33. Slope of the lines in this variation will be the apparent rate constants of the copper dissolution at different stirring speeds.

The apparent activation energy was determined by carrying out the dissolution at different time and temperature. To reduce the variability in the temperature effect, the

141

subsequent experiments were carried out without mechanical stirring, except at the beginning of reaction for particle suspension homogenization purpose.

5.3.2   Effect of Temperature

As has been mentioned previously, on the effect of temperature, the reaction was performed statically, i.e. no mechanical stirring, except at the beginning of the reaction for the purpose of homogenization of the particle suspension. The rate of copper dissolution by hydrogen peroxide was determined by carrying out the reactions at 5 different temperatures: 283, 293, 303, 313, and 323 K for 3 hours. However, as for the effect of stirring, after one hour of reaction time, the fraction of copper dissolved became constant. Because of that, the reactions showed were only for that of maximum time of 60 minutes. Even in 60 minutes of dissolution time, as can be seen in Figure 32, the fraction of copper dissolved increases with the increase of temperature is only of up to about 15 minutes of the reaction time, after then the fraction of copper dissolved becomes constant. Hence, the activation energy determination from Arrhenius plot was based on the fraction of copper dissolved for the reaction time of up to 15 minutes only.

The variation of $1 - (1 - X)^{1/3}$, where X represents the fraction of copper dissolved, in this case $[C]_t/[C]_\infty$ as in Equation 14, with time for various copper dissolution temperatures is shown in Figure 34. Slope of the lines in this variation will be the apparent rate constant of the copper dissolution. The apparent rate constants obtained from these slopes were then used in Arrhenius equation (Equation 15) to determine the apparent activation energy of 19 kJ/mol as can be seen in Figure 35. The activation energy for copper dissolution in several media has been determined by several

142

investigators: about 5.6 kJ/mol in aqueous ammonia [208], 12.6-16.6 kJ/mol by acidified iron in acetonitrile-water solutions [209], 18.4 kJ/mol in aqueous alkaline 2-2'-dipyridyl solutions [210], 36.3 kJ/mol in acidic ferric sulfate solutions [211], 40 kJ/mol from molybdenite concentrate by sodium dichromate leaching [212], and 54 kJ/mol in monoethanolamine-complexed cupric ion solution [213]. Thus, it is clear that different media solution gives different activation energy due to the change in the reaction pathway [213]. A low value of activation energy, in the range of about 5 kJ up to 45 kJ, is an indication that the mechanism is a diffusion controlled, while a value of activation energy higher than 45 kJ is an indication that the mechanism is a chemical reaction-controlled [187, 208-214]. Since the value of activation energy obtained in this work is in the range of what have been obtained by others, it is assumed that similar dissolution mechanism can be applied to the dissolution of copper into hydrogen peroxide, i.e. diffusion-controlled.
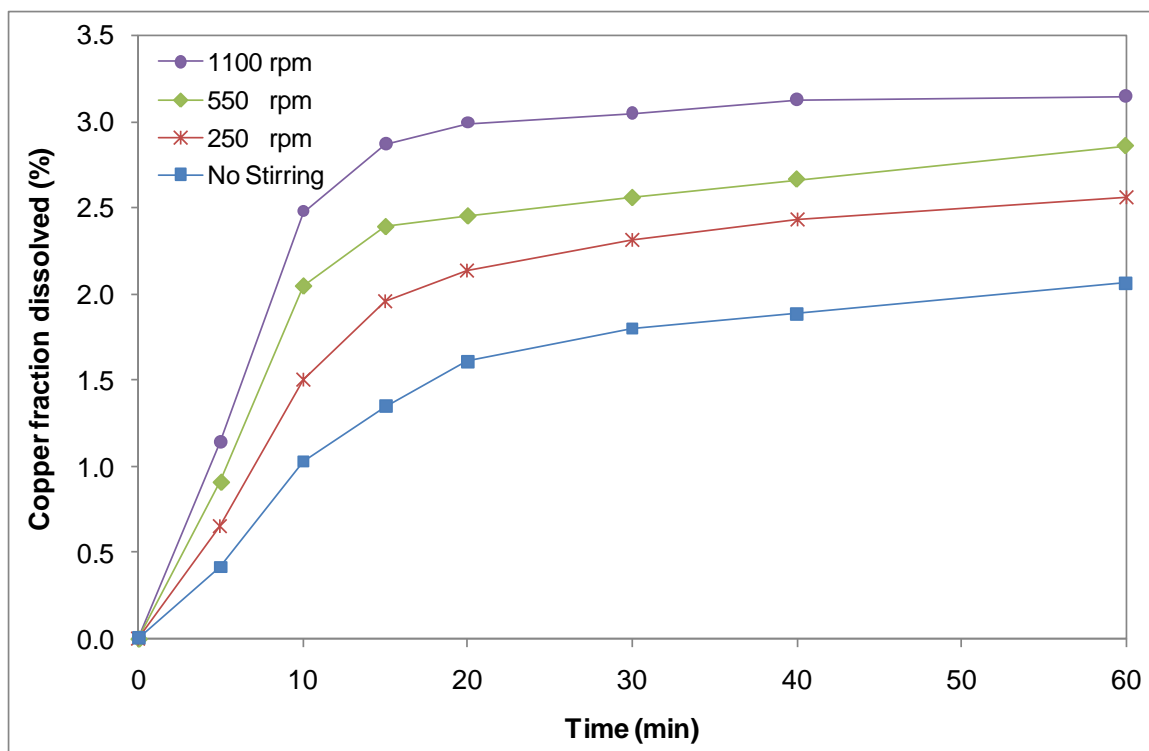
Figure 31–Effect of stirring speed on the fraction of copper dissolved into 35% liquid hydrogen peroxide.
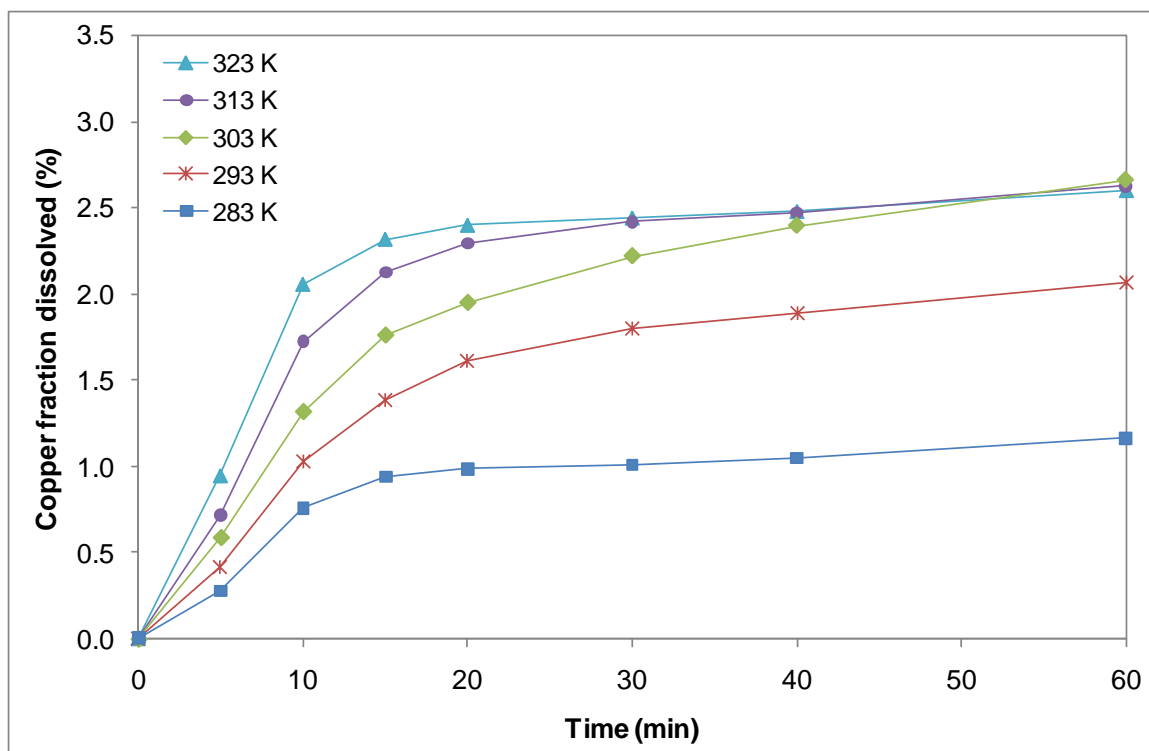
Figure 32–Effect of temperature in the range of 283-323 K on the fraction of copper dissolved into 35% liquid hydrogen peroxide.
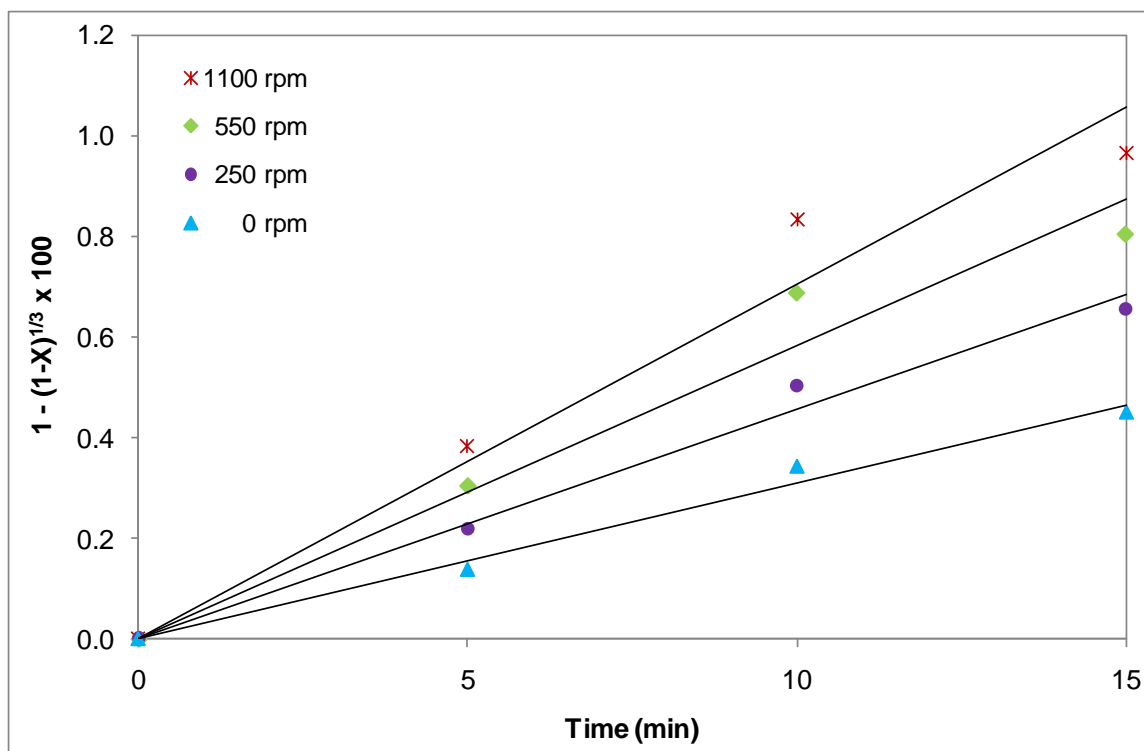
Figure 33–The variation of $1 - (1 - X)^{1/3}$ with time for various copper dissolution by 35% liquid hydrogen peroxide at different stirring speeds. In this case, X represents $[C]_t/[C]_\infty$ as in Equation 14.
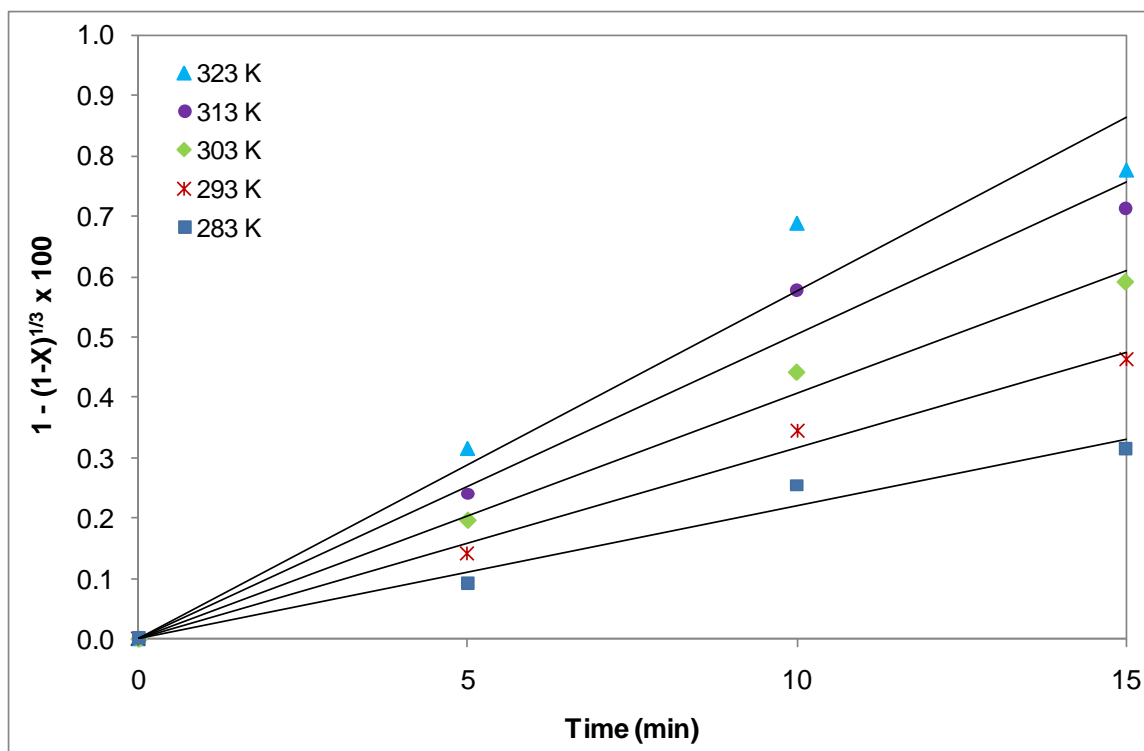
Figure 34–The variation of $1 - (1 - X)^{1/3}$ with time for various copper dissolution by 35% liquid hydrogen peroxide at different temperatures. In this case, X represents $[C]_t/[C]_\infty$ as in Equation 14.
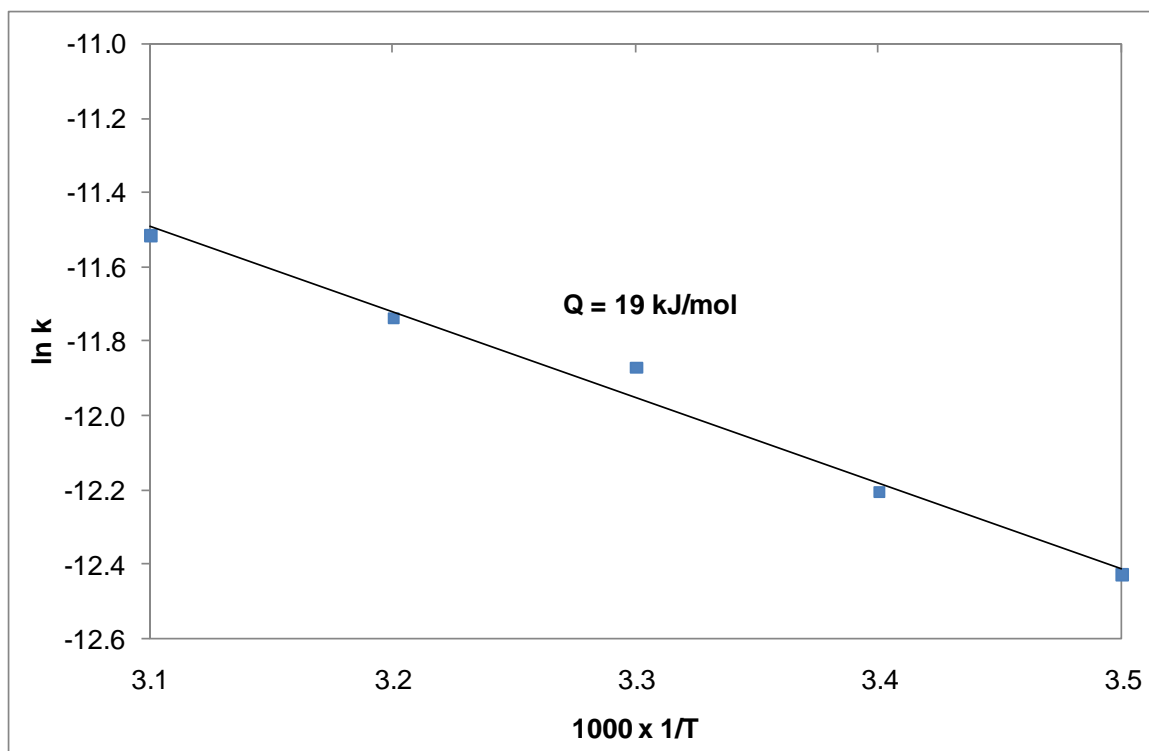
Figure 35–Activation energy determined from Arrhenius plot of linear data for the time 0 – 15 minutes of reaction.

As a comparison, dissolution of metal from a copper plate into the hydrogen peroxide solution at different time and temperature also has been performed. This experiment was performed statically by adopting an empirical theory [172] due to the unavailability of the equipment needed to run the rotating disk experiment. Fraction of copper plate dissolved into 35% liquid hydrogen peroxide as function of reaction time is shown in Figure 36. As can be seen from the figure, the fraction of copper dissolved from the copper plate is much lower compared to that from powder particles due to the smaller surface area. The activation energy calculated using an empirical theory, see Equation 5, gives a value of 8.6 kJ/mol as can be seen in Figure 37. However, as has been pointed out in the previous section, the value calculated by using this method cannot be confirmed because other factors, such as the diffusion layer thickness and kinematic viscosity, which would affect the diffusivity, was not included in the calculation.

For the two aluminum alloy plates of 2024-T3 and 7075-T6, as opposed to the copper powder, the data obtained was inconsistent. This inconsistency was expected to be due to the small area of the bulk specimens, inhomogeneity of copper distribution on the specimen surfaces, and/or small amount of copper content within the alloys. It would have been helpful if those two aluminum alloy samples were also in the form of powder so the surface area to the volume ratio would be large. Since there was no aluminum alloy material powders available, while the equipment setup for the rotating disk was not available, for the time being the data was just discarded. However, in its relation to the decontamination process, it seems that copper leaching during the aluminum alloys dip testing in the concentrated liquid hydrogen peroxide is supported by this result. Nonetheless, cyclic voltammetry test on 2024-T3 and 7075-T6 aluminum alloys in 0.1 M

NaCl after dip testing in 35% liquid hydrogen peroxide for up to 120 hours by Gale *et.al* [83] has shown that the impact of subsequent corrosion on aluminum alloys was insignificant.
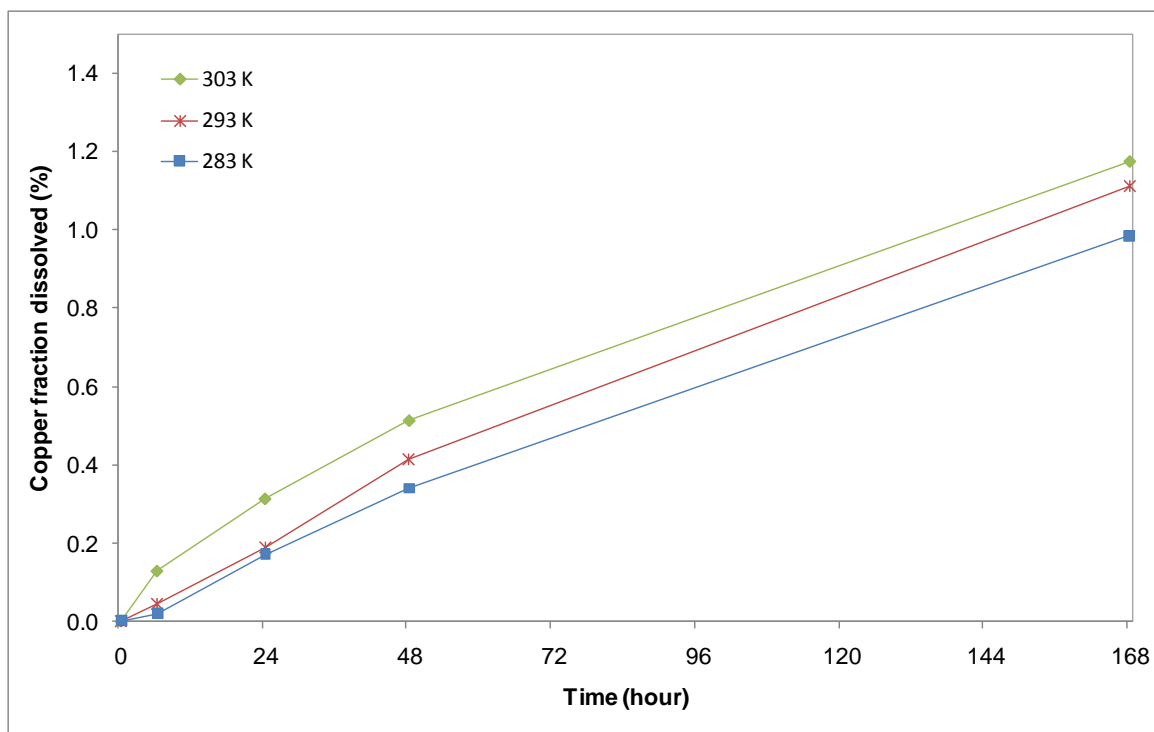
Figure 36–Fraction of copper plate dissolved into 35% liquid hydrogen peroxide as function of reaction time.
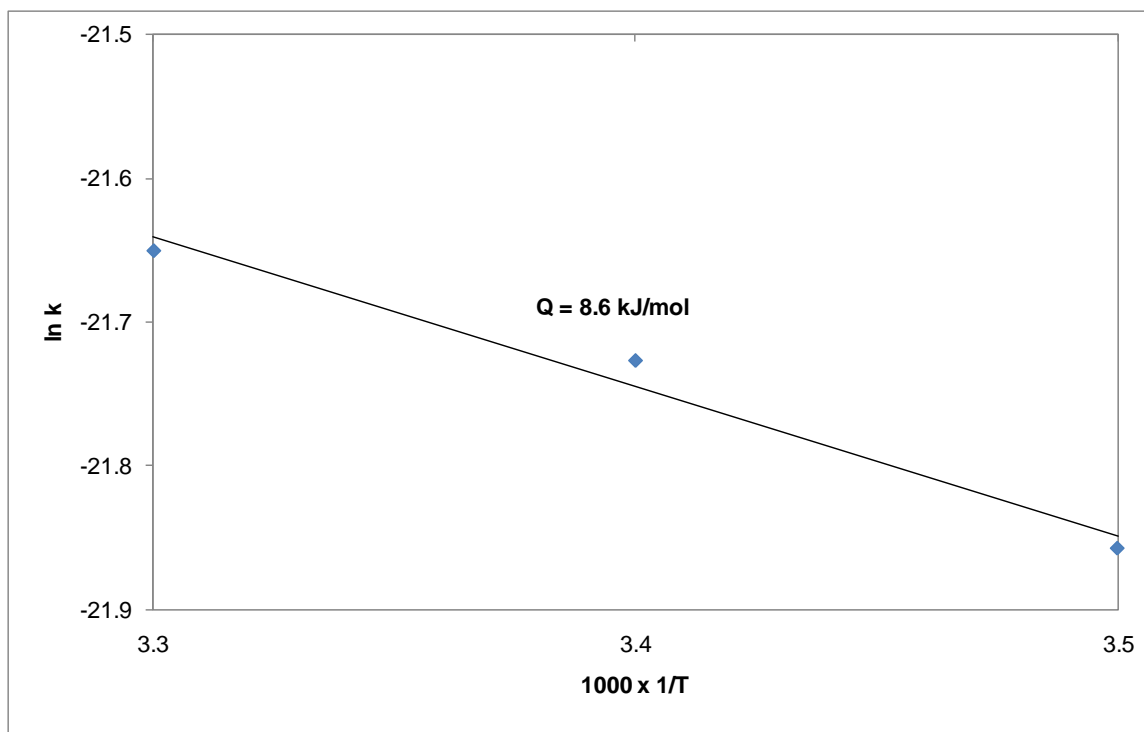
Figure 37– Activation energy of copper plate dissolution into 35% liquid hydrogen peroxide determined from empirical theory.

6. CONCLUSIONS

From what have been discussed previously, the outcomes of this work are summarized in the following.

6.1   Bacterial Attachment

1. The results from the first bacterial attachment work showed that surfaces of higher roughness distributed the *L. monocytogenes* suspension over larger area than the surface of lower roughness and the overall wettability of the surfaces appeared to be a primary determinant of the bacterial attachment results. The results also indicated that welding of austenitic stainless steel 304 followed by mirror polishing does not affect the ability of *L. monocytogenes* to attach to the surface under the conditions examined; however, corrosion of the welded stainless steels does promote the attachment of *L. monocytogenes* with the largest effect occurring in the HAZ. In its relation to the decontamination process, the more the spreading of bacteria over a surface, the more it likely prevents or at least affects the decontamination process. The results also indicated that corrosion site, especially on the austenitic stainless steel 304 welded joining and its surrounding HAZ should need more attention because it could become a source or a harborage after either incident or intentional release of bio-contaminant agents.

2. On the second work of bacterial attachment, the results showed that when the contact angle of a liquid on a surface increased to a certain degree, detachment of bacteria on that surface was observed to become more difficult resulting in more bacterial attachment occurred on surfaces with lower wettability and higher contact angle. This result might indicate that other factors, such as an optimum value for a surface roughness and contact angle or rate of spreading, need to be considered. In its relation to the decontamination, the major finding of this second work is that polishing an austenitic stainless steel 304 surface to a mirror finish, which would influence contact angle and rate of spreading, may give rise to more adhesion of bacteria on the surface. Thereby, it might take more time to decontaminate bio-contaminant on that type of surface finish compared to other certain type of surface finish. On the other hand, this mirror finish surface might give impact on decontamination process or any given decontamination setup by reducing the ability of decontamination treatments to remove or inactivate attached cells.

6.2   Effect of Decontamination on Materials Properties

On the effect of decontamination, and thus the effect of hydrogen peroxide, on the aircraft metallic structural materials properties of 2024-T3 and 7075 T-6 aluminum alloys and austenitic stainless steel 304, as used in galley and lavatory surfaces, the following conclusions are drawn:

1. There was no effect of vaporized hydrogen peroxide on the surface chemical composition change of all aircraft metallic materials examined up to 25 cycles of decontamination process. There was also no effect of concentrated liquid hydrogen peroxide tested up to 7 days on the surface chemical composition change of austenitic

stainless steel 304 and 7075-T6 aluminum alloy; however a significant effect on the surface chemical composition change of large intermetallic particles containing copper was found on 2024-T3 aluminum alloy. This compositional change indicates that copper is leached selectively from coarse intermetallic particles in 2024-T3 aluminum alloy.

2. A small but measurable weight loss occurred on the exposure of the two aluminum alloys to the concentrate liquid hydrogen peroxide. This weight loss indicates that some leaching occurs during the dip testing. On the contrary, repeated exposure to the vaporized hydrogen peroxide produced a small weight gain. This weight gain seems to indicate a limited amount of oxidation on the surface of aluminum alloys by the vapor of hydrogen peroxide.

3. There was no significant effect of both liquid and vaporized hydrogen peroxide on the microhardness and nanohardness of all of aircraft metallic materials; however, little effect was found on the nanohardness of 2024-T3 aluminum alloy after dip testing. This effect might indicate that there was a tendency towards surface softening very slightly after liquid hydrogen peroxide dip testing but was only confined to the immediate vicinity of the 2024-T3 aluminum alloy surface.

4. There was no significant effect of vaporized hydrogen peroxide exposure on the microstructure and mechanical properties of all of the metallic airliner materials examined up to 25 cycles of decontamination process. There was also no significant effect of concentrated liquid hydrogen peroxide tested up to 7 days on the microstructure and mechanical properties of austenitic stainless steel 304; however, little effect on the second phase particles containing copper was found on the 2024-

T3 and 7075-T6 aluminum alloys. This negligible effect seems to support copper leaching during the dip testing; however, there was no immediate loss or degradation in the materials properties and hence performance of all of aircraft metallic materials under the conditions examined.

5. In terms of overall effects of decontamination, and thus the effect of hydrogen peroxide as a decontaminant on the properties of aircraft metallic structural materials, the results of the testing in general are promising. These are included microstructure and mechanical properties tested under the most severe circumstances that could occur; in this case prolonged dip testing to the liquid concentrated hydrogen peroxide up to 168 hours. Most of the results under the conditions examined showed that only very limited damage was observed.

6.3   Copper Dissolution in Hydrogen Peroxide

The results from copper dissolution into hydrogen peroxide are concluded in the following:

1. The dissolution of copper into 35% liquid hydrogen peroxide occurs intensely only for up to 15 minutes of reaction time with an apparent activation energy of 19 kJ/mol during that stage of dissolution, after then the rate becomes constant due to the formation of copper hydroxide, which was observed to precipitate after the solution settled for some time.

2. In its relation to the decontamination process, it seems that copper leaching during the aluminum alloys dip testing in concentrated liquid hydrogen peroxide is supported by this result.

7. SUGGESTIONS FOR FUTURE WORK

The following suggestions are encourage to be performed for future expansion in scope of the project and/or application of the work to other area:

7.1   Bacterial Attachment

1. In the first bacterial attachment work, the results have shown that the increases of surface roughness plays a role on the decreases of the contact angle measurements of the samples and thus in the increase of wettability over the surface. However, a direct correlation between surface roughness and wettability cannot be precisely determined in this work since a detailed statistical analysis of the correlation of surface roughness to wettability was not included because the effect of surface roughness in this work was basically due to the accelerated corrosion process, which would likely entail other process as a result of the corrosion induced product(s). Thus, more investigation is needed to fully determine the direct correlation between surface roughness and wettability, independent of other factors associated with corrosion, for example potential reduction in solid-vapor interfacial energy which may be induced by the formation of corrosion products. This work can be used in support of the current project and/or can also be applied to other areas such as the food industry.

157

2. In terms of solely surface roughness, the result of the second work on the bacterial attachment does not fully agree with the previous assumption that the increase in the surface roughness would increase the wettability. Thus, there might be an optimum value for a surface roughness and contact angle and/or rate of spreading at which the bacterial attachment would be minimized. The suggestion would be to perform work to determine the optimum value for a surface roughness, wettability, contact angle, and/or rate of spreading at which bacterial attachment is minimized. This can be performed by employing different type and value of a surface roughness and then evaluating the effect of contact angle and rate of spreading of a liquid on that surface on the bacterial attachment.

7.2 Effect of Decontamination on Materials Properties

1. The present research actually does not yet address the predictions of effect of the chemical used as the decontaminant agent on the aircraft's flightworthiness. However, what has been performed in the present work is a necessary precursor to such predictions. Thus, the work on this prediction is suggested to be done to accomplish all of the goals mentioned in the broader objectives of the research.

2. Establishment of life prediction after decontamination on the aircraft structural materials would be desirable, especially to get a quantitative understanding on the nature of decontamination process impact on the material properties. Hence, fatigue testing is also needed, particularly to reveal subtle, incipient damage that could induce subsequent degradation in the airliner structural materials performance.

3. Since the range of materials examined in this work is still inadequate to cover all of complex aircraft structural materials, further work is still needed to cover more

aircraft materials such as composite materials, textiles and fabrics, and polymeric materials. Some of these activities are being performed by others in the same research group as of the date of writing.

7.3 Copper Dissolution in Hydrogen Peroxide

The result from copper dissolution showed that after 15 minutes of reaction, the fraction of copper dissolved, became constant. This was expected to be due to the formation of copper hydroxide, which was observed to precipitate after the solution settled for some time. However, because the final consumption of hydrogen peroxide was not controlled, the exact reason for this constant rate cannot be determined at this time. Hence, the following suggestions need to be addressed:

1. The final consumption of hydrogen peroxide and real time copper concentration needs to be controlled so the exact reason for the constant rate after 15 minutes of reaction time can be confirmed. This can be done by using the combination of real time hydrogen peroxide consumption and copper dissolution rate monitoring so the rate and mechanism can be determined exactly.

2. Since it was hard to make a comparison between dissolution of pure copper powder and dissolution of copper from 2024-T3 and 7075-T6 aluminum alloy plates due to the specimen shape difference and small amount of copper concentration in the aluminum alloys, it might be helpful if the comparison would have been started from aluminum copper alloys with the same shape and controlled concentration. Hence, it is suggested that this work would be also done in the near future so the comparison can be justified.

REFERENCES

1. Bio Warfare, available online from http://library.thinkquest.org/27393/tqtranslate.htm, accessed on June 7, 2005.

2. United Nations, Convention on the Prohibition of the Development, Production, and Stockpiling of Bacteriological and Toxin Weapons and Their Destruction, 1972.

3. H.W. Herrmann, *et al.*, *Physics of Plasmas*, 6 (1999) 2284-2289.

4. The Chemical/Biological Weapons Threat, available online from http://usmilitary.about.com/od/weapons/a/chemwarfare_4.htm accessed on June 2, 2006.

5. E.A.S. Whitney, *et al.*, *Emerg. Infect. Dis*., 9 (2003) 623-627.

6. U.S. State Department of State, *Decontamination of Sterling Mail Facility*, available online at http://www.state.gov/r/pa/prs/ps/2002/15992.htm, accessed on December 8, 2007.

7. S. Coll, *Ghost Wars: The Secret History of the CIA, Afghanistan, and Bin Laden, from the Soviet Invasion to September 10, 2001*, Penguin Books, New York, 2004, pp. 240-279.

8. Iraq gas attack makes hundreds ill, available online from http://www.cnn.com/2007/WORLD/meast/03/17/iraq.main/index.html accessed on July 17, 2007.

9. B. Pfefferbaum, *Lancet*, 358 (2001) 940.

10. M. Mines, *et al.*, *Ophthalmology*, 107 (2000) 837-843.

11. J.A. Davis, *Accident Emerg. Nursing*, 4 (1996) 59-64.

12. M. Varia, *et al.*, *Can. Med. Assoc. J*., 169 (2003) 285-292.

13. A.A. Edler, *J. Clin. Anesthesia,* 18 (2006) 1-4.

14. J.C. de Jong, *et al.*, *Nature*, 389 (1997) 554.

15. E.C.J. Claas, *et al.*, *Lancet*, 351 (1998) 472-477.

16. A.D.M.E. Osterhaus, *et al.*, *Vaccine*, 20 (2002) S82-S83.

17. K. Ungchusak, *et al.*, *N. Engl. J. Med.*, 352 (2005) 333-340.

18. WHO, Avian influenza – the latest situation in Indonesia – update 21, http://www.who.int/csr/don/2006_07_04/en/index.html, accessed on July 4, 2006.

19. A.S. Ho, J.J.Y. Sung, and M. Chan-Yeung, *Ann. Intern. Med.*, 139 (2003) 564-567.

20. Z. Zhao, *et al.*, *J. Med. Microbiol.*, 52 (2003) 715-720.

21. G. Gopalakrishna, *et al.*, *Emerg. Infect. Dis.*, 10 (2004) 395-400.

22. S.J. Twu, *et al.*, *Emerg. Infect. Dis.*, 9 (2003) 718-720.

23. L.D. Ha, *et al.*, *Emerg. Infect. Dis.*, 10 (2004) 265-268.

24. P.M. Hawkey, S. Bhagani, and S.H. Gillespie, *J. Med. Microbiol.*, 52 (2003) 609-613.

25. M. Varia, *et al.*, *Can. Med. Assoc. J.*, 169 (2003) 285-292.

26. T. Wong, *et al.*, *Emerg. Infect. Dis.*, 11 (2005) 322-325.

27. I.T.S Yu, *et al.*, *N. Engl. J. Med.*, 352 (2005) 333-340.

28. S.M. Poutanen, *et al.*, *N. Engl. J. Med.*, 348 (2003) 1995-2005.

29. WHO, Consensus document on the epidemiology of severe acute respiratory syndrome (SARS). Available from: http://www.who.int/csr/sars/en/WHO consensus.pdf, accessed on October 10, 2006.

30. A.H. Reid, J.K. Taubenberger, and T.G. Fanning, *Microbes Infect.*, 3 (2001) 81-87.

31. J.K. Taubenberger, A.H. Reid, and T.G. Fanning, *Virology*, 274 (2000) 241-245.

32. J.K. Taubenberger and D.M. Morens, *Emerg. Infect. Dis.*, 12 (2006) 1-2.

33. C.J. Luke and K. Subbarao, *Emerg. Infect. Dis.*, 12 (2006) 66-72

34. J.K. Taubenberger and D.M. Morens, *Emerg. Infect. Dis.*, 12 (2006) 15-22.

35. Greater New York Hospital Association (GNYHA), Nuclear, biological, and chemical decontamination; in *Joint Commission Perspectives*, 21 (2001) 20-21.

36. T.H.G. Megson, *Aircraft Structures*, 3rd Ed., Butterworth-Heinemann, Burlington, MA, 2003, pp. 211-232.

37. A. Baker, S. Dutton, and D. Kelly, *Composite Materials for Aircraft Structures*, American Institute of Aeronautics and Astronautics, New York, NY 2004, pp. 1-2.

38. H.M. Lappin-Scott, C. Bass, *Am. J. Infect. Control*, 29 (2001) 250-251.

39. International Air Transport Association (IATA), *General Guidelines for Cleaning Crew*, available online at http://www.iata.org/nr/rdonlyres/23ea32b7-ec3e-4eed-b4fa-efd7c07b58bc/0/guidelines_cleaning_crew_112006.pdf, accessed October 2, 2007.

40. E.A. Zottola and K. C. Sasahara, *Int. J. Food Microbiol.*, 23 (1994) 125–148.

41. A.S. Gordon, F.J. Millero, *Appl. Microbiol.*, 47 (1984) 495-499.

42. E. Sinde and J. Carballo, *Food Microbiol.*, 17 (2000) 439–447.

43. J.W. Arnold and S. Silvers, *Poultry Sci.*, 79 (2000) 1215 – 1221.

44. K. Bidle, H.H. Wickman, and M. Fletcher, *J. General Microbiol.*, 139 (1993) 1891-1897.

45. L.K. Ista, *et al.*, *FEMS Microbiol. Let.*, 142 (1996) 59-63.

46. C. Tide, *et al.*, *J. Food Eng.*, 42 (1999) 85–96.

47. T.L. Mai, *et al.*, *J. Food Prot.*, 69 (2006) 1527-1532.

48. N.I. Sofyan, *et al.*, *Food Prot. Trend*, 26 (2006) 926-929.

49. F.W. Hyde, M. Alberg, and K. Smith., *J. Ind. Microbiol. Biotech.*, 19 (1997) 142-149.

50. S. McEldowney and M. Fletcher, *App. Environ. Microbiol.*, 52 (1986) 460-465.

51. M. Al-Ahmed, *et al.*, *Desalination*, 132 (2000) 173-179.

52. D.R. Oliveira, in L.F. Melo, *et al.* (Eds), *Biofilm–Science and Technology*, Kluwer Academic Publisher, Durdrecht, the Netherlands, 1992, pp. 45-58.

53. S.H. Flint, J. D. Brooks, and P. J. Bremer, *J. Appl. Microbiol.*, 83 (1997) 508-517.

54. M.S. Lou, J.C. Chen, and C.M. Li, *J. Ind. Technol.*, 15 (1998) 1-6.

55. R.F. Anastasi and E.I. Madaras, The 4th International Workshop on Ultrasonic and Advanced Methods for Nondestructive Testing and Material Characterization, June 19, N. Dartmouth, MA, 2006, pp. 57-62.

56. Surface Metrology Guide – Profile Parameters, available online at http://www.predev.com/smg/parameters.htm, accessed on August 19, 2004.

57. J.W. Arnold, D.H. Boothe, and G.W. Bailey, *Trans*. *ASAE*, 44 (2001) 347-356.

58. US Environmental Protection Agency, Terms of Environment: Glossary, Abbreviations and Acronyms, available online at www.epa.gov/OCEPAterms/wterms.html, accessed 09/13/07.

59. W.F. Gale and D.A. Butts, *Sci*. *Technol*. *Welding and Joining*, 9 (2004) 283-300.

60. J.W. Gibbs, On the Equilibrium of Heterogeneous Substances, 1876, reprinted in *The Scientific Papers of J. Willard Gibbs*, Vol. 1: *Thermodynamics*, Longmans, Green & Co., London, 1906.

61. T. Young, *Philos*. *Trans*. *Roy*. *Soc*., 95 (1805) 65–87.

62. G.R. Lester, *J*. *Colloid Sci*., 16 (1961) 315-326.

63. W.A. Zisman, *Adv*. *Chem*. *Ser*., 43 (1963) 1-51.

64. I.A. Aksay, C.E. Hoge, and J.A. Pask, *J*. *Phys*. *Chem*, 78 (1974) 1178-1183.

65. V. Roucoules, *et al*., in K. L. Mittal (Ed.), *Contact angle*, *Wettability*, *and Adhesion*, Vol. 2. VSP International Science Publishers, Utrecht, The Netherlands, 2002, pp. 387–402.

66. R.N. Wenzel, *Ind*. *Eng. Chem*., 28 (1936) 988-994.

67. R.E. Johnson, Jr. and R.H. Dettre, *Adv*. *Chem*. *Ser*., 43 (1963) 112-135.

68. R.H. Dettre and R.E. Johnson, Jr., *Adv*. *Chem*. *Ser*., 43 (1963) 136-144.

69. J.V. Rogers, *et al*., *Environmental Technology Verification Report: CLARUS C Hydrogen Peroxide Generator*, Battelle, Columbus, OH, 2004.

70. C. Chamberland, *J*. *de Médecine*, *de Chirurgie et de Pharmacologie*, 67 (1879) 61-62.

71. STERIS® Corp., Steris VHP Generator Operator Training Program.

72. R.J.W. Lambert, in A.P. Fraise, P.A. Lambert, and J.-Y.Maillard (Eds), *Russell*, *Hugo & Ayliffe's Principles and Practice of Disinfection*, *Preservation & Sterilization*, 4th Ed., Blackwell Publishing, Malden, MA, 2004, pp. 345-360.

73. G.W. Gould, in A.P. Fraise, P.A. Lambert, and J.-Y.Maillard (Eds), *Russell*, *Hugo & Ayliffe's Principles and Practice of Disinfection*, *Preservation & Sterilization*, 4th ed., Blackwell Publishing, Malden, MA, 2004, pp. 361-383.

74. P.A. Lambert, in A.P. Fraise, P.A. Lambert, and J.-Y.Maillard (Eds), *Russell*, *Hugo & Ayliffe's Principles and Practice of Disinfection*, *Preservation & Sterilization*, 4th Ed., Blackwell Publishing, Malden, MA, 2004, pp. 384-400.

75. J.-Y. Dusseau, P. Duroselle, and J. Freney, in A.P. Fraise, P.A. Lambert, and J.-Y.Maillard (Eds), *Russell*, *Hugo & Ayliffe's Principles and Practice of Disinfection*, *Preservation & Sterilization*, 4th Ed., Blackwell Publishing, Malden, MA, 2004, pp. 401-435.

76. G.W. Gould, in A.P. Fraise, P.A. Lambert, and J.-Y.Maillard (Eds), *Russell*, *Hugo & Ayliffe's Principles and Practice of Disinfection*, *Preservation & Sterilization*, 4th ed., Blackwell Publishing, Malden, MA, 2004, pp. 473-483.

77. T.K. Das, in Kirk-Othmer Encyclopedia of Chemical Technology, *Disinfection*, Vol. 8, pp. 605-672.

78. C.H. Shaffer, in Seymour S. Block (Ed), *Disinfection*, *Sterilization*, *and Preservation*, 2nd Ed., Lea & Febiger, Philadelphia, 1977, pp. 78-99.

79. EPA, *Summary of the Federal Insecticide, Fungicide, and Rodenticide Act*, available online at http://www.epa.gov/lawsregs/laws/fifra.html, accessed on December 25, 2007.

80. N. Omidbakhsh and S.A. Sattar, *Am*. *J*. *Infect*. *Control*, 34 (2006) 251-257.

81. R.A. Caputo and T.E. Odlaug, in Seymour S. Block (Ed), *Disinfection*, *Sterilization*, *and Preservation*, 2nd Ed., Lea & Febiger, Philadelphia, 1977, pp. 47-64.

82. D.M. Portner and R.K. Hoffman, *Appl*. *Microbiol*, 16 (1968) 1782-1785.

83. W.F. Gale, *et al*., *The Effect of Vapor Phase Hydrogen Peroxide, as a Decontaminant for Civil Aviation Applications, on the Microstructure and Tensile Properties of 2024 and 7075 Age Hardenable Aluminium Alloys and 304 Austenitic Stainless Steel*, *Mater*. *Sci*. *Technol*., in press.

84. FIFRA, as amended through P.L. 110-94, enacted October 9, 2007, available online at http://agriculture.senate.gov/Legislation/Compilations/Fifra/FIFRA.pdf, accessed on December 25, 2007.

85. EPA, *Pesticides: Topical & Chemical Fact Sheets*, available online at http://www.epa.gov/pesticides/factsheets/chemicals/hydrogenperoxide_peroxyaceti

cacid_factsheet.htm and http://www.epa.gov/pesticides/factsheets/chemicals/vhp_factsheet.htm, accessed on October 3, 2007.

86. EPA, *Alphabetical List of Pesticide Fact Sheets*, available online at http://www.epa.gov/pesticides/factsheets/alpha_fs.htm, accessed on October 3, 2007.

87. J.R. Rickloff, *J. Valid. Technol.*, 5 (1998) 61-71.

88. Bioquell HPV Generator, http://www.bioquell.com/lifescience.asp accessed on November 24, 2007.

89. W.F. Gale, *et al.*, *Biosecurity and Bioterrorism*: *Biodefense Strategy*, *Practice*, *and Science*, *Mater. Sci. Technol.*, submitted November 20, 2007.

90. Science Applications International Corporation, Report: EPA/600/R-05/036/2005.

91. E.D. Asbury, in S.S. Block (Ed), *Disinfection*, *Sterilization and Preservation*, 3rd Ed., Lea and Febiger, Philadelphia, 1983, pp. 964-980.

92. ASTM Designation: E2111-05, ASTM International.

93. C.L. Tornblom, Report Executive Research Project F12, The Industrial College of the Armed Forces, Washington DC., 1992.

94. J.S. Robinson, *Elements Magazine, a University of Limerick Publication*, 2 (1994) 19-20.

95. EPA's Chemical Compatibility Chart, EPA-600/2-80-076 April 1980.

96. Cole-Parmer Chemical Compatibility, available online at http://www.coleparmer.com/techinfo/chemcomp.asp, accessed on November 26, 2007.

97. W. Eul, A. Moeller, and N. Steiner, in Kirk-Othmer Encyclopedia of Chemical Technology, *Hydrogen Peroxide*, Vol. 13, pp. 1-58.

98. G.L. French, *et al.*, *J. Hosp. Infec.*, 57 (2004) 31-37.

99. B.M. Andersen, *J. Hosp. Infec.*, 62 (2006) 149-155.

100. W. Mueller, U.S. Patent No. 5,792,435, 1998.

101. W. Mueller, WIPO Patent No. WO 98/44958, 1998.

102. F. Bounoure, H. Fiquet, and P. Arnaud, *Am. J. Health-Syst. Pharm.*, 63 (2006) 451-455.

103. J.R. Rickloff, J.P. Dalmasso, and L.W. Lyhte, *Proc. PDA Annual Meeting*, 1992, pp. 1-14.

104. J.R. Rickloff, D.C. Upchurch, and R.W. Childers, U.S. Patent No. 5,445,792, 1995.

105. ACER, Center Highlight as of March 23, 2007, available online at http://acer-coe.org/flyers/acer_highlights_public_release.pdf, accessed on October 3, 2007.

106. M.J. Kempf, *et al.*, *Astrobiology*, 5 (2005) 391-405.

107. G.W. Wagner and Y.-C. Yang, *Ind. Eng. Chem. Res.*, 41 (2002) 1925-1928.

108. G. Marsh, *Reinforced Plastics* 50 (2006) 18-23.

109. National Research Council, *The Airliner Cabin Environment and the Health of Passengers and Crew*, National Academy Press, Washington, D.C., 2002, pp.98-99.

110. A. Sverdlin, in G.E. Totten and D.S. MacKenzie (Eds), *Handbook of Aluminum*, *Physical Metallurgy and Process*, Vol. 1, Marcel Dekker, Inc., New York, 2003, pp. 33-80.

111. R. Howard, N. Bogh, and D.S. MacKenzie, in G.E. Totten and D.S. MacKenzie (Eds), *Handbook of Aluminum*, *Physical Metallurgy and Process*, Vol. 1, Marcel Dekker, Inc., New York, 2003, pp. 881-970.

112. J.R. Davis, *Corrosion of Aluminum Alloy and Aluminum Alloys*, ASM International, Materials Park, OH, 1999.

113. L. Katgerman and D. Eskin, in G.E. Totten and D.S. MacKenzie (Eds), *Handbook of Aluminum*, *Physical Metallurgy and Process*, Vol. 1, Marcel Dekker, Inc., New York, 2003, pp. 259-303.

114. E.A. Starke, Jr., in A.K. Vasudevan and R.D. Doherty (Eds), *Aluminum Alloys – Contemporary Research and Applications*, Vol. 31, Academic Press, Inc., San Diego, 1989, pp. 35-63.

115. D.S. MacKenzie, in G.E. Totten and D.S. MacKenzie (Eds), *Handbook of Aluminum*, *Alloy Production and Materials Manufacturing*, Vol. 2, Marcel Dekker Inc., New York, 2003, pp. 343-419.

116. R.L. Fleischer, *Acta Met.*, 11 (1963) 203.

117. M. Tiryakioğlu and J.T. Staley, in G.E. Totten and D.S. MacKenzie (Eds), *Handbook of Aluminum*, *Physical Metallurgy and Process*, Vol. 1, Marcel Dekker, Inc., New York, 2003, pp. 81-209.

118. E.O. Hall, *Proc. Phys. Soc.*, B64, (1951) 747-753.

119. J.C.M. Li, *Trans. Met.* Soc. AIME., 227 (1963) 239-247.

120. R.W. Armstrong, *et al.*, *Philos. Mag.*, 14 (1966) 943-951.

121. R.W. Hertzberg, *Deformation and Fracture Mechanics of Engineering Materials*, 4th Ed., John Wiley & Sons, Inc., New York, 1996, p. 123.

122. C.G. Schmidt and A.K. Miller, *Acta Metall.*, 30 (1982) 615-625.

123. A. Guinier, *Nature* 142 (1938) 569–570.

124. G.D. Preston, *Proc. Roy. Soc.* A 167 (1938) 526–538.

125. T.H. Courtney, *Mechanical Behavior of Materials*, McGraw-Hill Publishing Inc., New York, 1990, pp. 207-212.

126. T.J. Konno, M. Kawasaki, and K. Hiraga, *JEOL News*, 36E (2001) 14-17.

127. J.D. Embury and J.P. Hirth, *Acta Metall. Mater.*, 42 (1994) 2051-2056.

128. A.R. Despić, *et al.*, *Electrochim. Acta*, 35 (1990) 1747-1755.

129. M.-H. Wang and K.R. Hebert, *J. Electrochem. Soc.*, 143 (1996) 2827-2834.

130. J.H. Seo and D.N. Lee, *J. Electrochem. Soc.*, 150 (2003) B329-B335.

131. T.D. Burleigh, in G.E. Totten and D.S. MacKenzie (Eds), *Handbook of Aluminum*, *Alloy Production and Materials Manufacturing*, Vol. 2, Marcel Dekker Inc., New York, 2003, pp. 421-463.

132. W. Zhang and G.S. Frankel, *J. Electrochem. Soc.*, 149 (2002) B510-B519.

133. N.J.H Holroyd, A.K. Vasudevan. And L. Christodoulou, in A.K. Vasudevan and R.D. Doherty (Eds), *Aluminum Alloys – Contemporary Research and Applications*, Vol. 31, Academic Press, Inc., San Diego, 1989, pp. 463-483.

134. G.S. Chen, *et* al., *Mater. Sci. Eng.*, A219 (1996) 126-132.

135. B.W. Lifka and D.O. Sprowls, *Localized Corrosion Cause of Metal Failure*, ASTM STP516 (1972) 120-144.

136. G.S. Chen, M. Gao, and R.P. Wei, *Corr. Sci.*, 52 (1996) 8-15.

137. M. Gao, C.R. Feng, and R.P. Wei, *Metall. Mater. Trans.* A29 (1998) 1145-1151.

138. R.P. Wei, C.-M. Liao, and M. Gao, *Metall. Mater. Trans.* A29 (1998) 1153-1160.

139. T. Suter and R.C. Alkire, *J. Electrochem. Soc.*, 148 (2001) B36-B42.

140. C. Blanc, S. Gastaud, and G. Mankowski, *J. Electrochem. Soc.*, 150 (2003) B396-B404.

141. A.F. Padilha and R.L. Plaut, in G.E. Totten and D.S. MacKenzie (Eds), *Handbook of Aluminum*, *Alloy Production and Materials Manufacturing*, Vol. 2, Marcel Dekker Inc., New York, 2003, pp. 193-220.

142. N. Birbilis and R.G. Buchneit, *J. Electrochem. Soc.* 152 (2005) B140-B151.

143. H.M. Obispo, *et al.*, *J. Mater. Sci.*, 35 (2000) 3479-3495.

144. C.M. Liao and R.P. Wei, *Electrochim. Acta*, 45 (1999) 881-888.

145. R.G. Buchheit, *et al.*, *J. Electrochem. Soc.* 144 (1997) 2621-2628.

146. M. Raghawan, J.Y. Koo, and R Petkovic-Luton, *J. Met.*, 35 (1983) 44-50.

147. P.P. Villars and L.D. Calvert, *Pearson's Handbook of Crystallographic Data for Intermetallic Phases*, ASM International, Materials Park OH, 1991.

148. J. T. Staley, in A. K. Vasudevan and R.D. Doherty (Eds), *Aluminum Alloys – Contemporary Research and Applications*, Vol. 31, Academic Press, Inc., San Diego (1989) pp. 1-31.

149. M. Shao, *et al.*, *Mater. Sci. Eng.* A344 (2003) 323-327.

150. D.G. Harlow and R.P. Wei, *Eng. Fracture Mechanics*, 59 (1998) 305-325.

151. ASTM Designation: A 240/A 240M-01, ASTM International.

152. J.R. Davis, *ASM Specialty Handbook, Stainless Steel*, ASM International, Materials Park, OH, 1996.

153. D. Peckner and I.M. Bernstein, *Handbook of Stainless Steels*, McGraw-Hill Book Company, New York, NY, 1977.

154. D.P. Gregory and A.C. Riddiford, *J. Electrochem. Soc.*, 107 (1960) 950-956.

155. P. Miečinskas, *Russian J. Electrochem.*, 41 (2005) 731-735.

156. E. D'Elia, *et al.*, *J. Electrochem. Soc.*, 143 (1996) 961-967.

157. V. Kreizer, *et al.*, *Protections of Metal*, 39 (2003) 30-33.

158. D.H. Hur, *et al.*, *Nuclear Eng. Design*, 224 (2003) 207-212.

159. R.L. Cervantes, L.E. Murr, and R.M. Arrowood, *J. Mater. Sci.*, 36 (2001) 4079-4088.

160. M.A. Alodan and W.H. Smyrl,, *J. Electrochem. Soc.*, 145 (1998) 1571-1577.

161. M.B. Vukmirovic, N. Dimitrov, and K. Sieradzki, *J. Electrochem. Soc.*, 149 (2002) B428-B439.

162. Q. Meng and G.S. Frankel, *J. Electrochem. Soc.*, 151 (2004) B271-B283.

163. K.Y. Tam, *J. Am. Chem. Soc.*, 118 (1996) 4419-4426.

164. R.G. Compton, *et al.*, *J. Phys. Chem.*, 97 (1993) 10416-10420.

165. V.G. Levich, *Physicochemical Hydrodynamics*, Prentice Hall, Englewood Cliffs, NJ, 1962, pp. 39-138.

166. R.B. Bird, W.E. Stewart, E.N. Lightfoot, *Transport Phenomena*, 2nd Ed., John Wiley & Son Inc., New York, 2002, pp. 513-542.

167. A.W. Hixson and J.H. Crowell, *Ind. Eng. Chem.*, 23 (1931) 923-931.

168. A. Noyes and W.R. Whitney, *J. Am. Chem. Soc.*, 19 (1897) 930-934.

169. W. D. MacDonald and T. W. Eagar, *Annu. Rev. Mater. Sci.*, 22 (1992) 23-46.

170. S. Chada, *et al.*, *J. Elec. Mater.*, 29 (2000) 1214-1221.

171. C.V. King, *J. Am. Chem. Soc.*, 57 (1935) 828-831.

172. V.G. Levich, Physicochemical Hydrodynamics, Prentice Hall, Englewood Cliffs, NJ, 1962, pp. 60-78.

173. W.G. Cochran, Proc. Camb. Philos. Soc., 30 (1934) 365–375.

174. A.W. Hixson and J.H. Crowell, *Ind. Eng. Chem.*, 23 (1931) 1002-1009.

175. W.I. Higuchi and E.N. Hiestand, *J. Pharm. Sci.*, 52 (1963) 67-71.

176. W.I. Higuchi, E.L. Rowe, and E.N. Hiestand, *J. Pharm. Sci.*, 52 (1963) 162-164.

177. P.J. Niebergall, *et al.*, *J. Pharm. Sci.*, 52 (1963) 236-241.

178. J. Wang and D.R. Flanagan, *J. Pharm. Sci.*, 88 (1999) 731-738.

179. J. Wang and D.R. Flanagan, *J. Pharm. Sci.*, 91 (2002) 534-542.

180. A. Mills, H.L. Davies, and M.S. Garley, *J. Chem. Soc. Faraday Trans.*, 86 (1990) 2163-2167.

181. M.G. Segal and R.M. Sellers, *J. Chem. Soc. Chem. Comm.*, 21 (1980) 991-993.

182. A.B. O'Brien, M.G. Segal, and W.J. Williams, *J. Chem. Soc. Faraday Trans*. 1, 83 (1987) 371-382.

183. M.G. Segal and W.J. Williams, *J. Chem. Soc. Faraday Trans*. 1, 82 (1986) 3245-3254.

184. M.G. Segal and R.M. Sellers, *J. Chem. Soc. Faraday Trans*. 1, 78 (1982) 1149-1164.

185. H.Y. Sohn and M.E. Wadsworth, *Rate Processes of Extractive Metallurgy*, Plenum Press, New York, 1979, pp. 133-186.

186. M.M. Antonijević, Z.D. Janković, and M.D. Dimitrijević, *Hydrometallurgy*, 71 (2004) 329-334.

187. M.M. Antonijević, M. Dimitrijević, and Z. Janković, *Hydrometallurgy*, 46 (1997) 71-83.

188. M. Dimitrijević, M.M. Antonijević, and Z. Janković, *Hydrometallurgy*, 42 (1996).

189. D.A. McQuarrie and P.A. Rock, *General Chemistry*, W.H. Freeman & Co., New York, 1984, pp. 623-657.

190. K.K. Sankaran, R. Perez, and K.V. Jata, *Mater. Sci. Eng*. A297 (2001) 223-229.

191. D.L. DuQuesnay, P.R. Underhill, and H.J. Britt, *Int. J. Fatigue*, 25 (2003) 371-377.

192. K. Jones and D.W. Hoeppner, *Corr. Sci*., 47 (2005) 2185-2198.

193. K. Jones and D.W. Hoeppner, *Corr. Sci*., 48 (2006) 3106-3122.

194. Y. Kondo, *Corr. Sci*., 45 (1989) 7-11.

195. M.L. Du, *et al*., *Int. J. Fatigue*, 20 (1998) 743-748.

196. V. Bystritskii, *et al*., *Theoretical Appl. Fract. Mech*., 32 (1999) 47-53.

197. What is Listeria monocytogenes? Available online at http://www.bionewsonline.com/f/what_is_listeria_monocytogenes.htm, accessed on April 20, 2008.

198. A.C. Davies, *The Science and Practice of Welding*, 10th Ed., Vol. 1, Cambridge University Press, New York, 1992, pp. 103-105.

199. E.L. Criscuolo, *et al*., in A.L. Phillips, *et al*., (Eds), *Welding Handbook*, 6th Ed., Vol. 1., American Welding Society, New York, 1968, pp. 6.1-6.66.

200. ASTM Designation: E8M-00b, ASTM International.

201. B. Chalmers, *Principles of Solidification*, John Wiley & Sons, Inc., New York, 1964, p. 78-79.

202. J. Drelich and J. D. Miller, *J. Colloid Interface Sci.*, 164 (1994) 252–259.

203. J. Drelich, J. D. Miller, and R. J. Good, *J. Colloid Interface Sci.*, 179 (1996) 37–50.

204. D.S. MacKenzie, in G.E. Totten, K. Funatani, and L. Xie, *Handbook of Metallurgical Process Design*, CRC Press, Boca Raton, FL, 2004, pp. 765-790.

205. K.R. Trethewey and J. Chamberlain, *Corrosion*, Longman Scientific & Technical, Harlow, England, 1988, pp. 241-270.

206. N.N. Greenwood and A. Earnshaw, *Chemistry of the Elements*, 2nd Ed., Butterworth-Heinemann, Oxford, 1998, pp. 1173-1226.

207. H. Aretz, *Modelling Simul. Mater. Sci. Eng.*, 12 (2004) 491-509

208. J. Halpern, *J. Electrochem. Soc.*, 100 (1953) 421-428.

209. R.A. Couche and I.M. Ritchie, *Aust. J. Chem.*, 37 (1984) 231-238.

210. L.L. Duda, *Corr. Sci.*, 44 (2002) 989-995.

211. F. Arslan, *et al.*, *Scandinavian J. Metall.*, 33 (2004) 6-14.

212. M.C. Ruiz and R. Padilla, *Hydrometallurgy*, 48 (1998) 313-325.

213. C-W. Shih, Y-Y. Wang, and C-C. Wan, *J. App. Electrochem.*, 32 (2002) 987-992.

214. M.M. Antonijević, Z. Janković, and M. Dimitrijević, *Hydrometallurgy*, 35 (1994) 187-201.